Dissertation zur Erlangung des Doktorgrades
der Fakultät für Chemie und Pharmazie
der Ludwig-Maximilians-Universität München

TLR8 Is a Sensor of RNase T2 Degradation Products

Wilhelm Marcus Michael Greulich

aus

München, Deutschland

2020

Erklärung:

Diese Dissertation wurde im Sinne von § 7 der Promotionsordnung vom 28. November 2011 von Herrn Prof. Dr. Veit Hornung betreut.

Eidesstattliche Versicherung:

Diese Dissertation wurde eigenständig und ohne unerlaubte Hilfe erarbeitet.

München, den 18.12.2020

Wilhelm Greulich

Dissertation eingereicht am:	09.10.2020
1. Gutachter:	Prof. Dr. Veit Hornung
2. Gutachter:	Prof. Dr. Karl-Klaus Conzelmann
Mündliche Prüfung am:	08.12.2020

Auszüge dieser Arbeit wurden bereits in folgender Publikation veröffentlicht:

Greulich, W., Wagner, M., Gaidt, M.M., Stafford, C., Cheng, Y., Linder, A., Carell, T., and Hornung, V. (2019). TLR8 Is a Sensor of RNase T2 Degradation Products. Cell *179*, 1264-1275 e1213.

Table of contents

1 Introduction

1.1 The immune system

Immune systems are essential defense mechanisms that protect various organisms from all kinds of pathogens including bacteria, fungi, parasites and viruses. In multicellular organisms, it has the additional function of containing the growth of aberrant cells such as cancer cells. Generally, the immune system can be divided into two lines of defense: the innate immune system, which can already be found in invertebrates and even non-eucaryotic cells; and the adaptive immune system present in vertebrates. The innate immune system is triggered within minutes to hours and provides an almost immediate, yet non-specific response to invading pathogens, whereas the adaptive immune system takes several days to take full effect and is more specific. However, the rapid response of the innate immune system is essential to defending against invading pathogens. This is explained by the fact that instead of recognizing specific pathogens, it is triggered by a broad variety of molecules found in all kind of microbes, so called pathogen-associated molecular patterns (PAMPs). The receptors responsible for PAMP recognition are germline-encoded and called pattern recognition receptors (PRR). This provides a non-specific defense mechanism recognizing core pathogen structures and triggering an almost immediate immune response. In many cases this is enough to fight the invader, however, the adaptive immune system is summoned if the system is overwhelmed (Murphy et al., 2012).

The adaptive immune system is the second line of defense and provides a specific pathogen recognition mechanism. In contrast to the innate immunity, the adaptive immune system evolves over an organism's lifetime and cannot be inherited. This makes the adaptive immune system an immensely powerful defense mechanism, providing the organism with immunological memory and protecting it against reinfection with the same pathogen. Depending on the severity and type of infection, this protective immunity can last a lifetime. The adaptive immune system possesses effector cells called B- and T-cells. They recognize diverse pathogenic molecular structures known as antigens. Their antigen binding proteins are extremely diverse and are generated in individual cells by recombination of specific gene segments. B-cell receptors are located on the cell surface and can directly bind to their corresponding antigen. Upon antigen recognition, B-cells start to proliferate and differentiate into plasma cells. These are producing soluble antigen binding proteins called immunoglobulins (or antibodies), which are secreted to the extracellular space where they can bind the corresponding antigen, neutralizing it or promoting an immune response. T-cell receptors on the other hand are membrane-bound proteins, located on the surface of T-cells

and do not bind to their corresponding antigen directly. Instead, they recognize antigens presented through the major histocompatibility complex (MHC) on the surface of other cells. Dendritic cells are an innate immune system cell-type that play a crucial role as professional antigen presenting cells (APCs). Once activated they travel to lymphoid tissues to interact with naïve B- and T-cells (Murphy et al., 2012). The immune system is critical for fighting invading pathogens and maintaining tissue homeostasis, however, it also needs to be tightly regulated to ensure proper function and prevent auto-activation. Dysfunction can cause severe tissue damage via chronic inflammation or the production of autoantibodies, attacking healthy cells. This leads to a huge variety of diseases broadly be categorized into autoinflammatory diseases (AIDs), caused by the innate immune system, and systemic autoimmune diseases (ADs), involving the adaptive immune system (Doria et al., 2012).

1.2 The innate immune system

The innate immune system provides fast acting, non-specific defense mechanisms to immediately react upon encountering pathogens, instantly preventing their growth and spread inside the body. It provides direct anti-pathogenic effector mechanisms – analogous to the adaptive immune system – divided into humoral (body fluid related) and cell mediated defense mechanisms. Furthermore, it plays an essential role in the activation of adaptive immunity as well as the maintenance of tissue integrity and repair. Physical barriers like the skin or the low pH environment in the stomach can also be considered to be part of the innate immune system, as they shield the body against pathogens or have anti-microbial properties (Murphy et al., 2012). Besides, the skin secretes anti-microbial proteins such as defensins to complement the physical barrier properties (Brogden, 2005).

The humoral component of the innate immune system is activated upon pathogens overcoming the physical barrier of the body leading to the production of proteins like collectins, ficolins and pentraxins, resulting in opsonophagocytosis or the activation of the complement system (Bottazzi et al., 2010; Ma and Garred, 2018). The complement system is a central defense mechanism of the humoral innate immune system, and was discovered in 1896 by Bordet as a heat-labile component of the human serum (Dunkelberger and Song, 2010). It consists of more than 30 soluble proteins, which can either be found in blood or other body fluids (Murphy et al., 2012; Walport, 2001). Upon encountering a pathogen, complement proteins accumulate on its surface leading to opsonization and activation of the complement system. This initiates the recruitment of phagocytic cells, which on the one hand promote inflammation and on the other hand engulf the opsonized pathogen to destroy it. Another effector mechanism of the complement system is the formation of a protein complex called membrane-attack complex (MAC) disrupting the cell membrane of the pathogen causing lysis

(Murphy et al., 2012). The second part of the innate immune system is the cellular response, which is mainly but not exclusively mediated by highly specialized cell types. Upon pathogen recognition these cells secrete a cocktail of different cytokines and chemokines, recruiting immune cells from surrounding tissue and bloodstream, which is often accompanied by tissue swelling (inflammation). These recruited cell types include monocytes, macrophages, granulocytes (neutrophils, basophils, eosinophils and mast cells), and innate lymphoid cells, such as natural killer (NK) cells (Murphy et al., 2012).

Phagocytosis (or other forms of endocytosis), the engulfment and destruction of invading microorganisms, is a critical mechanism of the innate immune system. It plays an important role in the clearance of apoptotic bodies, being critically required for tissue homeostasis and remodeling. Phagocytosis is mainly performed by professional phagocytes like macrophages, neutrophils or dendritic cells. Pathogen destruction occurs inside the endolysosomal compartment and is facilitated by its uniquely hostile environment including low pH, the presence of several hydrolases and antimicrobial proteins like lysozyme. Furthermore, production of reactive oxygen species (ROS) by nicotinamide adenine dinucleotide phosphate (NADPH) and nitric oxide (NO) by inducible nitric oxide synthase (iNOS) are microbicidal mechanisms (Flannagan et al., 2012). Phagocytes are critical for innate immune defense but are also involved in activating the adaptive immune system in a two-step approach. Initially, contact with the pathogen promotes the release of pro-inflammatory cytokines, recruiting lymphoid cells. Subsequently, when the pathogen has been phagocytosed and digested, its constituent fragments are presented as antigens to the cells of the adaptive immune system, activating them (Flannagan et al., 2012). Apart from directly killing the pathogen, another defense mechanism is killing the infected cell by inducing cell death. This can either be initiated in a cell-independent fashion or be dependent on cell-to-cell interaction between the infected and the killer cell. The cell-independent ‘suicide’ results in either an immunologically silent death (apoptosis) or the release of cellular content (pyroptosis and necroptosis) leading to the activation of surrounding immune cells and an amplified immune response (Morizot and Saleh, 2012). Contact induced cell death on the other hand is mediated by NK cells, which unlike other cells of the innate immune system are not derived from myeloid but from lymphoid progenitors. They comprise the third largest population of lymphocytes (after B and T cells) and do not need pre-stimulation to perform their effector function. NK cells are large granular cells with various functions, like killing infected or neoplastic cells. Under steady state conditions NK cells are in resting state, however, they start to infiltrate infected or malignant tissues upon cytokine induced activation (Mandal and Viswanathan, 2015). The innate immune system includes a diverse array of intrinsic restriction factors important for defending against viral infections. SAM domain and HD domain-containing protein 1 (SAMHD1) for example has been shown to reduce the dNTP pool by hydrolysis, thus blocking replication of

human immunodeficiency virus (HIV) (Yan and Chen, 2012). Another example is the activation of 2'-5'-oligoadenylate synthetase (OAS) by viral RNA leading to RNase L activation, which in turn is blocking viral replication by degrading ssRNA (Chakrabarti et al., 2011). All in all, the innate immune system has evolved diverse mechanisms to immediately defend against invading pathogens on a cellular level, which can either directly clear the infection or buy time for the adaptive immune system to be activated.

1.3 Pattern recognition receptors (PRRs)

In order to be able to respond properly to threats and trigger an appropriate immune response, cells have developed diverse detection mechanisms. At first it was thought that pathogen recognition is a non-specific process, until a group of proteins called toll-like receptors (TLR) was found in the 1990s clearly showing specific recognition of distinct molecules. It soon became clear that TLRs are not the only group of germline-encoded pattern recognition receptors (PRR), which are able to detect various evolutionary conserved pathogen-associated molecular patterns (PAMPs) (Kawai and Akira, 2010). Yet it was not known how strong immune responses could be triggered under sterile conditions, for example after tissue transplantation or in the course of autoimmune diseases. It turned out, the immune system is not only capable of recognizing pathogen derived molecules, but is also triggered by cytoplasmic content released from damaged cells, called damage-associated molecular patterns (DAMP) (Venereau et al., 2015). The first molecules to be identified as such were high mobility group box 1 (HMGB1) and uric acid crystals (Scaffidi et al., 2002; Shi et al., 2003), however, over the years many other molecules like histones, genomic DNA (Gould et al., 2015) and ATP (Idzko et al., 2014) were recognized as DAMPs. This clearly shows that our body is not necessarily distinguishing between self and non-self molecules, but is rather sensitive to the localization of certain patterns allowing the discrimination between damaged and healthy tissue (Amarante-Mendes et al., 2018). Generally, there are four main classes of PRR including toll-like receptors (TLRs), NOD-like receptors (nucleotide-binding and oligomerization domain like receptors, NLRs), RIG-I like receptors (retinoic acid-inducible gene-I-like receptors, RLRs) and C-type lectin receptors (CLRs) (Walsh et al., 2013). Activation of these proteins induces a pro-inflammatory immune response, resulting in the release of cytokines or the killing of infected cells (Amarante-Mendes et al., 2018).

The first class of PRRs is the TLR family comprised of TLR1-10 in humans and TLR1-9 as well as TLR11-13 in mice. TLRs are type 1 transmembrane proteins and either located in the outer cellular membrane or inside the endolysosome. They can recognize quite diverse molecular patterns ranging from nucleic acids to bacterial cell wall components (Fitzgerald and Kagan, 2020). TLRs will be discussed in more detail in section 1.4-1.6. The next class of PRRs are CLRs,

a group of transmembrane and soluble proteins which have a C-type lectin domain and recognize a variety of glycans (Chiffoleau, 2018; Walsh et al., 2013). Another key feature of classical CLRs is their Ca^{2+} dependency for ligand recognition, though some CLRs are independent of calcium and are therefore referred to as C-type lectin-like receptors (CTLRs). In addition to their ability to detect carbohydrates, CTLRS are able to recognize a more diverse ligand spectrum including lipids and proteins (Dambuza and Brown, 2015). The third group of PRR are RLRs, including the proteins RIG-I (retinoic acid-inducible gene I), MDA5 (melanoma differentiation-associated gene 5), and LGP2 (laboratory of genetics and physiology 2) (Takeuchi and Akira, 2009; Yoneyama and Fujita, 2008). All RLRs are located in the cytosol and recognize RNA, which leads to the release of type I interferons (IFN) as well as pro-inflammatory cytokines (Yoneyama and Fujita, 2008). RIG-I, for example, was discovered to specifically detect viral RNA molecules bearing a 5'-triphosphate end (Hornung et al., 2006; Pichlmair et al., 2006). The last group of PRRs are NLRs, which are known to activate the innate immune system upon cellular injury or stress (Platnich and Muruve, 2019). All NLRs share a similar basic structure consisting of a variable number of C-terminal leucine-rich repeat domains (LRR) and a nucleotide-binding and oligomerization (NACHT) domain (Lamkanfi and Dixit, 2014). They can be divided into several subgroups with the most important ones being NLRCs and NLRPs. They are further distinguished by functional domains like the caspase recruitment domain (CARD) in the case of NLRC receptors, or the pyrin domain (PYD), which can be found in NLRP proteins (Platnich and Muruve, 2019). Another important feature of some NLRs (NLRP3, NLRP1, NLRC4) is their ability to form large multiprotein complexes called inflammasomes. They are formed inside the cytosol and result in the activation of the proinflammatory caspases 1 and 11 (caspase 4/5 in humans) as well as the release of mature IL-1β and IL-18 (Kayagaki et al., 2011; Martinon et al., 2002; Shi et al., 2014). The activated caspases can subsequently cleave a number of distinct substrates including GSDMD, which leads to pore formation in the outer cellular membrane and a lytic cell death, called pyroptosis (Gaidt and Hornung, 2016; Kayagaki et al., 2015; Sborgi et al., 2016; Shi et al., 2015). Apart from the four big PRR families, two additional DNA sensing pathways can be found inside the cytosol: the cGAS (cyclic GMP AMP synthase) -STING (stimulator of interferon genes) axis; the AIM2 inflammasome. Like most other PRRs, activation of the cGAS-STING pathway leads to the production of pro-inflammatory cytokines and type I interferons (Ishikawa and Barber, 2008; Wu et al., 2013). Upon recognition of cytosolic DNA by cGAS, the protein starts to produce the second messenger cyclic-GMP-AMP (cGAMP). cGAMP can then travel to the endoplasmic reticulum (ER) bound protein STING and activate it. This causes STING to travel to the Golgi apparatus where it recruits TBK1 as well as the IKKs initiating downstream signaling (Dobbs et al., 2015; Hornung et al., 2014; Motwani et al., 2019; Mukai et al., 2016).

Additionally, cytosolic DNA can be recognized by the Aim2 inflammasome, leading to pyroptotic cell death and the release of IL-1β (Hornung et al., 2009; Unterholzner et al., 2010).

Upon PRRs recognizing a ligand, different downstream signaling pathways are engaged. One of them is leading to the activation of the transcription factor NF-κB, which can travel to the nucleus and regulate a huge number of genes modulating the inflammatory immune response (Liu et al., 2017). A major protein class regulated by NF-kB are cytokines, a group of small, low molecular weight proteins critically involved in the regulation of acute and chronic inflammations. Key pro-inflammatory cytokines are interleukin-1 (IL-1), IL-6 or tumor necrosis factor (TNF), all signaling via type I cytokine receptors. However, this is not true for all cytokines, as IL-8 is for example signaling via G protein-coupled receptors (GPCRs) (Turner et al., 2014). As already mentioned, one important cytokine which is also often used as read-out for TLR activation is IL-6. It is a soluble glycosylated protein with a size of 21-26 kDa and is modulating different cellular processes like the immune response, tissue homeostasis and hematopoiesis (Tanaka et al., 2014). The cytokine is mainly produced by monocytes and macrophages upon PAMP or DAMP detection, but also downstream of IL-1 or TNF stimulation (Tanaka et al., 2014). Nevertheless, it can also be produced by other cell types like keratinocytes or fibroblasts (Turner et al., 2014). Once released into the extracellular space, IL-6 can bind to the receptor IL-6R, which in turn induces dimerization of the signal transducing chain gp130 (Murakami et al., 1993). Downstream of gp130 activation, the JAK-STAT3 (Janus kinase - signal transducers and activators of transcription) as well as the JAK-SHP-2-MAPK (mitogen-activated protein kinase) pathways are activated (Tanaka et al., 2014). Another very important class of cytokines expressed upon PRR activation are type I interferons which are playing an important role especially during viral infections. Secreted type I interferons signal through a heterodimeric receptor composed of the proteins IFNARI and IFNARII (interferon-α/β receptor). Upon activation, the receptor is endocytosed and recruits JAK1 and tyrosine kinase 2 (TYK2) leading to the phosphorylation of different STAT proteins (mainly STAT1 and STAT2). The STAT1/2 heterodimer can then form a complex with IRF9 modulating the transcription of IFN-stimulated genes (ISGs) (Chmiest et al., 2016; Ivashkiv and Donlin, 2014; Lee and Ashkar, 2018). Interferons can act in a paracrine, autocrine or systemic fashion and can for example lead to the transcription of OAS genes as well as the upregulation of MHC II proteins and the maturation of dendritic cells (Lee and Ashkar, 2018).

Besides cytokine release, different forms of induced cell death are powerful tools to control infections and modulate the innate as well as the adaptive immune response (Amarante-Mendes et al., 2018). Generally, regulated cell death can be divided into apoptosis and forms of induced necrosis (Tait et al., 2014). Apoptosis was already described in 1972 and is an evolutionary highly conserved form of cell death, which is very well studied (Kerr et al., 1972;

Tait et al., 2014). Besides its important role during immune responses, it is critically involved in the control of cell populations during development and aging (Elmore, 2007). Classical features of apoptosis are chromatin condensation, nuclear fragmentation and the formation of apoptotic bodies, which are normally removed by phagocytic cells (Elmore, 2007; Szondy et al., 2017). During this process the cellular contents are kept entirely inside the apoptotic bodies, thus it is a non-inflammatory and immunogenic silent form of cell death (Szondy et al., 2017). Apoptosis is categorized based on whether the initiating signal is derived from intracellular or extracellular sources, intrinsic or extrinsic apoptosis respectively. Downstream, the initiator caspases (caspase 8 and 9) are activated which in turn can cleave the executioner caspases (caspase 3, 6 and 7), leading to cell death (D'Arcy, 2019). In contrast to apoptosis, all forms of regulated necrosis lead to the release of cellular contents into the extracellular space, which can result in the release of DAMPs and hence activate the innate immune system. A well-studied form of regulated necrosis is called pyroptosis and is mediated by inflammatory caspases (Caspase 1, 11 in mice and 1, 4, 5 in humans) (Man et al., 2017). Pyroptosis can mainly be observed in professional phagocytic cells like macrophages, dendritic cells or neutrophils and is initiated downstream of inflammasome activation (Vande Walle and Lamkanfi, 2016). Another important form is necroptosis, which is caspase independent and instead executed by the activation of RIPK3 and MLKL. It can be induced downstream of TLRs, death receptors and interferon (Dhuriya and Sharma, 2018).

1.4 Toll-like receptors (TLRs)

The Toll protein from Drosophila was already studied in the 90's and was found to be involved in anti-microbial responses (Lemaitre et al., 1996). Shortly after, the human homolog, today known as TLR4, was discovered. It was shown to be a transmembrane protein consisting of an extracellular leucine-rich repeat (LRR) domain and a cytoplasmic domain similar to the one of IL-1 receptor, today known as TIR (Toll/Interleukin-1 receptor) domain (Medzhitov et al., 1997). In the following years it was published by three different groups, that TLR4 is recognizing lipopolysaccharide (LPS), which is part of the outer membrane of gram-negative bacteria (Poltorak et al., 1998; Qureshi et al., 1999; Takeuchi et al., 1999).

Like it was shown for TLR4, all TLRs are type I integral membrane proteins with a N-terminal leucine-rich repeat (LRR) domain, one single transmembrane domain and a TIR domain for downstream signaling (Bell et al., 2003; Botos et al., 2011). Ligand binding is mediated by the LRR domain, which is built up by leucine-rich repeats, a characteristic repetitive pattern rich in leucine and a length of 20-30 residues. When assembled, the domain forms a curved horseshoe like structure, mediating protein-protein interactions. Leucine-rich repeats are a widespread structural motif that can be found in all forms of life ranging from viruses to

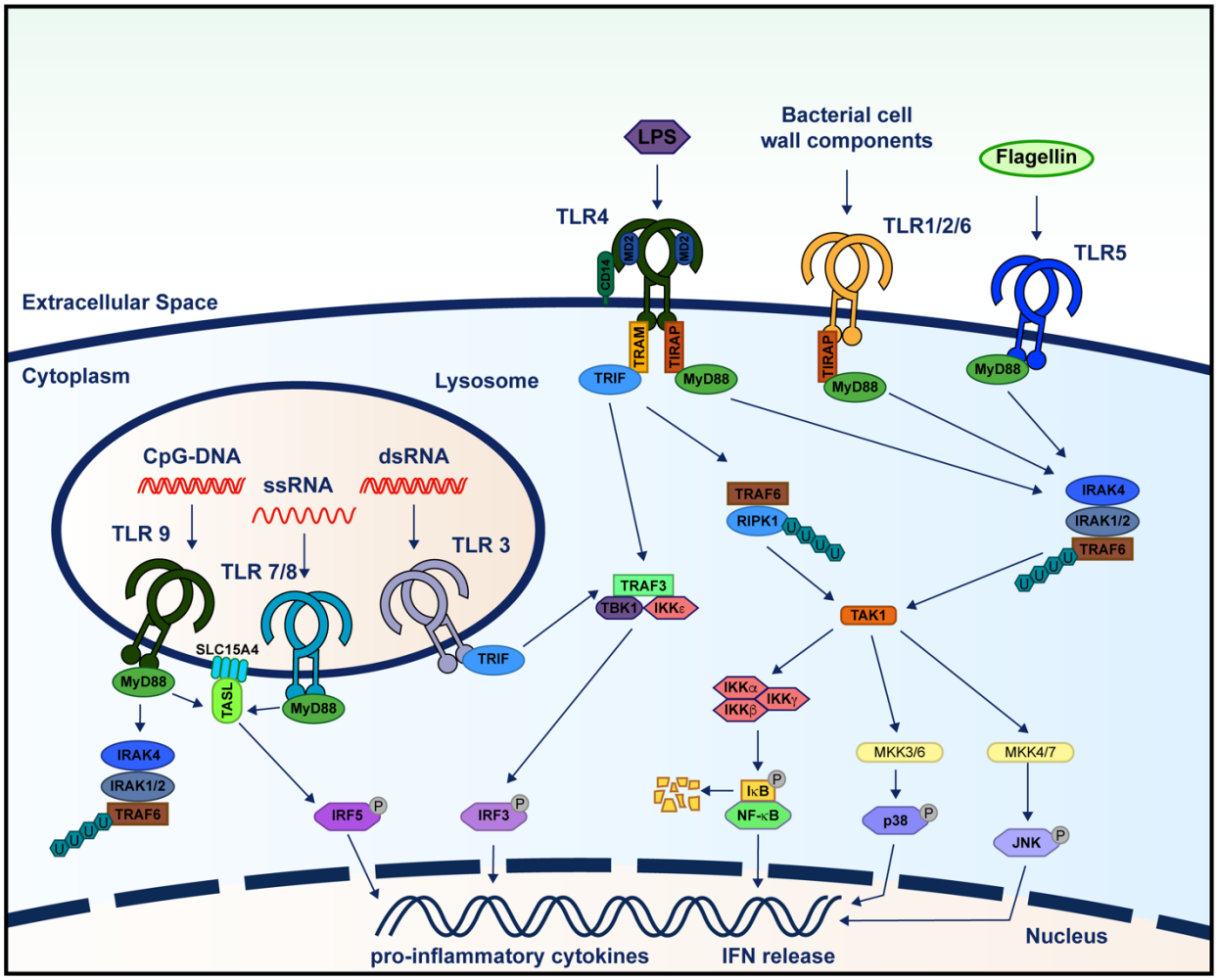

Figure 1.1 Toll-like receptor signaling pathways

Toll-like receptors (TLRs) belong to the class of pattern recognition receptors (PRR) and play an important role in innate immune defense. TLRs are located either on the cell surface or inside the endolysosomal compartment. They are able to recognize a broad spectrum of different molecules, including DNA, RNA and bacterial cell wall components like LPS. The receptors consist of a leucine-rich repeat (LRR) domain, one transmembrane domain and a TIR domain for downstream signaling. Upon activation all TLRs form a dimer and signal via the adapter proteins MyD88 or TRIF, resulting in the activation of diverse signaling pathways. This leads to cell survival, the NF-κB dependent release of pro-inflammatory cytokines and the release of type I interferons (IFN).

eukaryotes (Bella et al., 2008). TLRs are used by a huge variety of species including humans and mice, which encode 10 and 12 TLRs respectively. Other species like the sea urchin even encodes for 222 TLR genes (Imler and Hoffmann, 2002; Satake and Sekiguchi, 2012). TLRs are synthesized inside the endoplasmic reticulum (ER) before being transported to either the plasma membrane or the endolysosomal compartment. Therefore, it is not surprising that the lack of ER localized chaperones like gp96, PRAT4A and Unc93B1 leads to compromised TLRs function. Intriguingly, this is not true for TLR3, the reason for which remains elusive (Fitzgerald and Kagan, 2020). Unc93B1, for example, is involved in intracellular transport of TLRs, which renders it essential for proper receptor function (Kim et al., 2008). Furthermore, binding of

Unc93B1 to the receptors is critically required to maintain stability of the proteins after synthesis (Pelka et al., 2018). After reaching the acidic milieu of the endolysosome, TLR3, TLR7, TLR8 and TLR9 are cleaved within their leucine-rich-repeat domain (Z-loop), which is mediated by various cathepsins (Ewald et al., 2011; Fukui et al., 2018). Uncleaved receptors are unable to dimerize, hence the necessity for LRR domain cleavage to occur for TLR activation is essential. Nevertheless, the two fragments always stay associated with one another (Ohto et al., 2018; Tanji et al., 2016).

TLRs in humans have evolved to recognize a broad variety of pathogen-associated molecular pattern (PAMPs) and can be divided into two groups. One group including TLR1, TLR2, TLR4, TLR5 and TLR6, is located at the cell surface and is responsible for recognition of extracellular molecules. The second group is localized inside the endolysosomal compartment composed of TLR3, TLR7, TLR8 and TLR9 (Satake and Sekiguchi, 2012). One of the TLRs found at the cell surface is TLR2, forming a heterodimer with either TLR1 or TLR6 (Jin et al., 2007; Kang et al., 2009), recognizing lipid containing PAMPs from the extracellular space. Its ligands include lipoteichoic acid as well as di- and tri-acetylated cysteine-containing lipopeptides (Takeda et al., 2003). As previously mentioned, TLR4 recognizes the bacterial cell wall component LPS. For proper signaling it requires the co-receptor MD-2, which is bound to the LRR region of TLR4 via several hydrogen bonds (Kim et al., 2007). Furthermore, CD14 is needed to deliver LPS to the receptor, however, this can be overcome by high concentrations of LPS. However, CD14 is critically required for TLR4 mediated TRIF signaling, which cannot be compensated by high LPS concentrations (Zanoni et al., 2011). Interestingly, the potency of endotoxins like LPS is significantly dependent on its acetylation status (Teghanemt et al., 2005). The last TLR found on the cell surface is TLR5 and in contrast to other TLRs it recognizes a critical protein component of bacterial flagella, flagellin (Hayashi et al., 2001). It is mostly expressed in intestinal lamina propria cells controlling the microbiota of the gut (Vijay-Kumar et al., 2010). An intracellular, endolysosomally located TLR receptor is TLR3, recognizing dsRNA produced by most viruses at some point during their life cycle. Under steady-state conditions TLR3 exists in a monomeric state, but dimerizes upon recognition of RNA with a length of at least 40-50 bp. In line with its endolysosomal localization the receptor can only be activated at low pH (below pH 6.5) (Leonard et al., 2008). The next receptors found in this acidic milieu of the endolysosome are TLR7 and TLR8. Both proteins recognize single stranded RNA (ssRNA) and have two distinct binding pockets, for either a single nucleotide or a short RNA fragment (Miyake et al., 2017). The two TLRs differ in that TLR7 recognizes guanosine in its first pocket and uridine containing ssRNA in its second (Zhang et al., 2016), while TLR8 binds to uridine in its first and purine terminated fragments in its second pocket (Tanji et al., 2015). Interestingly, for both TLR7 and TLR8, binding of ssRNA to the second pocket seems to enhance the binding of guanosine or uridine to the first pocket, respectively (Shibata et al., 2016; Tanji et al., 2015).

The last member of the endolysosomal TLR family is TLR9, which recognizes CpG sequences in single-stranded DNA (ssDNA). It was shown that DNase II acts upstream of TLR9, generating appropriate ligands by cleaving CpG-A into 11-12mer fragments needed for receptor activation. Intriguingly, even though the absence of DNase II leads to DNA accumulation inside the endolysosome, *DNASE2*$^{-/-}$ mice show activation of cGAS-STING rather than TLR9 (Chan et al., 2015; Okabe et al., 2005). This strongly indicates that in the absence of DNase II, accumulated DNA leaks from the endolysosome into the cytoplasm, where it can activate the cGAS-STING pathway. To-date, TLR10 is the only member of the TLR family that is poorly studied and whose corresponding ligand remains elusive (Fitzgerald and Kagan, 2020).

Different signaling pathways can be engaged downstream of TLRs, all requiring close proximity of the TIR domains via receptor dimerization or conformational change of the preformed dimer (Latz et al., 2007; Tanji et al., 2013). Activation of these downstream pathways can lead to significant changes in cellular processes like gene transcription, translation, splicing, autophagy and glycolysis. Upon TIR domain approximation, a large protein complex, the supramolecular organizing center (SMOC), is formed inside the cytosol. Generally, TLRs can initiate the formation of either the myddosome or triffosome, which assemble within minutes after receptor activation (Fitzgerald and Kagan, 2020). In case of the myddosome, TIR domain dimerization is in most cases recognized by a membrane protein called TIRAP (or MAL) leading to MyD88 recruitment. However, not all MyD88 dependent responses are TIRAP dependent (Bonham et al., 2014; Horng et al., 2002). Apart from MyD88, the myddosome consists of two different members of the IRAK family of serine-threonine kinases, IRAK2 and IRAK4. The crystal structure revealed that the protein complex is a single stranded left-handed helix of death domains (DD), consisting of six MyD88, four IRAK4 and four IRAK2 proteins (Lin et al., 2010). The C-terminal TIR domain of MyD88 is thereby interacting with the TIR domain of TLRs or TIRAP, whereas the N-terminal death domain mediates the binding of IRAKs (Fitzgerald and Kagan, 2020). The close proximity of IRAK proteins greatly enhances their autophosphorylation, leading to the subsequent recruitment of the E3 ubiquitin ligase TRAF6 (Cao et al., 1996; Ferrao et al., 2014; Lomaga et al., 1999). Downstream of TRAF6 recruitment, the kinase TAK1 gets activated, subsequentially leading to IKK mediated NF-κB activation as well as the initiation of MAPK signaling (Emmerich et al., 2013; Wang et al., 2001). Furthermore, TRAF6 can recruit TBK1, inducing rapid glycolysis mediated by the AKT kinase (Everts et al., 2014; Tan and Kagan, 2019). The second SMOC downstream of TLR signaling is the triffosome, which can only be activated after TLR3 or TLR4 activation (Akira and Hoshino, 2003; Yamamoto et al., 2003). However, TLR3 signaling is exclusively dependent on TRIF, whereas TLR4 can signal via both adapter proteins TRIF and MyD88 (Yamamoto et al., 2003). Analogous to MyD88-TIRAP, TRAM was reported to be the adapter for TRIF in TLR4 signaling. TRAM is a membrane bound protein anchored to the lipid bilayer by myristoylation (Rowe et

al., 2006). In contrast to TLR4, TLR3 can directly bind TRIF without an additional adapter protein (Kawasaki and Kawai, 2014). The first branch of TRIF signaling is activation of the NF-κB pathway by recruiting TRAF6 and receptor interacting protein kinase 1 (RIPK-1) leading to signal transduction via TAK1 (Anwar et al., 2019; Kawai and Akira, 2010). In contrast to MyD88, TRIF together with MAVS and STING contains a conserved amino acid sequence (pLxIS), which can be phosphorylated by the kinase TBK1 and lead to the activation of IFN signaling. Thus, TRIF recruits TRAF3, which in turn recruits TBK1 and IKKε. Upon TRIF phosphorylation IRF3 gets recruited through its positively charged binding domain, allowing its phosphorylation by TBK1. This results in dimerization of IRF3, which facilitates it to travel into the nucleus inducing type I IFN expression. TBK1 is, therefore, crucially required but not sufficient for IRF3 phosphorylation (Liu et al., 2015; Ullah et al., 2016). As interferons are potent regulators of innate immunity, they must be tightly regulated to prevent dysfunction like autoimmunity. To this end, the pLxIS motif is a critical control mechanism for IFN signaling, however, activation of the lysosomal nucleic acid sensors TLR7, TLR8 and TLR9 leads to type I interferon production, even though they are not signaling via the adaptor protein TRIF (Fitzgerald and Kagan, 2020; Schmacke and Hornung, 2020). Instead, they are published to signal via MyD88, lacking the pLxIS motif, and IRF5, which is structurally related to IRF3 and IRF7 (Ban et al., 2018; Schoenemeyer et al., 2005). Recently, the new protein TLR adaptor interacting with SLC15A4 on the lysosome (TASL), which is encoded by the gene *CXorf21*, was found to be involved in interferon signaling downstream of TLR7-9 (Heinz et al., 2020). Interestingly, the gene was already associated with the human disease systemic lupus erythematosus (SLE) (Bentham et al., 2015; Odhams et al., 2019) and was now found to interact with the endolysosomal transporter SLC15A4 (Heinz et al., 2020). SLC15A4 is published to transport oligopeptides and the amino acid histidine across the endolysosomal membrane and was already shown to be involved in TLR signaling (Blasius et al., 2010; Sisirak et al., 2014) as well as to be genetically associated with SLE (Han et al., 2009; Odhams et al., 2019). The recently published article proposes that SLC15A4 as well as TASL are both critically required for interferon signaling downstream of TLR7-9, whereas ligand interaction, NF-κB activation and MAPK pathways are unaffected by their absence. Interestingly, it seems as if this newly discovered pathway is independent of SLC15A4 transporter function, suggesting that the protein only serves as scaffold. TASL has a pLxIS motif analogous to STING, MAVS and TRIF, rendering it the fourth protein involved in type I interferon induction upon nucleic acid sensing (Heinz et al., 2020; Liu et al., 2015). Therefore, the following mechanism was suggested: downstream of TLR7-9 activation, TASL binds to SLC14A4, gets phosphorylated and recruits IRF5, which in turn also gets phosphorylated leading to dimerization. The dimer can then enter the nucleus to induce type I IFN transcription. The kinase involved in phosphorylation of TASL and IRF5 was suggested to be IKKβ (Heinz et al., 2020).

1.5 ssRNA recognition by TLR7 and TLR8

As previously mentioned, TLR7 and TLR8 are both localized inside the endolysosome and recognize ssRNA. They both consist of a cytoplasmic TIR domain, one transmembrane domain and an endolysosomal LRR domain (Botos et al., 2011). As mice are the predominant model organisms used to investigate TLRs, TLR8's inability to be activated by natural ssRNA in mice has proven to be an impendence to the thorough investigation of TLR8 compared to TLR7. To this end, it was initially believed that murine TLR8 is nonfunctional, however, was shown to be activated by a combination of imidazoquinoline compounds and poly-T oligodeoxynucleotides (Gorden et al., 2006).

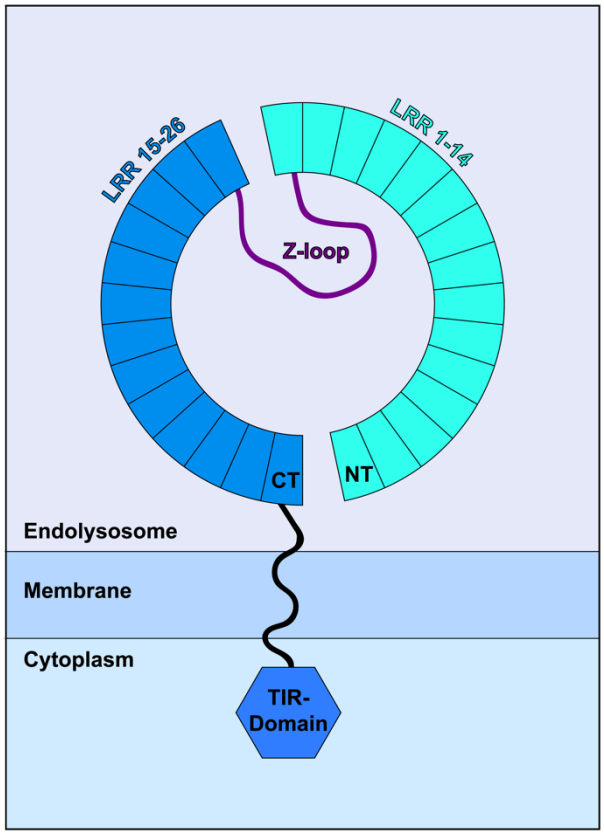

Figure 1.2 Domain organization of TLR7 and TLR8

The receptors TLR7 and TLR8 are build up by a leucine-rich repeat (LRR) domain, one transmembrane domain and a TIR domain for downstream signaling. The LRR domain consists of 26 repeats and is either located in the extracellular space or the lysosomal lumen. Between LRR 14 and 15 a flexible structure, called Z-loop, can be found, which has to be cleaved to allow receptor dimerization. The LRR domain is essential for ligand binding and forms the first and second binding pocket of TLR7 and TLR8.

Nevertheless, some years ago the crystal structure of human TLR8 was solved providing an improved understanding of its mode of action (Tanji et al., 2013; Tanji et al., 2015). The crystal structure revealed that the N-terminal region of the receptor consists of 26 leucine-rich repeat domains (Figure 1.2). Between LRR14 and LRR15 an approximately 40 amino acids long

insertion region was found, named the Z-loop. This Z-loop gets cleaved inside the endolysosomal compartment, however, the two TLR8 fragments stay associated with one another as the β-strands of LRR14 and LRR15 are forming a β-sheet structure (Tanji et al., 2013). Notably, the uncleaved Z-loop serves an autoinhibitory function – preventing receptor dimerization. Therefore, the cleavage of the Z-loop is necessary for TLR8 activation (Tanji et al., 2016). Upon ligand binding to the preformed TLR8 dimer, a conformational change is induced which brings the TIR domains in close proximity resulting in downstream signaling. This stands in contrast to TLR7, which exists in a monomeric state and only dimerizes after ligand binding (Tanji et al., 2013).

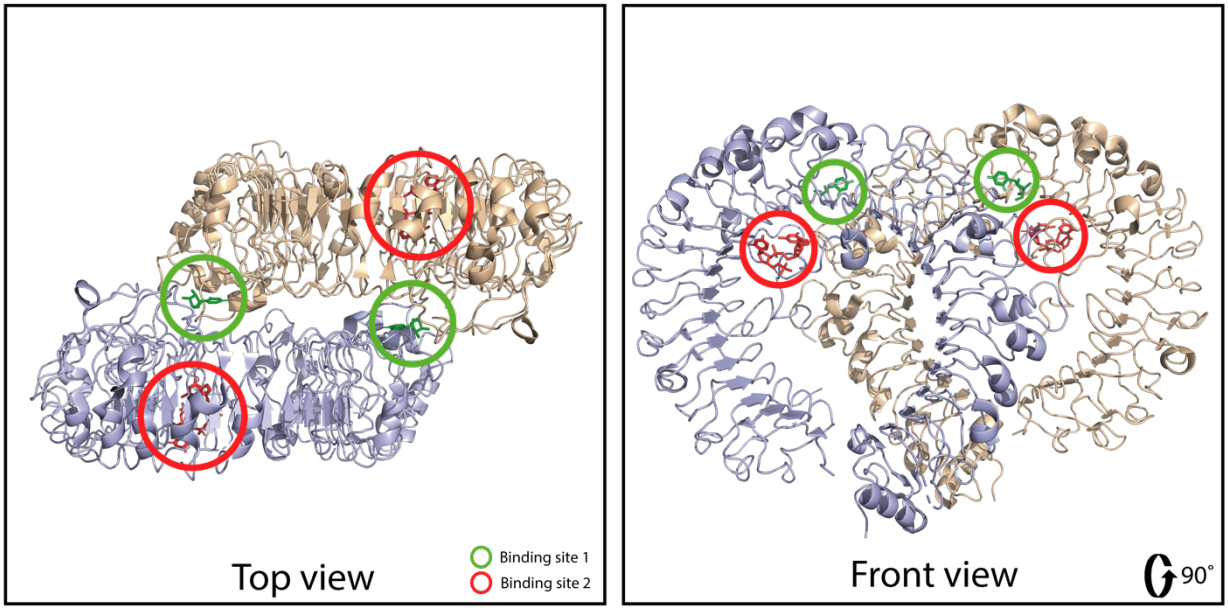

Figure 1.3 Crystal structure of human TLR8

The crystal structure of the human TLR8 homodimer is shown. The first binding pocket of TLR8 is bound to uridine (green), whereas the second one is occupied by a UG dinucleotide (red). Of note, as it is a dimer each binding site is present twice (PDB, 4R07).

TLR8 has two distinct ligand binding pockets located inside the LRR domain. The first pocket can be found within the dimerization interface at LRR11-14 in TLR8; and LRR 16*-18* in TLR8*. It preferentially binds uridine or small chemical compounds like R848 (Tanji et al., 2013; Tanji et al., 2015). The second pocket is located in the concave surface of TLR8 and binds to small ssRNA fragments like UG or UUG (Tanji et al., 2015). Interestingly, the ON $(UUA)_6UU$ is also capable of activating TLR8, indicating that guanosine can also be replaced by adenosine (Forsbach et al., 2008). As TLR8 is a homodimer, each binding pocket is present twice. Importantly, the occupation of the first binding pocket by small chemical compounds like R848 is sufficient for receptor activation. However, the affinity of uridine is not high enough to directly bind the first pocket under physiological conditions. Hence, the second pocket must be initially occupied to increase the first pocket's binding affinity for uridine ultimately leading

to receptor activation. The binding affinity of compounds like R848 on the other hand is high enough to overcome the need of a second pocket ligand allowing the direct activation of the receptor (Tanji et al., 2015). Intriguingly, an un-cleavable Z-loop that keeps TLR8 at a monomeric state, still results in binding of short ssRNA fragments at the second but not at the first binding site. This can easily be explained by the fact that the first pocket is located within the dimerization interface and can only be occupied upon dimerization (Tanji et al., 2016). A similar effect was observed for TLR9, which can only dimerize upon Z-loop cleavage but can bind to agonistic DNA in an uncleaved state (Ohto et al., 2015).

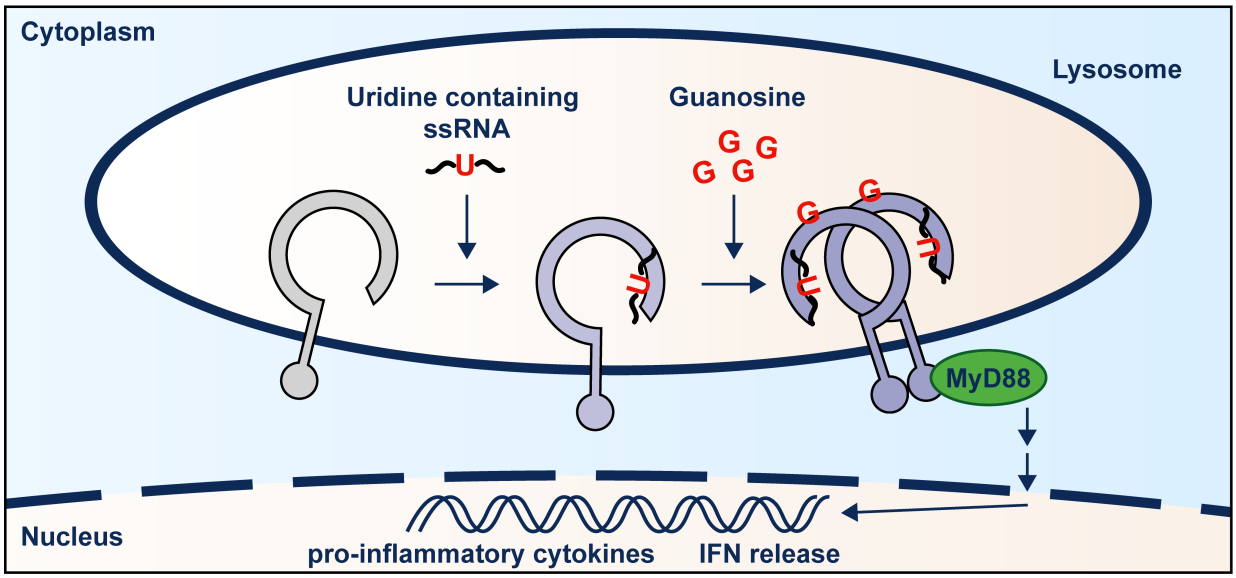

Figure 1.4 Activation mechanism of human TLR7

Under steady-state conditions human TLR7 exists in a monomeric state. Generally, ligand binding to the first pocket of TLR7 was shown to be necessary and sufficient for receptor activation. However, this is only true for chemical compounds like R848, which have a very high affinity towards the first binding site of TLR7. Under physiological conditions, ligand binding to the second pocket is essential to increase the affinity of guanosine towards the fist pocket. The binding of guanosine leads to receptor dimerization and downstream signaling (release of pro-inflammatory cytokines and IFN).

The second endolysosomal protein recognizing ssRNA is TLR7. Unlike TLR8, which exists as preformed dimer, TLR7 only dimerizes upon ligand binding (Petes et al., 2017). The receptor has two distinct binding pockets, one for single nucleotides and one for short ssRNA fragments (Zhang et al., 2016). However, in contrast to TLR8 the first pocket is occupied by guanosine, not uridine (Shibata et al., 2016; Tanji et al., 2015). Nevertheless, the first pocket of TLR7 and TLR8 exhibits homology in amino acid sequence and structure (72 % similarity). This explains why both TLR7 and TLR8 can be activated by the same imidazoquinoline compounds (Zhang et al., 2016). Analogous to TLR8, guanosine is not capable of efficiently activating TLR7 on its own (Lee et al., 2003; Shibata et al., 2016), but relies on the binding of ssRNA to the second pocket (Zhang et al., 2016). This initial binding of ssRNA dramatically increases the affinity of

guanosine towards the first pocket of TLR7 enabling receptor activation. Interestingly, binding of chemical compounds like R848 to the first pocket is sufficient to initiate TLR7 dimerization. In contrast to the first binding site, which is located at the same position for TLR7 and TLR8, the position and structure of the second pocket is distinct. While in TLR8 it is located completely outside the dimerization interface, TLR7's second pocket is close to the dimerization site (Zhang et al., 2016). Due to the TLR7 first binding site's capacity to be occupied by deoxyguanosine (dG) in addition to guanosine, TLR7 is capable of recognizing DNA degradation, provided ssRNA has already occupied the second pocket (Shibata et al., 2016).

RNA modifications like methylation or hydroxylation are very common in eukaryotes. RNA molecules especially heavily modified are tRNA and rRNA (de Crecy-Lagard et al., 2019; Taoka et al., 2018), suggesting that RNA modifications could be critically involved in self versus non-self-discrimination. In line with this notion, RNA modifications like pseudouridine (Y), 5-methyluridine (m5U) or N6-methyladenosine (m6A) drastically reduce TLR7 and TLR8 activation (Kariko et al., 2005). Yet, other RNA modifications like 8-hydroxyguanosine (8-OHG) or 8-hydroxydeoxyguanosine (8-OHdG) are able to activate TLR7 in the presence of ssRNA (Shibata et al., 2016). Intriguingly, 8-hydroxylation of guanosine is the most prominent natural DNA modification induced by reactive oxygen species (ROS) (Wiseman and Halliwell, 1996). 8-OHdG modifications on the other hand, turn DNA resistant to TREX1 degradation leading to DNA accumulation inside the cell. However, despite its resistance, the modified DNA eventually releases 8-OHdG, which can be recognized by TLR7 (Gehrke et al., 2013; Kroese and Scheffer, 2014). This suggests that modifications like 8-OHG and 8-OHdG play an important role in TLR7 activation under oxidative stress conditions (Shibata et al., 2016). Furthermore, even if 8-OHdG modified DNA is resistant to degradation, it can still be recognized by the cytosolic DNA sensor STING (Gehrke et al., 2013).

1.6 Endolysosomal TLRs in autoimmunity

The recognition of pathogens by PRRs like TLRs, is an essential feature in all different forms of life to fight invading microbes by triggering an immune response. Thus, it is equally important to tightly control these defense mechanisms to avoid excessive activation resulting in disrupted immune homeostasis and all kinds of inflammatory and autoimmune diseases such as SLE, infection-associated sepsis, atherosclerosis or asthma (Gao et al., 2017; Marshak-Rothstein, 2006; Tsujimoto et al., 2008). To this end, TLRs became an important drug target trying to control these diseases by either interfering with ligand binding, or intracellular signaling pathways to stop signal transduction (Gao et al., 2017).

SLE is one of the main systemic autoimmune disease with a compelling worldwide impact across all age and ethical groups (Stojan and Petri, 2018). It is a complex disease defined by the recognition of self-antigens and increased type I interferon release, leading to the production of autoantibodies attacking healthy tissue (Gao et al., 2017). SLE prevalence is highly biased toward women (9:1) and is typically observed at the age of 16-55 years (Scofield et al., 2008). It leads to a broad variety of clinical symptoms that can affect almost all organs and tissues including fever, mucocutaneous lesions, malar rash and arthritis (Cojocaru et al., 2011; Tamirou et al., 2018). Although SLE is a complex disease, it is strongly associated with endolysosomal TLR activation. It was shown that in the course of SLE, TLR7 and TLR9 are detecting autoantigens like endogenous nucleic acids, which leads to the activation of immune cells including DC and autoreactive B-cells (Santiago-Raber et al., 2009). Additionally, the overexpression of TLR7 in several mouse models causes severe autoimmune phenotypes (Celhar et al., 2012), whereas TLR7 deletion results in the decrease of autoantibodies and pro-inflammatory cytokines production (Gao et al., 2017). Furthermore, recent studies uncovered a link between SLE and the protein *CXorf21* (TASL), which was now found to be critically involved in interferon signaling via the endolysosomal receptors TLR7-9 (Heinz et al., 2020; Odhams et al., 2019). The critical involvement of TLR7 in the course of SLE can also partly explain the much higher incidence in women, by an X-chromosome gene-dose effect (Scofield et al., 2008). Despite the similar mode of action between TLR7 and TLR8, not many studies have been published investigating the role of TLR8 in SLE. It was, however, shown that TLR8 deletion leads to accelerated autoimmunity in lupus-prone mice (Tran et al., 2015; Wu et al., 2015). Apart from SLE, the overactivation of TLR7 by endogenous RNAs like the micro RNA let-7 can cause severe damage to the central nervous system (CNS). Intriguingly, the amount of let-7b is increased in the cerebrospinal fluid (CSF) of patients suffering from Alzheimer's disease (Lehmann et al., 2012).

1.7 The RNase T2 superfamily

As a consequence of their involvement in many cellular processes such as DNA replication, control of gene expression and the defense against invading pathogens, RNases play an important role in prokaryotes and eukaryotes. A subset of theses RNases, which are either secreted into the extracellular space or can be found inside the endolysosomal compartment and the vacuole, are cleaving their substrates via a 2'-3' cyclic phosphate intermediate (MacIntosh, 2011). Generally speaking, this set of RNases can, according to their properties, be classified into three superfamilies: RNase T1, RNase T2 and RNase A (Irie, 1999). In contrast to RNaseT1 and RNase A proteins, RNase T2 enzymes can, due to their diversity, not be classified by mass or pH activity. They are instead identified by their active center, as the

amino acid sequence is very conserved throughout all members of this family (MacIntosh, 2011). Interestingly, at least one protein of the RNase T2 family can be found in nearly every eukaryote as well as in many bacteria and viruses. The only organisms missing RNase T2 enzymes are archaea (Condon and Putzer, 2002). The size of RNase T2 family members ranges from 19 to 97 kDa, however, the majority has a mass between 20 and 40 kDa and consists of a single polypeptide chain (Deshpande and Shankar, 2002). Yet, there are some exceptions like E^{rns} from the classical swine fever virus (CSFV), which are multimeric proteins (Schneider et al., 1993). Another feature of RNase T2-like enzymes is their glycosylation pattern – the most common modification is N-glycosylation of the motif Asn-X-Thr/Ser (Deshpande and Shankar, 2002), whereas O-glycosylation is rarely observed (Inokuchi et al., 2000). Enzymes from the RNase T2 family cannot be inhibited by EDTA as they are not metalloenzymes. Nevertheless, some bivalent metal ions like Zn^{2+} or Cu^{2+} are potent inhibitors of human RNase T2, whereas Mg^{2+}, Ni^{2+}, and Co^{2+} have no effect (Thorn et al., 2012). Several crystal structures of RNase T2 proteins like MC1 from bitter ground (Nakagawa et al., 1999) or EcRNase I from *E. coli* are available and despite their low sequence similarity, all of them have a core of hydrophobic residues at comparable locations (Deshpande and Shankar, 2002; Rodriguez et al., 2008). Analysis of the different crystal structures revealed a high level of conservation only for residues located at the active center of the enzymes (MacIntosh, 2011). All RNase T2 enzymes belong to the class of transferase-type endoribonucleases and cleave their substrates via a 2'-3'-cyclic phosphate intermediate state, before hydrolyzing it to a 3'-phosphate (Figure 1.4) (Irie, 1999; Tanaka et al., 2000). Yet, some members of the T2 family were also reported to mainly generate 2'-3'-terminated fragments as a final product (Chacko and Shankar, 1998; Nurnberger et al., 1990). The cleavage mechanism was mostly studied for fungal enzymes, however, the high level of conservation between the active sites of known enzymes suggests a similar mode of action for all members of the RNase T2 family. It was shown that two histidine residues within the active center of the proteins are essential for enzymatic function (Kawata et al., 1990; Parry et al., 1997). They are located at two particularly conserved regions, the CAS I (conserved active site) and CAS II site, with the amino acid sequence F/WTL/IHGLWP and FWXHEWXKHGTC, respectively (Irie, 1999). According to RNase A nomenclature the active center of the enzyme was named P1 site, which is flanked by two nucleotide binding pockets, called B1 and B2 (MacIntosh, 2011). Most RNase T2 enzymes do not have a substrate specificity, however, some members preferentially cleave between two specific bases (Deshpande and Shankar, 2002). Although at least one member of the RNase T2 family can be found in nearly all kingdoms of life, the proteins seem to be particularly widespread in plants, resulting in a huge variety and number of gene duplications. Hence, plant enzymes can be divided into three classes: class I enzymes, a diverse group of stress regulated and tissue specifically expressed enzymes (MacIntosh et al., 2010); class III

enzymes correspond to S-RNases, seeming to share a common ancestor which originated from a class I enzyme (Igic and Kohn, 2001; Roalson and McCubbin, 2003; Steinbachs and Holsinger, 2002); and class II enzymes, which are much more conserved, resulting in usually only one copy per genome. The high level of conservation of class II proteins suggests, that these enzymes are involved in essential cellular processes like housekeeping (MacIntosh et al., 2010). In contrast to plants, only one member of the RNase T2 family can be found in most animals including humans (Hillwig et al., 2009). This could indicate, that RNase T2 enzymes in vertebrates are comparably involved in housekeeping functions to class II RNases from plants (MacIntosh, 2011).

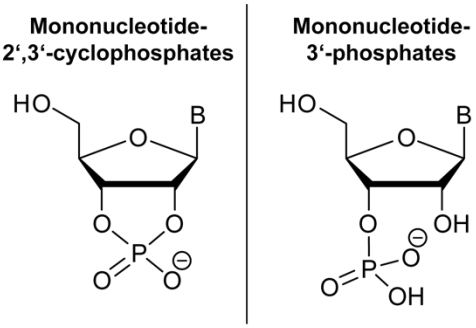

Figure 1.5 Phosphate configurations at the 3’ end of RNA
The most common phosphate configuration after cleavage is the open 3’ phosphate (right panel). However, some transfer type RNases like RNase T2 seem to mainly generate a 2’-3’-cyclophosphate (left panel) at the 3’ end.

The functions of RNase T2 enzymes are quite diverse and include tasks like housekeeping, rRNA degradation and antimicrobial defense (MacIntosh, 2011). Some plants such as Solanaceae, Scrophulariaceae, and Rosaceae use S-RNases to assure self-incompatibility and prevent self-pollination. To this end, the plants have S-RNases in the pistils and the S-locus F-box (SLF) protein in the pollen. If the haplotype of the pollen matches the one of the pistil, it is recognized as self-pollen and fertilization is prevented (Kumar and McClure, 2010; Meng et al., 2011). Other plant RNases were published to have antimicrobial features namely, RNase NE from tobacco plants is thought to be involved in the defense against *Phytophthora parasitica* and *Fusarium oxysporum (*Hugot et al., 2002*)*. Furthermore, it was suggested that RNases can provide antimicrobial activities in nectar (Hillwig et al., 2010). Nevertheless, other members of the RNase T2 family have functions independent of their catalytic activities: Rny1 for example, the only member of the RNase T2 superfamily present in *Saccharomyces cerevisiae*, is not only involved in cytotoxic responses and the cleavage of tRNA and rRNA, but can also induce cell death independent of its catalytic activity (MacIntosh et al., 2001; Thompson and Parker, 2009). Interestingly, some RNase T2 enzymes are even thought to have tumor suppression functions, although the mechanism is not understood (MacIntosh, 2011).

Only one member of the RNase T2 family, called RNase T2, is expressed in humans. It is composed of seven α-helices and eight β-strands building a central β-sheet structure. It has four essential disulfide bonds between the cysteine residues 48/55, 75/121, 184/241 and 202/213. Furthermore, the protein is glycosylated at the asparagine residues 76, 106 and 212. As already mentioned, the protein can be inhibited by zinc and copper ions, however, its catalytic activity is independent of its glycosylation status (Thorn et al., 2012). The structure of human RNase T2 is related to RNase LE from *Solanum lycopersicum* (Tanaka et al., 2000), RNase MC from *Momordica charantia* (Nakagawa et al., 1999; Numata et al., 2003) and RNase NW from *Nicotiana glutinosa* (Kawano et al., 2002). Analysis revealed that the core structure harboring the active center of the protein is very conserved between species, whereas the outer loops are rather variable (Thorn et al., 2012). Loss-of-function mutations in human RNase T2 leads to severe diseases mimicking an congenital cytomegalovirus (CMV) brain infection. The MRI of such patients shows multifocal white matter lesions and in rare cases calcifications, leading to impairment, spasticity and sometimes epilepsy (Henneke et al., 2009). A transgenic zebrafish model showed comparable brain abnormalities together with RNA accumulation in the lysosomal compartment of cerebral neurons (Haud et al., 2011). Most known clinically relevant mutations have severe impact on the protein conformation - the C184R mutation for example disrupts the disulfide bond between cysteine 184 and 241, whereas most other mutations result in altered mRNA splicing leading to a disrupted α-β-core motif (Thorn et al., 2012).

1.8 The RNase A superfamily

The second big family of RNases is the RNase A superfamily. The protein RNase A was originally purified from bovine pancreatic tissue and is one of the best studied mammalian proteins. Over time, other closely related RNases were discovered in mammalians and other vertebrates, becoming the first members of the RNase A superfamily (Koczera et al., 2016). All members of this family are stabilized by several disulfide bonds and have two catalytic histidines (H) as well as one lysine (K), which are located within the CKXXNTF motif. RNase A enzymes do not have a common substrate specificity but seem to preferentially cleave pyrimidines (Raines, 1998). The enzymes efficiently cut ssRNA, however, some members of this family, including human RNase 1, also very potently cut dsRNA and even DNA-RNA hybrids (Potenza et al., 2006; Sorrentino, 2010). Generally, 13 representatives of the RNase A family can be found in humans (RNase 1-13) (Gupta et al., 2013). These enzymes play an important role in many different cellular processes like antiviral, antibacterial and antifungal defense as well as cytotoxic activities. The canonical RNase A proteins (RNase 1-8), secreted by several tissues and immune cells, are important players during acute infections that possess critical

immunomodulatory functions (Boix and Nogues, 2007; Gupta et al., 2013; Martin et al., 2016). RNases 9-13 on the other hand seem to be involved in male reproductive functions (Cho et al., 2005). Of note, all human RNase A proteins are single exon genes and are all located on chromosome 14 (Rosenberg, 2008).

2 Aims of this work

The central dogma of innate immune defense is the recognition of all kinds of PAMPs, DAMPs and MAMPs by cellular pattern recognition receptors. The detection of RNA molecules is especially essential for the defense against a broad variety of viral and bacterial infections. Thus, several PRRs are located in different cellular compartments to ensure proper RNA recognition, including MDA5 and RIG-I, located inside the cytoplasm (Hornung et al., 2006; Kato et al., 2006), as well as TLR7 and TLR8, which can be found in the endolysosomal compartment. The recently solved crystal structures of TLR7 and TLR8 revealed two distinct RNA binding pockets for either receptor. It was shown that the first pocket binds a single nucleotide (uridine for TLR8 and guanosine for TLR7), whereas the second one recognizes at least di- or trinucleotides (Tanji et al., 2015; Zhang et al., 2016). However, the exact substrate specificity as well as the activation mechanism of either receptor is not fully understood. This is especially true since most foreign RNA molecules entering the cell are complex in sequence and therefore not suitable ligands for TLR7 or TLR8 activation. Furthermore, TLR8 is particularly poorly studied as ssRNA ligands cannot activate the receptor under physiological conditions in murine models (Gorden et al., 2006; Hemmi et al., 2002). Analogous to TLR9 whereby DNase II generates appropriate ligands upstream of the receptor (Chan et al., 2015), it is tempting to assume that an enzyme with RNase activity acts upstream of lysosomal RNA recognition.

In this study we exploit the human myeloid BLaER1 cells to investigate the exact substrate specificity and activation mechanism of TLR8. Using this cell line, we aimed to identify potential enzymes acting upstream of the receptor, by systematically knocking out proteins with RNase activity located in either the endolysosomal compartment or the extracellular space, using CRISPR/Cas9 mediated genome editing. Subsequently, a minimal motif for TLR8 activation was determined by mass spectrometry and validated in an *in vitro* infection model.

3 Materials and Methods

3.1 Material

3.1.1 Antibodies

Antibody	Source	Identifier
Anti-β-Actin-HRP-coupled	Santa Cruz	Cat#sc-47778 HRP
Direct-Blot HRP anti-FLAG tag	BioLegend	Cat#637311
Anti-RNase T2	Sigma-Aldrich	Cat#HPA029013
Anti-rabbit IgG HRP linked	Cell Signaling Technology	Cat#7074
Anti-TLR8 (D3Z6J)	Cell Signaling Technology	Cat#11886S

3.1.2 Bacterial strains

Strain	Source	Identifier
S. aureus subsp. aureus	ATCC	ATCC 6538

3.1.3 Chemicals

Chemicals and Reagents	Source	Identifier
Agilent RNA 6000 Nano Kit	Agilent	Cat#5067-1511
Ammonium persulfate	Sigma-Aldrich	Cat#A3678
Blood agar plate	OXOID	Cat#PB5039A
Doxycycline hyclate	Sigma-Aldrich	Cat#D9891
EDTA (0.5M)	Thermo Fisher	Cat#15575020
GeneJuice® Transfection Reagent	Merck Chemicals GmbH	Cat#70967
Gentamicin	Thermo Fisher	Cat#15750060
HisTrap™	GE Healthcare	Cat#17-5247-01
ISOGRO®-^{15}N Powder-Growth Medium	Sigma-Aldrich	Cat#606871
Lipofectamine 2000 Transfection Reagent	Thermo Fisher Scientific	Cat#11668019
LPS-EB Ultrapure	InvivoGen	Cat#tlrl-3pelps
nitrocellulose membrane (0.45µm)	GE Healthcare	Cat#10600002
Pam3CSK4	InvivoGen	Cat#tlrl-pms
Penicillin-Streptomycin	Life Technologies	Cat#15140122

Phenol/Chloroform/Isoamyl alcohol	Roth	Cat#A156.3
Phorbol 12-myristate 13-acetate (PMA)	Enzo Life Sciences	Cat#BML-PE160-0005
poly-L-arginine	Sigma-Aldrich	Cat#P7762
Recombinant Human IL-3	MPI of Biochemistry, Munich	N/A
Recombinant Human IFN-γ	PeproTech	Cat#300-02
Recombinant Human M-CSF	MPI of Biochemistry, Munich	N/A
R848	InvivoGen	Cat# tlrl-r848
SequaGel Concentrate	national diagnostics	Cat#EC8301L
SequaGel Buffer	national diagnostics	Cat#EC835200ML
SequaGel Diluent	national diagnostics	Cat# EC8401L
Superdex-200 16/600	GE Healthcare	Cat#28989335
SYBR Gold Nucleic Acid Gel Stain	Thermo Fisher Scientific	Cat#S11494
TL8-506	InvivoGen	Cat# tlrl-tl8506
TEMED	Roth	Cat#2367.3
UltraPure 0.5M EDTA, pH 8.0	Thermo Fisher Scientific	Cat#15575020
ß-Estradiol	Sigma-Aldrich	Cat#E8875-250MG

3.1.4 Critical commercial assays

Kit	**Source**	**Identifier**
Human IL-6 ELISA Set	BD Biosciences	Cat#555220

3.1.5 Cell lines

Cell Lines	**Source**	**Identifier**
BLaER1 human b-cell to monocyte trans-differentiation cell line	(Rapino et al., 2013)	N/A
HEK293T	(Gaidt et al., 2017)	N/A
THP-1	ATCC	TIB202

3.1.6 Oligonucleotides

Oligonucleotide	Source	Identifier
RNA40S (rG*rC*rC*rC*rG*rU*rC*rU*rG*rU*rU*rG*rU*rG*rU*rG*rA*rC*rU*rC)	Miltenyi	130-104-429
RNA40 (rGrCrCrCrGrUrCrUrGrUrUrGrUrGrUrGrArCrUrC)	IDT	N/A
P20 (rUrUrGrArArGrGrArCrArUrGrUrCrCrUrUrCrArA)	IDT	N/A
P20-5M (rUrGrUrCrCrUrGrArCrArUrGrUrCrCrUrUrCrArA)	IDT	N/A
dN*dN*dN*dN*dN*dN*U*U*G*U*dN*dN*dN*dN*dN*dN*dN*dN	IDT	N/A
dN*dN*dN*dN*dN*dN*U*U*G*A*dN*dN*dN*dN*dN*dN*dN*dN	IDT	N/A
dN*dN*dN*dN*dN*dN*U*U*G*G*dN*dN*dN*dN*dN*dN*dN*dN	IDT	N/A
dN*dN*dN*dN*dN*dN*U*U*G*C*dN*dN*dN*dN*dN*dN*dN*dN	IDT	N/A
dN*dN*dN*dN*dN*dN*U*U*G*dN*dN*dN*dN*dN*dN*dN*dN	IDT	N/A
dN*dN*dN*dN*dN*dN*U*U*A*U*dN*dN*dN*dN*dN*dN*dN*dN	IDT	N/A
dN*dN*dN*dN*dN*dN*U*U*A*A*dN*dN*dN*dN*dN*dN*dN*dN	IDT	N/A
rArArArGrGrArArA	IDT	N/A
rArArArGrArArArA	IDT	N/A
rArArArGrUrArArA	IDT	N/A
rArArArGrCrArArA	IDT	N/A
rArArArArGrArArA	IDT	N/A
rArArArArArArArA	IDT	N/A
rArArArArUrArArA	IDT	N/A
rArArArArCrArArA	IDT	N/A
rArArArUrGrArArA	IDT	N/A
rArArArUrArArArA	IDT	N/A
rArArArUrUrArArA	IDT	N/A
rArArArUrCrArArA	IDT	N/A
rArArArCrGrArArA	IDT	N/A
rArArArCrArArArA	IDT	N/A
rArArArCrUrArArA	IDT	N/A
rArArArCrCrArArA	IDT	N/A
rA*rC*rA*rC*rA*rC*rA*rC*rA*rC*rA*rC*rA*rC*rU*rU*rG*rU*rC*rU	IDT	N/A
dAdCdAdCdAdCdAdCdAdCdAdCdAdCdAdC	IDT	N/A
dAdCdAdCdAdCdAdCdAdCdAdCdAdC*rU*rU*rG*rU*rC*rU	IDT	N/A

dAdCdAdCdAdCdAdCdAdCdAdCdAdC*rU*rU*rG	IDT	N/A
dAdCdAdCdAdCdAdCdAdCdAdCdAdC*rU*rU*rG-3‘-phosphate	IDT	N/A
dAdCdAdCdAdCdAdCdAdCdAdCdAdC*rU*rU	IDT	N/A

3.1.7 Plasmids

Plasmids	**Source**	**Identifier**
pcDNA3.1_RNase T2_PreScission_6xHis	This study	N/A
pLI_hu_RNase T2_FLAG_Puro	This study	N/A
pLI_mScarlet _Puro	This study	N/A
CMV-mCherry-Cas9	(Schmid-Burgk et al., 2014)	N/A
pLK0.1-gRNA-CMV-GFP	(Schmid-Burgk et al., 2014)	N/A
pCAS9-mCherry -gRNA	(Schmid-Burgk et al., 2016)	N/A

3.1.8 Software and algorithms

Plasmids	**Source**	**Identifier**
GraphPad Prism 8	GraphPad	N/A
Outknocker	(Schmid-Burgk et al., 2014)	N/A
Adobe Illustrator v21.0.0	Adobe	N/A

3.1.9 Primer

Name	**Sequence**	**Used for**
TLR7_Fwd	ACACTCTTTCCCTACACGACGctcttccgatctAATGTCACAGCCGTCCCTAC	MiSeq
TLR7_Rev	TGACTGGAGTTCAGACGTGTGctcttccgatctAACTTTTAATTCTGTCAGCGCATC	MiSeq
TLR8_Fwd	ACACTCTTTCCCTACACGACGctcttccgatctAATGCTGACCTGCATTTTCC	MiSeq
TLR8_Rev	TGACTGGAGTTCAGACGTGTGctcttccgatctATTTTGCAGCCCTTGAAATG	MiSeq
RNaseT2_Fwd	ACACTCTTTCCCTACACGACGctcttccgatctTGCAGTACCTGTATCTCGTTGG	MiSeq
RNaseT2_Rev	TGACTGGAGTTCAGACGTGTGctcttccgatctCAAGCTAGGGTTCCCAGTCA	MiSeq
RNase1_Fwd	ACACTCTTTCCCTACACGACGctcttccgatctTCCTGATACTGCTGGTGCTG	MiSeq
RNase1_Rev	TGACTGGAGTTCAGACGTGTGctcttccgatctTCTTGCAGGTGACCTTTTCC	MiSeq
RNase2_Fwd	ACACTCTTTCCCTACACGACGctcttccgatctGTTGGGGCTTCTGGCTGT	MiSeq

RNase2_Rev	TGACTGGAGTTCAGACGTGTGctcttccgatctTGGTGACAATTTTTGCGAGT	MiSeq
RNase6_Fwd	ACACTCTTTCCCTACACGACGctcttccgatctTGGTGCTATGCTTTCCTCTTC	MiSeq
RNase6_Rev	TGACTGGAGTTCAGACGTGTGctcttccgatctATCACAGACAGCAGCCACAT	MiSeq
RNAseT2_cDNA_F	ATTAGCTAGCATGCGCCCTGCAGCCCT	Cloning
RNAseT2_cDNA_R	ATTAGGATCCTCAATGCTTGGTCTTTTTAGGTGGGG	Cloning
RNAseT2_cDNA_BshTI_R	ATTAACCGGTTCAATGCTTGGTCTTTTTAGGTGGG	Cloning
RNAseT2_BshTI_no stop_R	ATTAACCGGTATGCTTGGTCTTTTTAGGTGGGGGATAGAAGAC	Cloning
RNAseT2_PreScission_6xHis_BamHI_R	ATTAGGATCCTCAGTGGTGATGGTGATGATGCAGTTCAACCAGGAACTGCCCGGGATGCTTGGTCTTTTTAGGTGG	Cloning
RNAseT2_NheI_F	ATTAGCTAGCATGCGCCCTGC	Cloning
CMV-F	CGCAAATGGGCGGTAGGCGTG	Sequencing
U6_Fwd	GAGGGCCTATTTCCCATGATTCCT	Sequencing
LICsgRNA_rev	P-AACGGACTAGCCTTATTTTAACTTGCTATTTCTAGCTCTAAAAC	

3.1.10 sgRNA

The sgRNAs were designed using a web tool called CHOPCHOP. The oligonucleotide for LIC cloning is composed of 5'-GGAAAGGACGAAACACCG-3' followed by the target sequence without the PAM and without the first nucleotide, followed by 5'-GTTTTAGAGCTAGAAATAGCAAGTTAAAATAAGG-3'.

Target Gene	**Target Site and PAM**
RNASE1	GAGGCGCCGGAATATGACAC**AGG**
RNASE2	GCGAGTTTTGTTACTAGGAC**AGG**
RNASE6	TGAGCCTTGGTGAGACGCTT**AGG**
RNASET2	GTATTGTCCAGTAATCCGGA**GGG**
TLR7	ATGGGGCATTATAACAACGA**GGG**
TLR8	GGAAGTTCCCCAAACGGT**GGG**

3.1.11 Media and buffers

Buffer	Ingrediencies
Cell culture medium	500 ml RPMI or DMEM 10% heat inactivated FCS (v/v) Sodium pyruvate (1 mM) 100 U/ml Penicillin-Streptomycin
Direct lysis buffer	0.2 mg/ml Proteinase K 1 mM $CaCl_2$ 3 mM $MgCl_2$ 1 mM EDTA 1 % Triton X-100 10 mM Tris pH 7.5
DISC	30 mM Tris-HCl 150 mM NaCl 10 % Glycerol (v/v) 1 % Triton-X-100 (v/v) pH 7.5
LB agar	20 g LB 15 g Agar 1 l H_2O Autoclave before usage
LB medium	20 g LB 1 l H2O Autoclave before usage
Miniprep buffer P1	50 mM Tris pH 8.0 10 mM EDTA 100 µg/ml RNase A
Miniprep buffer P2	200 mM NaOH 1 % SDS
Miniprep buffer N3	4.2 M guanidine hydrochloride 0.9 M Potassium acetate pH 4.8
Miniprep buffer PE	10 mM Tris pH 7.5 80 % ethanol
TAE buffer	40 mM Tris pH 8.0 20 mM acetic acid 1 mM EDTA
10x TBE buffer	1 M Tris 1 M boric acid 0.02 M EDTA pH 8.3

TBS-T buffer	137 mM NaCl 2.7 mM KCKl 19 mM Tris 0.05 % Tween 20 pH 7.4
TFBI	100 mM RbCl 50 mM $MnCl_2$ 30 mM KAc 10 mM $CaCl_2$ 15 % Glycerol pH 5.8
TFBII	10 mM MOPS 10 mM RbCl 75 mM $CaCl_2$ 15 % Glycerol pH 6.8
6x Lämmli buffer	60 mM Tris pH 6.8 9,3 % DTT (w/v) 12 % SDS (w/v) 47 % glycerol (v/v) 0,06 % bromophenol blue (w/v)

3.1.12 Laboratory equipment

Device	**Supplier**
Absorbance readers	TECAN/ Epoch
Biomek FX Robot	Beckmann Coulter
Chemidoc imaging system	Bio-Rad
Fusion Fx device	Vilber
Gene Pulser Xcell	Bio-Rad
Nanodrop	Peqlab
PCR cycler	Bio-Rad
Sony sorter SH800Z	Sony
Thermoshaker	Eppendorf
Centrifuge (5920R, 5424R, 5810R)	Eppendorf

3.2 Molecular biology methods

3.2.1 Generation of chemically competent *E. coli*

200 ml LB medium was inoculated with *E. coli* (DH5α) and incubated over night at 37 °C. The next day 200 ml of LB medium was inoculated 1:100 with the overnight culture and grown for 3 h. Bacteria were incubated on ice for 15 min before they were centrifuged for 10 min at 2700 g at 4 °C. The pellet was resuspended in 30 ml chilled TFBI buffer and incubated on ice for 10 min. Cells were centrifuged at 600 g in 4 °C for 10 min. After removing the supernatant cells were gently resuspended in 4 ml chilled TFBII and aliquoted (40 µl). After snap freezing in liquid nitrogen competent bacteria were stored at -80 °C.

3.2.2 Restriction enzyme cloning

To obtain the needed DNA plasmids, genes were amplified from human cDNA by PCR. The needed restriction sites were added by overhanging primers in a second PCR step. The insert as well as the vector were digested with the respective restriction enzymes (Thermo Scientific, FastDigest) according to supplier's protocol. The plasmid was furthermore incubated with Fast AP (Thermo Scientific, #EF0651) for 15 min, to remove the 5'-phosphate and prevent re-ligation of the vector. The digested DNA fragments were purified by agarose gel purification (QIAquick Gel Extraction Kit) and ligated with T4 ligase (Thermo Scientific, #EL0011) in a molecular ratio of 1:3 (vector:insert). The ligation was also performed according to the supplier's protocol. The ligation mixture was transformed into *E. coli*.

3.2.3 Generation of gRNA-plasmids by ligation independent cloning (LIC)

If the needed sgRNA could not be found in the sgRNA library (Schmidt et al., 2015), a new sgRNA plasmid was generated by ligation independent cloning (LIC). To design an early targeting sgRNA, present in all annotated splice variants, the web based tool CHOPCHOP was used (Montague et al., 2014). The according DNA with overhangs complementary to the vector was ordered and cloned into an expression plasmid:

2 µg empty expression vector was digested with the FastDigest enzymes ApaI and SpeI and purified by agarose gel extraction. The essential overhangs were generated by the 3'-5' exonuclease activity of T4 polymerase in the presence of dTTP as stop nucleotide:

10 µl	10x NEB2 buffer
10 µl	Vector 70ng/µl
1 µl	BSA 10mg/ml
1 µl	dTTP 100 mM
74.66 µl	H_2O
3.33 µl	T4 DNA polymerase 3 U/µl

The reaction mixture was incubated for 5 min at 27 °C, put on ice and heat inactivated for 20 min at 75 °C. The chewed vector was mixed with the universal reverse binding oligonucleotide LICsgRNA_rev (PAGE purified, IDT):

20 µl	10x NEB2-puffer
10 µl	Chewed vector
0.5 µl	LICsgRNA_rev 100µM
69.5 µl	H_2O

2.5 µl master mix was added to 2.5 µl of sgRNA oligonucleotide (0,25 µM) and annealed according to the following protocol:

70 °C	1 min	
65 °C	1min	
60 °C	30 sec	29 cycle; -1 °C/cycle
55 °C	2.5 min	
25 °C	∞	

Afterwards the mixture was transformed into chemically competent *E. coli*.

3.2.4 *E. coli* transformation

Chemically competent *E. coli* were thawed on ice before adding the plasmid DNA and incubated 15 min on ice. Cells were heat shocked at 42 °C for 45 s and put back on ice for 2 min. After adding 250 µl LB medium bacteria were shaken for 30 min at 37 °C. They were plated on an agar plate with appropriate antibiotics.

3.2.5 Plasmid isolation from *E. coli*

Plasmids were isolated according to the protocol of the QIAprep Spin Miniprep Kit (Qiagen). The buffers for the purification are self-made. For higher yield and purification, the Midi and Maxi Kits from Invitrogen (#K210014, #K210006) were used.

3.2.6 Sanger sequencing

Sanger sequencing was performed by Eurofins (TubeSeq service).

3.2.7 PCR

For all performed PCRs Phusion High-Fidelity DNA Polymerase (Thermo Scientific, #F530L) was used according to the manufacture's protocol.

3.2.8 Agarose gel electrophoresis

To analyze the size of DNA fragments a 1 % (w/v) agarose gel was cast. For visualization ROTI GelStain (#3865.2) was used in a final concentration of 0.005 %. Samples were mixed with loading dye and run at 120 V for 30-40 min.

3.2.9 Bioanalyzer

S. aureus total RNA analysis was performed using the Agilent Bioanalyzer device. The RNA 6000 Nano kit (#5067-1511) was used according to the supplier's protocol.

3.2.10 Urea gel

Urea Gels were cast using SequaGel Concentrate, SequaGel Diluent and SequaGel Buffer according to the supplier's protocol. Samples were loaded using 2x RNA gel loading dye (Thermo Fisher #R0641) and the gel was run at 250 V for 70 min in TBE buffer. It was stained with SYBR Gold and imaged using a UV table.

3.2.11 RNA precipitation

RNA was purified by sodium acetate precipitation. Samples were mixed with a 3 M sodium acetate solution, resulting in a final concentration of 0.3 M. 4 volumes 100 % EtOH were added to the samples and incubated for 1 h at -20 °C. After centrifugation for 30 min at full speed the RNA washed twice with 80 % EtOH. The pellet was air dried and dissolved in RNase free water.

3.3 Cell culture methods

3.3.1 Cell lines

BLaER1: a subclone of human B cell Lymphoma expressing the transdifferentiation construct CEBPα-ER-GFP.

THP-1 (ATCC® TIB202™): monocytic cell line obtained from human leukemia patient.

HEK 293T (ATCC® CRL-3216™): HEK 293T human embryonic kidney cells stably expressing SV40 large T antigen.

3.3.2 Cell culture

BLaER1 (Rapino et al., 2013) and THP-1 cells were cultured in RPMI medium whereas HEK293T were grown in DMEM. BLaER1 cells were trans-differentiated for 5-6 days with medium containing 10 ng/ml IL-3, 10 ng/ml CSF-1 (M-CSF) (MPI of Biochemistry, Munich) and 100 nM ß-estradiol. All experiments were carried out in a 96-well format with 80,000 cells/well. In this study BLaER1 cells with a $CASP4^{-/-}$ genetic background were used. Furthermore, we noticed the infection of this cell line by SMRV (Squirrel monkey retrovirus). Further experiments confirmed the integration of viral DNA into the BLaER1 genome. However, testing early passages of BLaER1 cells confirmed that the parental cell line was already infected with SMRV. Of note, the extensive testing of BLaER1 cells also in comparison with other human myeloid cells did not give any indication that the SMRV infection would influence the experimental outcome of the cell line.

THP-1 cells were differentiated in 10 cm dishes using RPMI medium supplemented with 100 ng/ml PMA for 16 h. Cells were washed with PBS twice, detached and seeded into 96-well plate (80,000 cells/well). After a resting phase of 3 days cells were stimulated with IFN-γ for 6 h.

3.3.3 Cell stimulation

BLaER1 cells were stimulated with all different kind of RNA oligonucleotides which either had a phosphorothioate backbone stabilization or a normal phosphodiester backbone. For cellular delivery the RNA was complexed with poly-L-arginine in a 1:1 ratio (Ablasser et al., 2009). If not otherwise indicated, stimulation with RNA 40 was performed with 0.6 µg/well. For all condition involving *ex cellulo* digestion of any ONs, 1.2 µg was transfected to account for cleavage activity of RNaseT2. The transfection was performed as follows: RNA and Poly-L-arginine were separately incubated in Opti-MEM (Gibco®) (25 µl per 96-well each) for 5min.

Afterwards the two components were mixed and incubated for 20 min at room temperature. After exchanging the medium (100 µl/well), 50 µl transfection mix was added. The transfection of RNA with Lipofectamine 2000 (LF) was performed according to the supplier's protocol. As control, cells were stimulated with either 200 ng/ml LPS, 1 µg/ml R848 or 100 ng/ml TL8-506. Stimulations were carried out at 37 °C for 14-16 h.

To stimulate cells with RNA degradation products, 1-2 µg of ONs was digested with either RNaseT2 (made in this study) or RNase A (Invitrogen, Maxiprep Kit, #K210017). The digest was performed for 20 min at 30 °C in a total volume of 10 µl (IDTE buffer pH 8). After digest, the RNA fragments were transfected using poly-L-arginine and cells were stimulated for 14-16 h at 37 °C.

For bacterial infections with *S. aureus* subsp. *aureus* (ATCC® 6538™), bacteria were grown overnight on blood agar plate at 37 °C. The next day bacteria were scraped and resuspended in PBS. After centrifugation for 5 min at 4000 g cells were resuspended in RPMI medium without antibiotics. 100µl (per 96-well) of bacteria containing medium (with the indicated MOI) was added onto cells and incubated for 1 h at 37 °C. Afterwards the medium was topped up with 50 µl RPMI containing gentamicin, resulting in a final concentration of 50 µg/ml. Stimulation was carried out for another 14 h at 37 °C. Stimulation with ^{15}N labeled *S. aureus* was performed according to the same protocol.

Differentiated THP-1 cells were stimulated with 1.2 µg RNA40, complexed with poly-L-arginine in a 1:1 ratio. RNA and Poly-L-arginine were separately incubated in Opti-MEM (Gibco®) (25 µl per 96-well each). After 5 min the two components were mixed and incubated for 20 min at room temperature. After exchanging the medium (100 µl/well), 50 µl transfection mix were added on top. As control, THP-1 cells were stimulated with either 0,33 µg/ml Pam3CSK4, 2 µg/ml R848 or 200 ng/ml TL8-506. All stimulations were carried out for 14-16 h at 37 °C.

3.4 Cell biology methods

3.4.1 ^{15}N-labeling of *S. aureus*

S. aureus were labeled as follows: ISOGRO-^{15}N powder was purchased and dissolved in water to a final concentration of 0.5g/50ml and supplemented with K_2HPO_4 (10 mM), KH_2PO_4 (10 mM), $MgSO_4$ (10 mM) and $CaCl_2$ (0,1 mM). 5 ml medium were inoculated with *S. aureus* subsp. *aureus* (ATCC® 6538™), grown for 16 h and harvested by centrifugation (8min at 5000 g). Bacteria were washed twice with PBS to remove remaining salts.

3.4.2 Lentiviral expression and transduction of BLaER1 cells

To generate cell lines expressing the gene of interest in an inducible fashion, the third-generation lentiviral vector system was used. This system is extremely safe as the needed proteins for viral particle formation are separated on four plasmids: pLI_GeneOfInterest (transfer plasmid), pMDLg/pRRE and pRSV-rev (packaging plasmids) and pCMV-VSV-G (envelope plasmid). The DNA (1 µg transfer plasmid, 1.5 µg pMDLg/pRRE, 0.5 µg pRSV-rev and 1 µg pCMV-VSV-G in 200 µl opti-MEM) and PEI Max mix (10.6 µl PEI Max in 200 µl Opti-MEM) were prepared separately and incubated for 5 min at room temperature. Afterwards they were mixed and incubated another 25 min at room temperature. 300 µl transfection mix was added to 1 ml cell suspension containing $2x10^6$ HEK 293T cells and put into a 6-well. After 2 h the medium was topped up with FCS containing DMEM medium resulting in a final FCS concentration of 30 %. After 16 h the supernatant was harvested, centrifuged for 5 min at 500 g and filtered (0.45 µm). 750 µl of virus supernatant were mixed with 750 µl cell suspension containing $2x10^6$ BLaER1 cells and put in a 6-well plate. After 24 h the medium was exchanged with fresh RPMI and cells were transferred to a T25 flask. For selection of transduced cells, puromycin (1.25 µg/ml) was added to the medium. Selection pressure was kept up for one week prior to analysis of surviving cells.

3.4.3 RNA-seq

Undifferentiated as well as differentiated BLaER1 cells were lysed in Trizol ($2x10^6$/1ml) and total RNA was purified using the Zymo Direct-zol RNA Miniprep. Total RNA was used to generate stranded RNA sequencing libraries using the Encore Complete RNA-Seq™ library system of NuGEN. The libraries were sequenced on an Illumina HiSeq1500 device. The reads were aligned to the human reference genome (Ensemble genome version 91) using STAR (Dobin et al., 2013). The transcripts were quantified using RSEM (Li and Dewey, 2011) and TPM (Transcripts Per Kilobase Million) values are shown as normalized gene expression. All RNA-seq datasets were generated in this study, except for THP-1 data which are derived from a public database (GEO, GSE 62171).

3.5 Mass spectrometry

All mass spectrometry measurements (LC/MS and MALDI) were performed by Mirko Wagner from the group of Thomas Carell.

3.5.1 LC/MS

For LC/MS analysis $3x10^6$ BLaER1 cells were lysed in 750 µl of a 1:1 mixture of water and acetonitrile for 10 min. The samples were centrifuged for 10 min at 21,000 g and the supernatant was flash frozen. After freeze-drying, the samples were re-dissolved in 300 µl miliQ water. The samples were centrifuged for 30 min at 21,000 g in 4 °C and the supernatant transferred to a new tube to solely obtain the soluble cell pool. Before mass spectrometry measurement, 10 µl of a 0.3 µM 2-(D3-methyl)guanosine (D3-m2G; 3 pmol; synthesized in the Carell group (Globisch et al., 2011)) solution (dissolved in milliQ-water) was added to 90 µl of the sample serving as internal standard. The mixture was vortexed for 60 s and analyzed by LC-HESI-MS using a Dionex Ultimate 3000 HPLC system coupled to a Thermo Fisher LTQ Orbitrap XL mass spectrometer. For comparability, the injection volume was constantly kept at 90 µl (out of 300 µl total volume) per technical replicate. Nucleoside / nucleotide separation was performed using an Interchim Uptisphere 120-3HDO C18 column with a constant temperature of 30 °C. For elution the buffers A (2 mM NH4HCOO in H2O; pH 5.5) and B (2 mM NH4HCOO in H2O/MeCN 20/80 v/v; pH 5.5) were used at a constant flow rate of 0.15 ml/min. The two buffers were gradually mixed over time: 0→10 min, 0% B; 10→15 min, 0→0.1% B; 15→50 min, 0.1→5% B; 50→90 min, 5→100% B. The chromatogram was recorded at 260 nm with a Dionex Ultimate 3000 Diode Array Detector. The eluent was directly injected into the mass spectrometer without splitting. Samples were measured in the positive polarity mode scanning the full range between *m/z* 225-2000 with a resolution of 60,000. The mass spectrometer was calibrated using a freshly mixed inosine (5µM) solution in buffer A. The parameters were set as follows: capillary temperature 275.00 °C; source voltage 4.80 kV; capillary voltage 0.00 V; tube lens voltage 45.00 V. The areas under the curve were integrated after the ion chromatograms of the compounds of interest were extracted from the total ion current (TIC) chromatogram. To make the samples more comparable, the integrals of the found molecules were divided by integral of the internal standard D3-m2G. Importantly, the sulfur atom in $RNA40^S$ derived fragments led to diastereomeric configurations, generating several peaks for each molecule in the liquid chromatography. To this end, we only used the most abundant peak for quantification.

In samples stimulated with ^{15}N-labeled *S. aureus*, the fully labeled fragments were by far more abundant than the respective fragment with less ^{15}N-atoms. Therefore, only the fully labeled fragments were considered for MS-based quantifications.

To determine the substrate specificity of RNase T2 basically the same HPLC-ESI-MS setup was used (a Dionex Ultimate 3000 HPLC system coupled to a Thermo Fisher LTQ Orbitrap XL mass spectrometer). While buffer A and buffer B were identically, the flowrate was changed to

0.2 ml/min. Furthermore, the gradient was altered: 0→5 min, 0% B; 5→20 min, 0→5% B; 20→30 min, 5→100% B. The chromatogram was also recorded at 260 nm using a Dionex Ultimate 3000 Diode Array Detector. Whereas the MS analysis was critical to identify the found fragments, the UV trace was used to calculate how efficient the RNA molecule was cleaved. Therefore, the sum of the integrals of all cleaved fragments was divided by the integrals of all found fragments (including the full length). As the oligonucleotides were bearing multiple charges the MS full-scan range of *m/z* 225-2000 was used.

3.5.2 MALDI

1200 ng of the respective RNA ON was digested by adding either RNase T2 (5-50 pg/µl) or RNase A (5-50 pg/µl) for 20 min at 37°C. The total reaction volume was 10 µl, which was filled up to 300µl after digestion using water. To inactivate the enzyme and for further purification the samples were mixed with Roti®-Phenol/Chloroform/Isoamyl alcohol in a 1:1 ratio and flash frozen. If not otherwise indicated, all following steps were performed at room temperature. The thawed samples were centrifuged for 3 min at 21,000 g and the aqueous (upper) phase was transferred to a new tube. To remove the remaining phenol, the samples were washed twice with chloroform as follows: The aqueous phase was mixed with equal amounts of chloroform and vortexed for 30 s. After centrifugation at 21,000 g for 3 min the aqueous phase was again transferred to a fresh tube. Subsequent of the two washing steps the samples were freeze-dried. After re-dissolving them in 60 µl milliQ-water, they were centrifuged for 30 min at 21,000 g and 4 °C. The supernatant was taken and analyzed by HPLC (Waters e2695 Separations Module) using an injection volume of 50 µl. For separation an EC 250/4 Nucleodur 100-3 C18ec column was used, which was constantly kept at room temperature. The chromatogram was recorded at 260 nm using a Waters 2489 UV/Visible Detector. For elution buffer C (0.1 M NEt_3/HOAc in H_2O) and buffer D (0.1 M NEt_3/HOAc in H_2O/MeCN 20/80 v/v) were used at a constant flowrate of 0.5 ml/min. The following gradient was used: 0→45 min, 0→25% D; 45→47 min, 25→100% D. The fractions were freeze-dried and re-dissolved in 10 µl milliQ-water. The samples were desalted for 3 h using a MF-Millipore Membrane Filter with a pore size of 0.025 µm. Subsequent a MALDI-MS analysis was performed using an autoflex II system (Bruker Daltonics) in the negative polarity mode. Therefore, 1.5 µl of HPA-matrix (3-hydroxypicolinic acid) was used per 1.5 µl desalted sample. All MALDI experiments were done in duplicates.

3.6 Biochemical methods

3.6.1 Protein purification

The human RNase T2 protein (residues 1-256) was amplified from cDNA derived from BLaER1 cells. It was either cloned in a pcDNA3.1 vector or the piggyBAC vector system (Li et al., 2013), using conventional enzyme cloning. Both systems were used for protein purification and yielded RNase T2 with over 90% purity, which was determined by Coomassie stanning and mass spectrometry. Protein activity was comparable between both approaches.

Using the pcDNA3.1 vector system the plasmid (pcDNA3.1_RNase T2_PreScission_6xHis) was transfected into HEK293T cells. For protein purification the supernatant of six 10 cm dishes was harvested and centrifuged for 5 min at 500 g and 4 °C. The supernatant was filtered and loaded onto a 1 ml HisTrap™. The column was subsequently washed using 20 column volumes (CV) of wash buffer (20 mM K2HPO4, pH 7.5, 0.5 M NaCl, 20 mM Imidazole). The protein was eluted by using a gradient of Buffer A (wash buffer) and buffer B (1 M imidazole) over 10 CV. RNase T2 containing fractions were subsequently purified by size exclusion chromatography (SEC) using a Superdex-200 16/600 in SEC buffer (200 mM NaAc pH 6.0, 50 mM NaCl). The protein was concentrated and flash frozen for storage at -80 °C.

The piggyBac_RNase T2_PreScission_6xHis plasmid was used to generate stable HEK293T/17 SF cells. Stable cells were grown in 1 l medium to a density of 1 x 10^6 cells/ml. For selection cells were treated with Doxycycline (1 ug/ml). Supernatant was harvested after 7 days and concentrated using a Sartocon Slice 200, 10 kDa MW cutoff (Sartorius) in PBS. The protein was subjected to size exclusion chromatography in SEC buffer (200 mM NaAc, 50 mM NaCl, pH 6.0) using a HiLoad 26/60 Superdex 200 (GE healthcare). Fractions containing RNase T2 were concentrated using a 10 kDa cut-off, Amino Ultra 15 concentrator (Amicon), to a concentration of 11 mg/ml and flash frozen in liquid nitrogen.

3.6.2 Immunoblotting

For western blots of whole cell lysate, 1x10^6 cells were stimulated in a 96-well format for 14 h. Cells were detached from the dish using PBS-EDTA (Invitrogen, #15575020, 2 mM), pooled and centrifuged for 5 min at 500 g. The supernatant was removed, and cells were lysed in DISC buffer for 10 min on ice. To get rid of the nuclei, cells were centrifuged for 10 min at 16,000 g. The supernatant was mixed with 6x Lämmli buffer and denatured for 5 min at 85 °C. The proteins were separated using a precast tris-glycine denaturing SDS-PAGE (Invitrogen, Novex Tris-Glycine Gels) and transferred onto a 0.45 µm nitrocellulose membrane by wet blotting. The membrane was blocked in 5 % skim milk for 1 h and incubated with the primary antibody

overnight. The membrane was washed 3 times with TBS-T for 5 min and incubated with the corresponding secondary HRP-coupled antibody for 1 h. After another 3 washes chemiluminescence was measured using a CCD-camera and respective images were contrast-enhanced in a linear fashion. The antibodies were diluted as follows:

Anti-RNase T2	1:500
Anti-TLR8	1:1000
Anti-FLAG HRP	1:1000
Anti-β-Actin-HRP	1:1000
Anti-rabbit IgG HRP Antibody	1:1000

3.7 CRISPR/Cas9 mediated knockout-cell line generation

Knockouts were generated using the CRISPR/Cas9 system throughout the whole manuscript. BLaER1 KO generation was performed according to a published protocol (Schmid-Burgk et al., 2014). Therefore, sgRNAs (18- or 20-mer) targeting an early coding exon were designed and cloned into an expression plasmid. BLaER1 cells were electroporated with the plasmid carrying the respective sgRNA as well as Cas9-T2A-BFP. BLaER1 cells were sorted for high BFP expression and serially diluted to obtain monoclones.

As THP-1 cells could, due to their strong immune response upon DNA recognition, not be electroporated with plasmid DNA, ribonucleoprotein (RNP) complexes were delivered by nucleofection (Lonza). As this led to very efficient KO generation, cells were directly subjected to serial dilution. All genotypes (BLaER1 and THP-1) were subsequently analyzed by deep sequencing (MiSeq).

3.7.1 Electroporation of BLaER1 cells

Fresh BLaER1 cells were adjusted to $2.5x10^5$ cells /ml 24 h prior to electroporation. Cells were counted and adjusted to $1x10^7$ cells/ml in Opti-MEM. 250 µl cell suspension was mixed with a total of 5 µg DNA. The mixture was incubated for 15 min at room temperature and transferred to an electroporation cuvette. The electroporation was performed with the Gene Pulser Xcell Electroporation system from BIO-RAD using the following settings: 265 V, 975 µF and 720 Ω. Cells were quickly transferred into 2 ml prewarmed RPMI medium and incubated in a 6-well plate at 37 °C.

3.7.2 FACS sorting of BLaER1 cells

24 h to 48 h after electroporation cells were spun down for 5 min at 500 g, resuspended in 500 µl medium and put through a cell strainer. To sort the cells either the SONY SH800Z or the BD FACS Melody sorting device was used. BFP positive BLaER1 cells were sorted and used for serial dilution.

3.7.3 Nucleofection of THP-1 cells

As THP-1 cells were generated using RNPs and could therefore not be sorted to enrich for positive cells, each gene was targeted by two sgRNAs located in close proximity to increase the KO efficiency. First, the CRISPR RNA (crRNA) and the Trans-activating crRNA (tracrRNA) had to be annealed in a 1:1 ratio. The tracrRNA is identical for all genes and is essential for binding Cas9. The crRNA on the other hand provides specificity and guides the Cas9 protein to the target gene. The annealing was done as follows:

Temperature [°C]	Time [min]
78	10
37	0.5
36	0.5
34	1
32	1
30	1
28	1
26	1
24	1
22	∞

Afterwards, the nucleofection mix was prepared and incubated for 10 min at room temperature to allow RNP formation. It was prepared using the SG Cell Line 96-well Nucleofector™ Kit:

gRNA mix	5 µl
IDT Cas9 (c=62 µmol/l)	1.3 µl
Supplement	4.5 µl
Nucleofector™ solution	14.2 µl

Next, $5x10^5$ THP-1 cells were centrifuged for 5 min at 500 g washed with PBS and resuspended in 25 µl nucleofection mix. The mixture was transferred into a cuvette and nucleofected using the Lonza 4D-Nucleofector (protocol FF-100). Afterwards, cells were transferred into a 96-well

plate containing 200 µl prewarmed RPMI and incubated for 24 h at 37 °C. The next day cells were expanded into a 48-well and incubated another 24 h.

3.7.4 Monoclone generation by serial dilution

To obtain monoclones, cells were serially diluted. To this end, sorted (BLaER1) or unsorted (THP-1) cells were diluted and plated in a 96-well format. For BLaER1 cells three plates of each 4, 2 and 1 cell/well were plated. For THP-1 on the other hand six plates with only 1 cell/well were seeded. After 3-4 weeks grown colonies were re-formatted onto a new 96-well plate using a Beckmann Coulter Biomek FK robot. The genotype of picked cells was subsequently analyzed by deep sequencing.

3.7.5 K.O. Identification by deep sequencing

To analyze the genotype of generated monoclones a deep sequencing approach was performed using the illumina MiSeq (MiSeq reagent kit v2) device. Therefore, cells were lysed for 10 min at 65 °C using direct lysis buffer, followed by a heat inactivation step for 15 min at 95 °C. As it is essential for sequencing to label each amplicon with a unique barcode set, a two-step PCR approach was used. The first PCR specifically amplifies the gene of interest and generates an approximately 250 bp long DNA fragment located at the target site. Of note, it is essential for further analysis, that the targeted region is not within the first or last 50 bp of the amplicon. Furthermore, the primers carry overhanging adapter sequences, which serve as binding site for the second PCR primers rendering their sequence independent of the target sequence. The second PCR is essential to add a unique set of barcodes as well as the Illumina sequencing adapters to the PCR product. Therefore, 16 different forward and 24 different reverse barcode primers were mixed to obtain 384 unique primer combinations. All PCR products were then pooled subjected to agarose gel purification, precipitated and quantified. Both PCRs were performed using Phusion polymerase according to the supplier's protocol:

95 °C	3 min	
95 °C	30 sec	18 cycles
63 °C	30 sec	
72 °C	30 sec	
72 °C	3 min	
4 °C	∞	

Sequencing of the purified DNA was performed using an Illumina MiSeq device (MiSeq Reagent Kit v2, 300 Cycles, #MS-102-2002). Analysis of FastQ-files was done with help of the previously published web based tool "Outknocker" (Schmid-Burgk et al., 2014). This tool maps

the reads according to the barcodes as well as the amplicon sequence of the target gene and thereby identifies possible insertions or deletions. Only clones with both allelic out-of-frame insertion/deletions were picked. If possible 3-6 clones of each genotype were picked and tested for phenotypes.

3.8 Quantification and statistical analysis

If not otherwise indicated, statistical significance was determined by two-way ANOVA with Dunnett's or Tukey's correction for multiple testing using GraphPad Prism 8 (except for normalized LC/MS data): ****p ≤ 0.0001; *** p ≤ 0.001, ** p ≤ 0.01, * p ≤ 0.05, ns = not significant. If multiple comparisons are depicted with one comparison bar, the major tick of the comparison bar indicates the reference data to which the statements regarding the level of significance are made. LC/MS data was normalized by dividing the values of *RNASET2*$^{-/-}$ cells by the values of Ctrl cells. These values were then transformed into a Log_2 scale and a Welch's unequal variances t test was performed. Undetectable values were replaced with 1/10 of the lowest non-zero value of the corresponding dataset. The analysis was performed using R.

3.9 Data availability

BLaER1 RNA-Seq data can be accessed at Gene Expression Omnibus (GEO: GSE138913) or at Sequence Read Archive (SRA: SRP225808).

4 Results

4.1 TLR7 and TLR8 are functional TLRs in BLaER1 monocytes

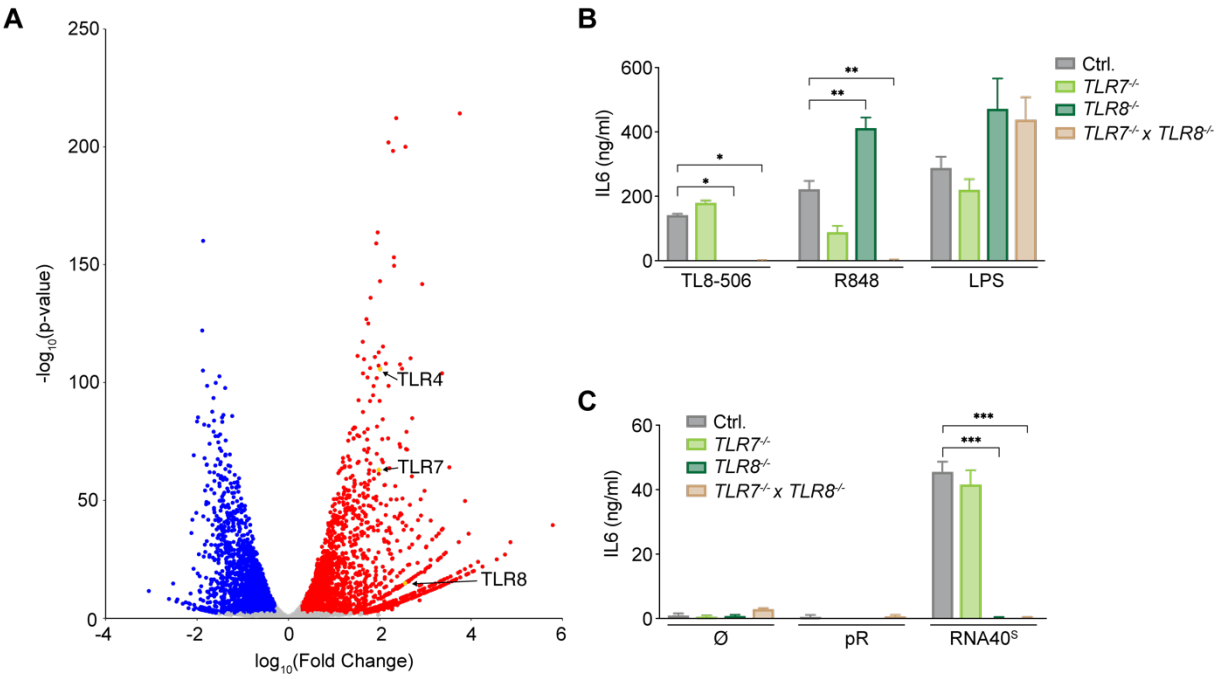

Figure 4.1 Characterization of TLR7 and TLR8 in BLaER1 cells

(A) Gene expression change of differentiated vs un- differentiated BLaER1 monocytes are shown as volcano plot with negative $\log_{10}$ p-values on the y-axis plotted against $\log_{10}$ changes in gene expression on the x-axis. Significantly upregulated genes are depicted in red whereas downregulated ones are shown in blue. Significance is defined by a p-value < 0.05 and absolute fold change > 2. The receptors TLR4, 7 and 8 are highlighted. **(B and C)** Differentiated BLaER1 cells of indicated genotype were stimulated with (B) TL8-506, R848 and LPS or (C) unstimulated, poly-L-arginine (pR) and transfected with RNA40^S. Supernatants were harvested 14 h after stimulation and analyzed by ELISA. Data are depicted as mean + SEM of three independent experiments. Statistical significance was calculated using two-way ANOVA: ***p ≤ 0.001; **p ≤ 0.01; *p ≤ 0.05; ns, not significant.

To study the activation mechanism of TLR8 we decided to exploit the BLaER1 cell system, which had already earlier been used to model human monocytes (Gaidt et al., 2017; Gaidt et al., 2016). This B-cell lymphoma cell line can be trans-differentiated into macrophage-like cells by adding a cytokines cocktail containing IL-3 and M-CSF as well as β-estradiol (Rapino et al., 2013). In these cells the endolysosomal receptors TLR7 and TLR8, recognizing ssRNA, are upregulated upon trans-differentiation. The same is true for the LPS sensor TLR4 which was stimulated as control (Figure 4.1A). As prototypic TLR8 agonist we used the well-established RNA40 ligand, a 20-mer ssRNA oligonucleotide (ON) derived from HIV-1 genome (Heil et al., 2004). In this study a modified version of RNA40 named RNA40^S was used, which has

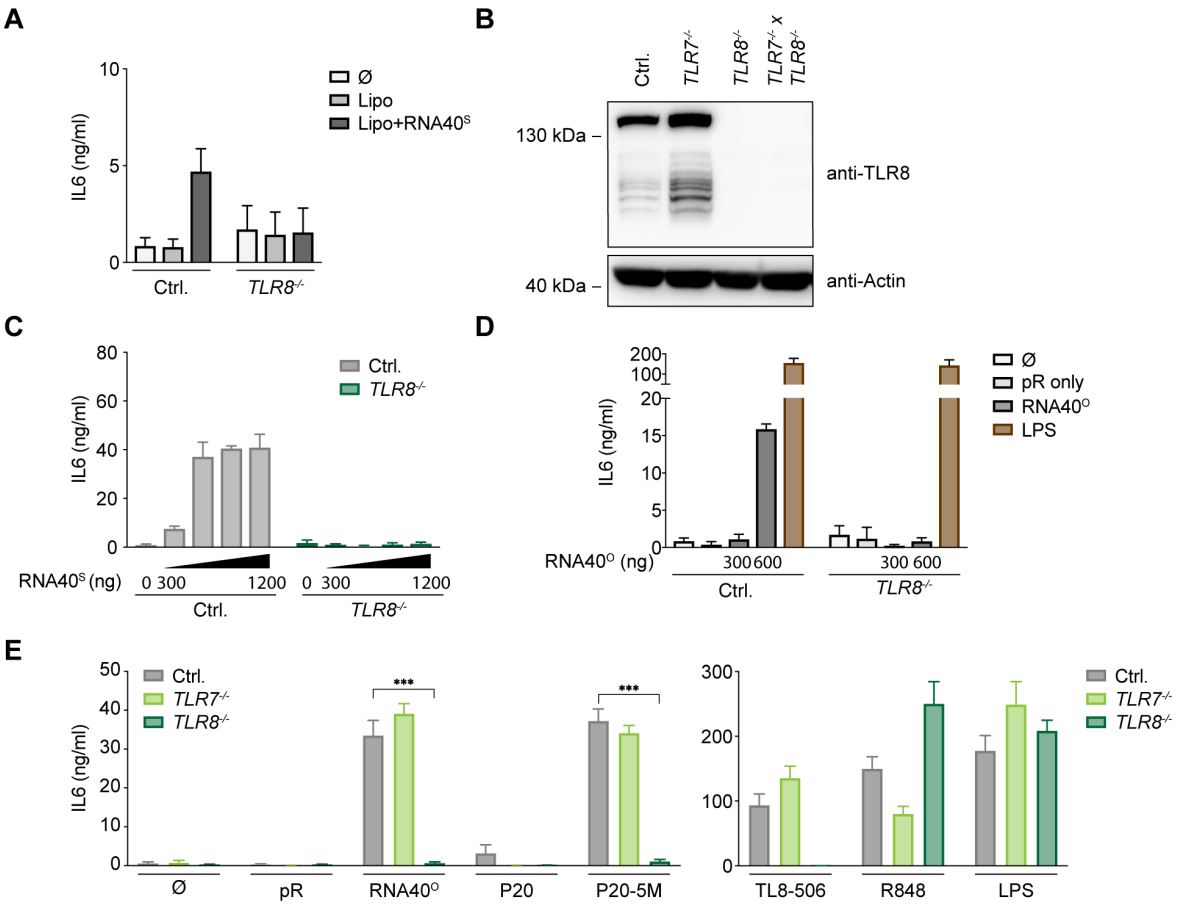

Figure 4.2 TLR7 and TLR8 are functional receptors in BLaER1 cells

(A) BLaER1 cells of indicated genotype were transfected with Lipofectamine 2000 either with or without RNA40^S. **(B)** TLR8 expression level in BLaER1 cells of indicated genotype was analyzed by immunoblotting. **(C)** Ctrl and *TLR8*$^{-/-}$ BLaER1 cells were stimulated with increasing amounts of RNA40^S. **(D)** BLaER1 cells were stimulated with increasing amounts of RNA40^O, LPS or were unstimulated. The unstimulated control shown in (A), (C) and (D) is the same as it is derived from the same experiment. **(E)** BLaER1 cells of indicated phenotype were stimulated with the indicated stimuli. P20 is a self-complementary RNA forming a hairpin structure, whereas P20-5M in only partially self-complementary and has single stranded stretches. All supernatants were harvested after 14 h and IL-6 was measured by ELSA. Data are depicted as mean + SEM of three (A, C and D) or four (E) independent experiments. Statistical significance was calculated using two-way ANOVA: ***p ≤ 0.001; **p ≤ 0.01; *p ≤ 0.05; ns, not significant.

phosphorothioate linked bases, instead of phosphodiester linkage. This protects it against degradation and increases its half-life compared to unmodified ONs. To deliver RNA40 specifically into the endolysosomal compartment, the polycationic polypeptide poly-L-arginine (pR) was used (Ablasser et al., 2009). As a proxy for TLR8 activation, the pro-inflammatory cytokine IL-6 was measured by ELISA, which gets expressed as a result of NF-κB activation downstream of the receptor. Stimulation of BLaER1 cells with either TL8-506 (TLR8 ligand), R848 (TLR7/8 ligand) or LPS (TLR4 Ligand) led to high IL-6 levels (Figure 4.1B). As expected, TL8-506 was TLR8 specific and IL-6 production was abolished in *TLR8*$^{-/-}$ cells. R848

on the other hand can activate TLR7 as well as TLR8 and cytokine production was only blunted if both receptors were absent. Stimulation only with the transfection reagent (pR) itself did not lead to any IL-6 release. TLR4 activation by its ligand LPS resulted in robust IL-6 expression in all tested genotypes. RNA40^{S} stimulation on the other hand, was completely TLR8 dependent (Figure 4.1C), which could also be observed after Lipofectamine transfection albeit at much lower levels (Figure 4.2A). The absence of TLR8 on a protein level in the respective cells was confirmed by western blot (WB) (Figure 4.2B). Increasing amounts of RNA40^{S} led to increased IL-6 release reaching a saturation at 600 ng (Figure 4.2C). Studying phosphodiester linked RNA40, from now on referred to as RNA40^{O}, also led to dose dependent IL-6 release, albeit resulting in lower cytokine levels compared to RNA40^{S} (Figure 4.2D). Similar results were obtained by stimulating with an unrelated phosphodiester linked RNA named P20-5M (Figure 4.2E). Whereas control BLaER1 monocytes produced robust amounts of IL-6 in response to P20-5M, *TLR8*$^{-/-}$ cells were unresponsive. As already published, a self-complementary version of the ON (P20) was not able to stimulate TLR8 at all (Ablasser et al., 2009). These results indicate that a certain degree of ssRNA is needed for TLR8 activation. All in all, these data establish the BLaER1 cells system as a good model to investigate the RNA dependent activation mechanism of TLR8 in the human context.

4.2 RNase T2 deficient cells fail to respond to RNA oligonucleotides

In 2015 the crystal structure of TLR8 was solved and reveled that the receptor has two distinct binding sites. The first binding site is occupied by a single nucleotide (uridine) whereas the second pocket can bind to small RNA fragments like di- or tri-nucleotides (Tanji et al., 2015). Furthermore, it is known, that DNase II is generating appropriate ligands for TLR9 by degradation, upstream of the receptor (Chan et al., 2015). Therefore, we hypothesized, that there must most likely be an enzyme with RNase activity upstream of TLR8 generating small RNA fragments needed for its activation. To address this question, we performed an RNA sequencing analysis of several cell lines. We focused on proteins, which according to their gene ontology (GO) terms are annotated as either lysosomal, extracellular space or ribonuclease activity (Figure 4.3A). Only the four RNases *RNASE2*, *RNASE3*, *RNASE6* and *RNASET2* matched all three conditions, however, as only *RNASE2*, *RNASE6* and *RNASET2* were highly expressed in differentiated BLaER1 cells as well as in primary human monocytes we initially focused on these three. Additionally, we included *RNASE1* as it is highly expressed in differentiated BLaER1 monocytes (Figure 4.3A, right panel). Using the CRISPR/Cas9 system we generated *RNASE1*$^{-/-}$, *RNASE2*$^{-/-}$, *RNASE6*$^{-/-}$ and *RNASET2*$^{-/-}$ single KOs in BLaER1 cells and stimulated them with RNA40^{S}. Studying the respective KO cell lines reveled a complete loss-of-function phenotype for *RNASET2*$^{-/-}$ cells (Figure 4.3B), whereas the other three RNase KOs

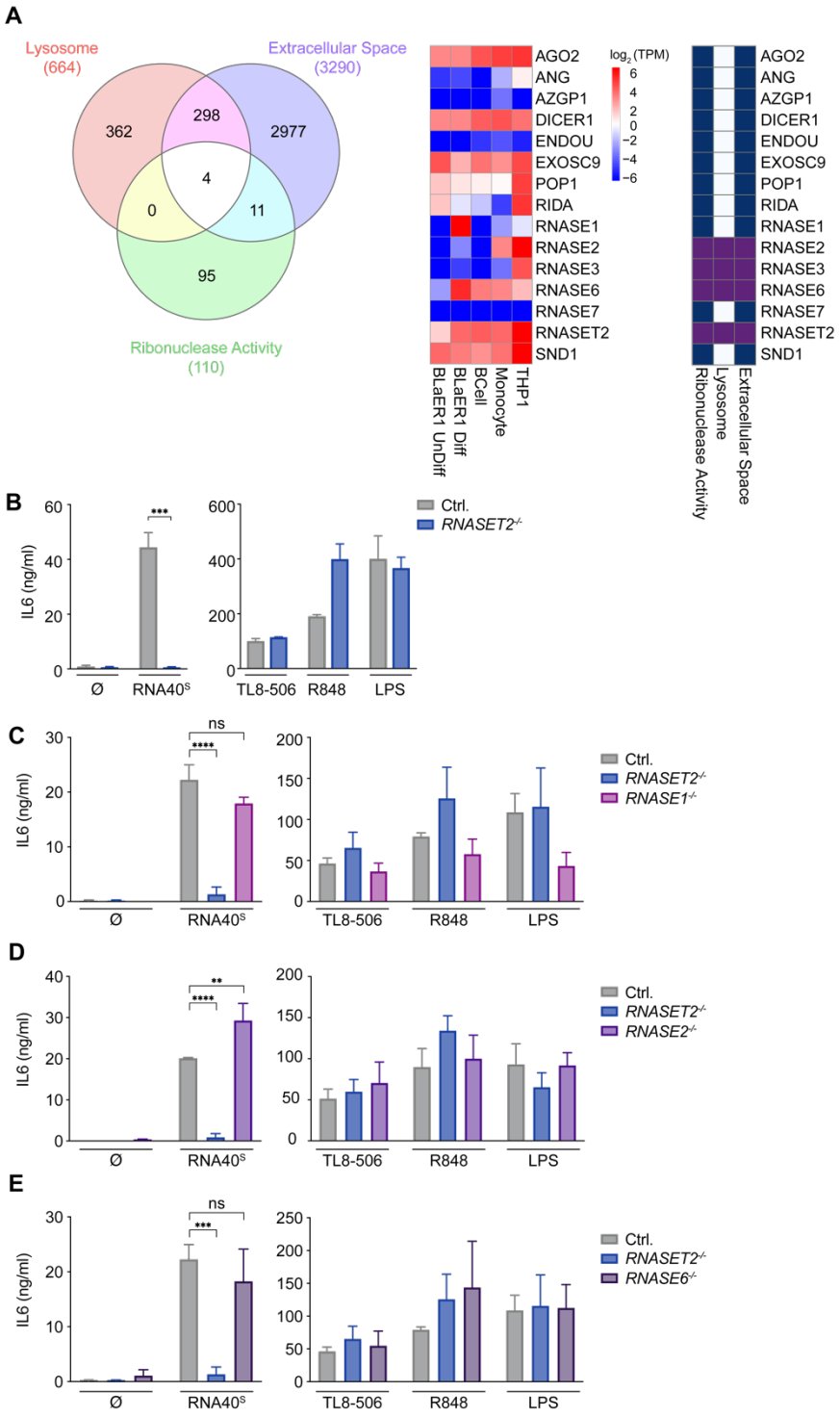

Figure 4.3 *RNaseT2*$^{-/-}$ cells do not produce IL-6 upon RNA40 stimulation

(A) Venn diagram of proteins which are due to their Gene Ontology (GO) term annotated as "lysosomal", "extracellular space" or "ribonuclease activity" (left panel). Heat map displaying gene expression of diverse RNases in different cell types (middle panel). Heat map of the same RNases with their corresponding GO terms (right panel) **(B)** Ctrl and *RNASET2*$^{-/-}$ BLaER1 cells were stimulated with RNA40^{S}, TL8-506, R848 and LPS. **(C-E)** BLaER1 cells of indicated genotypes were either unstimulated or stimulated with RNA40^{S}, TL8-506, R848 and LPS. Controls of *RNASE1*$^{-/-}$ and *RNASE6*$^{-/-}$ are indicial as they derive from the same experiment. Data are depicted as mean + SEM of three independent experiments. Statistical significance was calculated using two-way ANOVA: ****p ≤ 0.0001; ***p ≤ 0.001; **p ≤ 0.01; *p ≤ 0.05; ns, not significant.

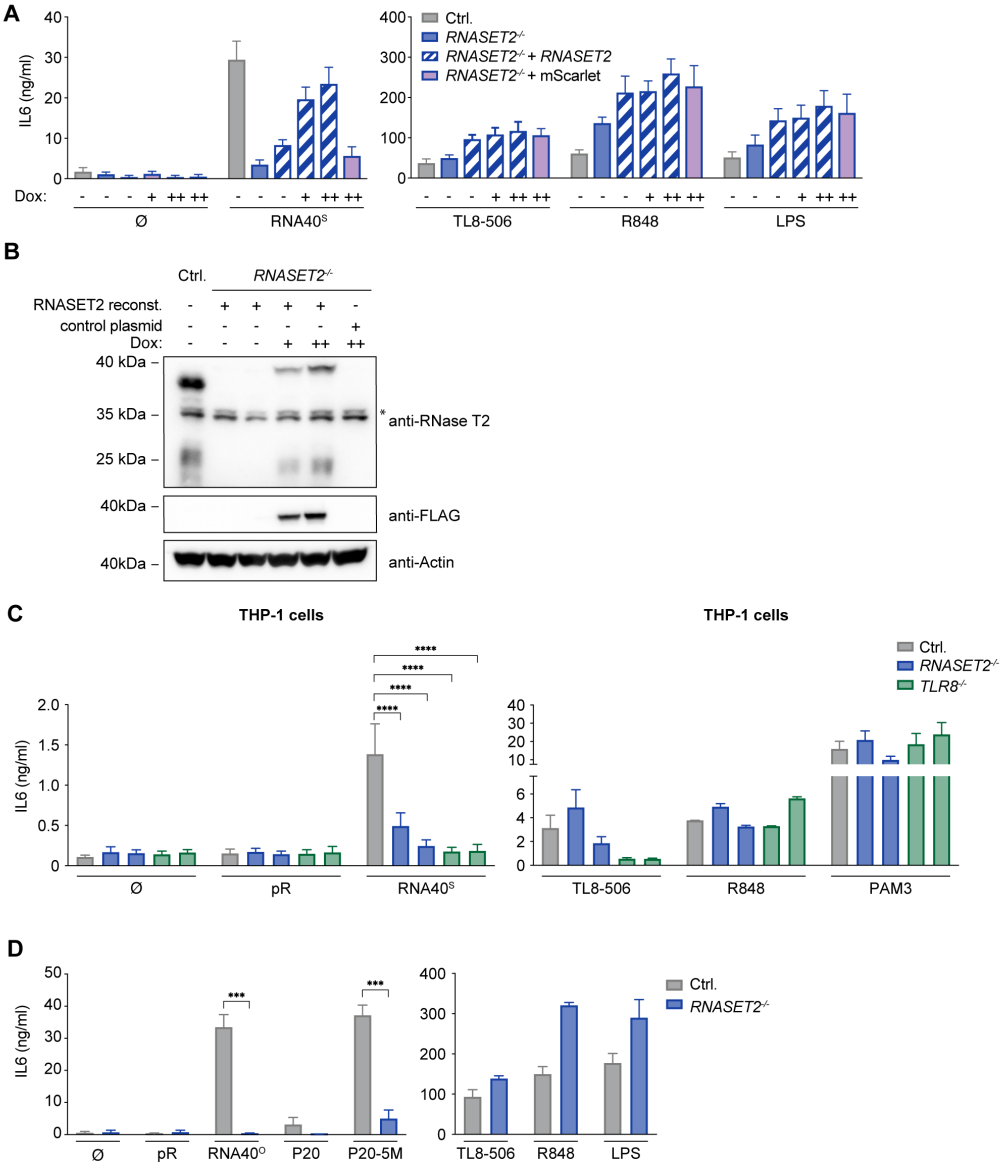

Figure 4.4 RNASE T2 deficiency can be rescued by lentiviral transduction of *RNASET2*

(A) Lentiviral delivery was used to reconstitute *RNASET2*$^{-/-}$ cells with either *RNASET2* or mScarlet (control). Gene expression was induced by doxycycline (++, 1 µg/ml; +, 0.5 µg/ml). **(B)** Immunoblot corresponding to the stimulation experiment in (A). Unspecific bands are indicated by asterisk. **(C)** THP-1 cells were differentiated with PMA and stimulated with poly-L-arginine (pR), RNA40^{S}, TL8-506, R848 or PAM3. **(D)** BLaER1 cells of indicated genotype were stimulated as shown. Data of Ctrl cells are identical to the ones in Figure 4.2E as they derive from the same experiment. All stimulations were carried out for 14 h prior to IL-6 measurement. Data are depicted as mean + SEM of three (A-C) or four (D) independent experiments. Statistical significance was calculated using two-way ANOVA: ****p ≤ 0.0001; ***p ≤ 0.001; **p ≤ 0.01; *p ≤ 0.05; ns, not significant.

did not lead to decreased IL-6 levels (Figure 4.3C-E). Interestingly, knocking out RNase T2 only led to blunted IL-6 levels upon RNA40^{S} stimulation, but not upon TL8-506, R848 or LPS treatment. This indicates that RNase T2 has no impact on TLR8 activation per se, rather it is functioning upstream of it. The *RNASET2*$^{-/-}$ phenotype in BLaER1 cells upon RNA40^{S} stimulation

could, however, be rescued by lentiviral transduction of *RNASET2* (Figure 4.4A). After doxycycline induction IL-6 levels could be increased in a dose dependent manner nearly reaching wild type (WT) levels. The lack of RNase T2 as well as its increasing amounts after doxycycline induction could also be visualized by western blotting (Figure 4.4B). Similar results were obtained in THP-1 cells, knocking out *RNASET2* or *TLR8* (Figure 4.4C). Whereas control THP-1 cells released robust amounts of IL-6 after RNA40^{S} stimulation, it was significantly reduced in both *RNASET2*$^{-/-}$ and *TLR8*$^{-/-}$ cells. Finally, we also tested the self-complementary ON P20 as well as the partially single stranded ON P20-5M in BLaER1 KO cells, showing that stimulation with P20-5M is significantly dependent on RNase T2 (Figure 4.4D). These data indicate that RNase T2 is critically and non-redundantly required to render RNA strands agonistic upstream of TLR8.

4.3 RNase T2 cleaves RNA between purine bases and uridine

The previous results led to the conclusion, that RNase T2 is likely to function upstream of TLR8 generating ligands for either its first or second binding pocket by RNA degradation. To further investigate this theory, we generated recombinant RNase T2 enzyme for subsequent *in vitro* analysis. Degradation of RNA40^{S} with increasing amounts of recombinant RNase T2 showed a very specific degradation pattern resulting in distinct fragments. Interestingly, the degradation products were substantially different from the ones obtained by digesting RNA40^{S} with bovine pancreatic RNase A which is orthologous to human RNase 1 (Figures 4.5A and B). To investigate the exact composition of these *in vitro* digests, RNase T2 as well as RNase A degradation mixtures were analyzed by HLPC and MALDI-TOF (all mass spectrometry experiments were measured by Mirko Wagner) (Figure 4.5C). Of note, to identify the cleavage pattern we initially studied degradation of RNA40^{O}, as the analysis of RNA40^{S} by HPLC is drastically more difficult: the phosphorothioate backbone of RNA40^{S} leads to numerous diastereomers which all behave unique during HPLC separation, resulting in less defined peaks of each product. HPLC analysis revealed at least nine distinct peaks of which eight could be assigned to the according masses by MALDI-TOF. In the next step we tried to match the found masses with the calculated masses of possible RNA40^{O} degradation products. As RNA40 is not very complex in terms of sequence, especially short fragments tend to have very similar masses, making it significantly harder to analyze. To this end, we assigned the found peaks not only by mass, but also by the notion that found fragments must in the end add up to a full-length RNA40 molecule. This allowed us to unequivocally identify six fragments (all terminal ones) and two with high probability (Figure 4.5D). Interestingly, the found degradation products were in line with a cleavage activity of RNase T2 between guanosine and uridine (GU).

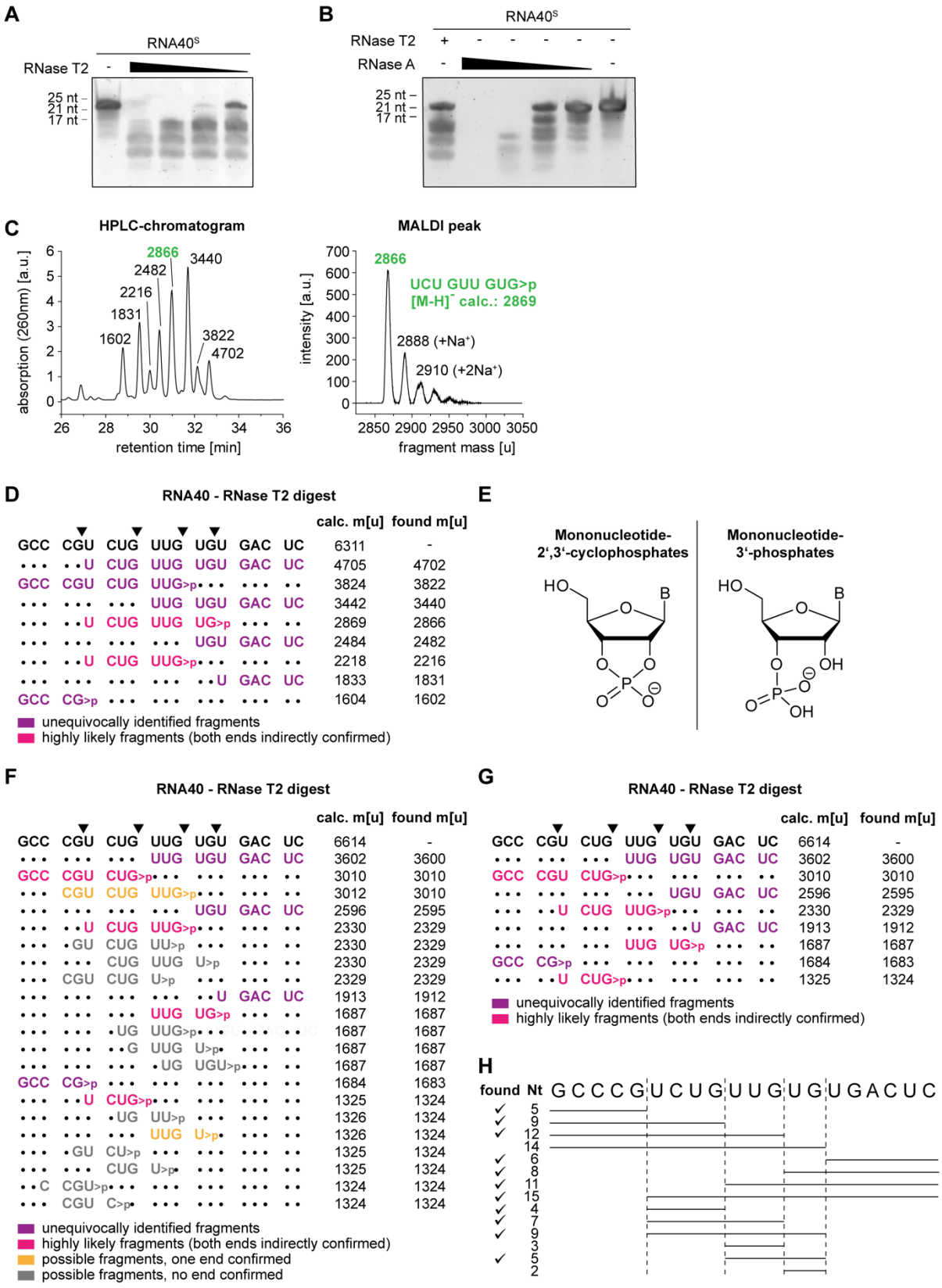

Figure 4.5 *In vitro* digest of RNA40 by RNase T2

(A and B) Urea gel of RNA40^S digested with decreasing amounts of either RNaseT2 (A) or RNase A (B). One representative gel of two independent experiments is shown. **(C)** The HPLC chromatogram of RNase T2 digested

RNA40^{O} fragments is shown (left, masses were determined by MALDI-TOF) and the corresponding MALDI peaks of a representative peak marked in green (right). **(D)** RNA40^{O} was digested *in vitro* with RNase T2. The analysis was performed using HPLC and MALDI-TOF. All found fragment masses (based on the MALDI-TOF analysis) are shown and were assigned to the most likely ONs. All calculated and found masses are depicted as $[M-H]^-$. **(E)** Shown are the structures of mononucleotide 2',3'-cyclophosphates (left) and Mononucleotide 3'-phosphates (right). (**F)** RNA40^{S} was digested with RNase T2 and analyzed by HPLC and MALDI-TOF. Shown are all possible fragments theoretically fitting to the found masses of the digest. The color code indicated the probability with which the masses could be assigned to the shown fragments. All fragment masses are shown as $[M-H]^-$. **(G)** Depicted are the most likely assigned fragments from the analysis in (F). **(H)** All theoretically possible fragments of RNA40 digested with RNase T2 are shown assuming that the enzyme can only cleave between G and U. The ticks in front of each fragment indicate if it could be found in one of the MALDI-TOF analysis.

Moreover, all ONs cleaved at their 3' end had a 2'- 3'-cyclophosphate rather than a 3'-phosphate configuration (Figure 4.5E). This is, however, in line with the published cleavage mechanism of RNase T2 suggesting a 2'- 3'-cyclophosphate configuration as an intermediate state which can then be hydrolyzed to an open 3'-phosphate (MacIntosh, 2011). Yet, hydrolysis seems to be quite inefficient under the used reaction conditions. Performing analogous experiments with RNA40^{S} showed comparable results, well in line with the notion of RNase T2 cleaving RNA between guanosine and uridine (Figure 4.5G). Interestingly, the same 2'- 3'-cyclophosphate configuration at the 3' end of cleaved fragments was found. Additionally, all possible fragments (according to their mass) were listed and color coded by their probability (Figure 4.5F). Like for RNA40^{O} all uncertain fragments were allocated according to the unequivocally identified ONs. Taken together, assuming RNase T2 is only capable of cleaving between guanosine and uridine, 11 out of 14 possible fragments of RNase T2 digested RNA40 could be assigned by mass spectrometry (Figure 4.5H).

To confirm the unique cleavage pattern of RNase T2 we repeated the degradation experiments, using RNase A instead of RNase T2. This analysis revealed, like already indicated by *in vitro* digested RNA40^{O}, a fundamentally different cleavage pattern. RNase A preferentially cuts RNA after pyrimidines (uridine or cytidine), which is in line with the already published literature. As observed for RNase T2 degradation, fragments digested by RNase A were likewise terminated by a 2'- 3'-cyclophosphate structure (Figure 4.6A). As RNA40 does not have a very complex sequence and therefore is not allowing the investigation of the exact substrate specificity of RNase T2, we switched to 16 different ONs containing all possible dinucleotide combinations. The ONs were flanked by adenosines and had the following sequence: A_4-NN-A_2 (Figure 4.6B). Due to their asymmetry, the cleavage products could easily be analyzed by LC-MALDI-TOF (Figure 4.6C) and revealed cleavage of RNase T2 between guanosine and uridine (GU) as well as between adenosine and uridine (AU) residues with comparable efficiency. This renders the cleavage specificity of RNase T2 to purine uridine (RU). Of note, no cleavage of the self-complementary RNA P20 was observed when digested with

RNase T2 whereas the partially single stranded RNA P20-5M was readily cleaved (Figure 4.6D). This indicates, that RNase T2 is not capable of cutting base-pairing RNA but rather needs ssRNA as a template, providing a rationale as to why ONs like P20 do not exert TLR8 activity (Ablasser et al., 2009). Together, these results indicate that under the conditions tested, RNase T2 is preferentially cleaving ssRNA between purine and uridine (RU) residues resulting in 2'- 3'-cyclophosphate terminated fragments.

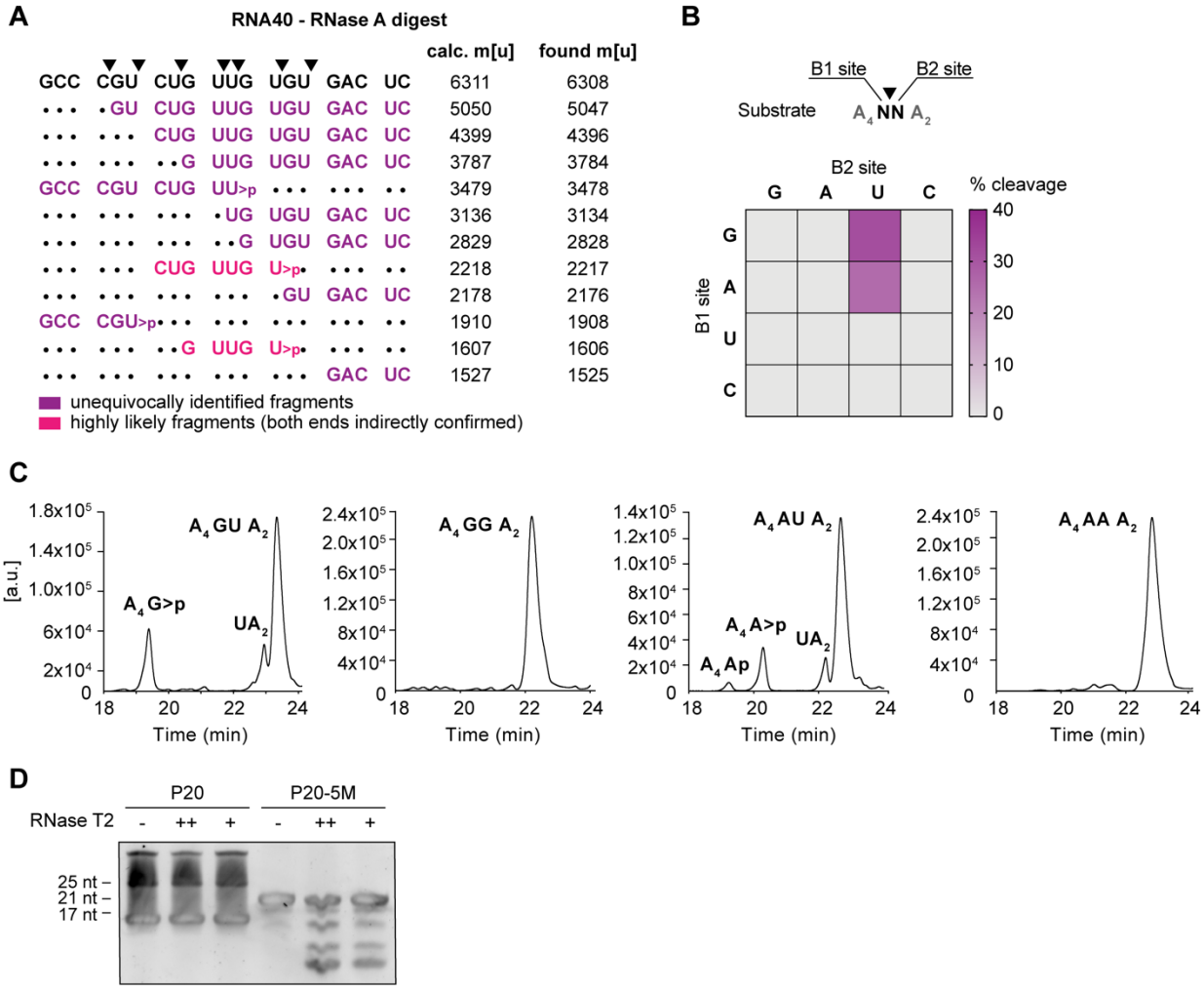

Figure 4.6 RNase T2 cleaves RNA between purine bases and uridine

(A) RNA40^{O} was *in vitro* digested with RNase A and analyzed as described above. All found and calculated masses are depicted as $[M-H]^-$. **(B)** To investigate the cleavage site of RNase T2, 16 ONs were digested carrying all possible dinucleotide combinations (A_4NNA_2) and analyzed by HPLC and MALDI-TOF. Of note, all ONs with uridine at the B1 site were cleaved between A and U but not between U and N. **(C)** HPLC chromatogram from the cleavage analysis in (G) corresponding to the ONs with the sequence GU, GG, AU and AA. **(D)** Urea gel of the *in vitro* digested ONs P20 and P20-5M are shown. P20 is a self-complementary RNA fragment forming a hairpin structure, whereas P20-5M is only partially self-complementary resulting in single stranded RNA stretches. One of two representative gels is shown.

4.4 Altered RNA catabolism *in cellulo* in the absence of RNase T2

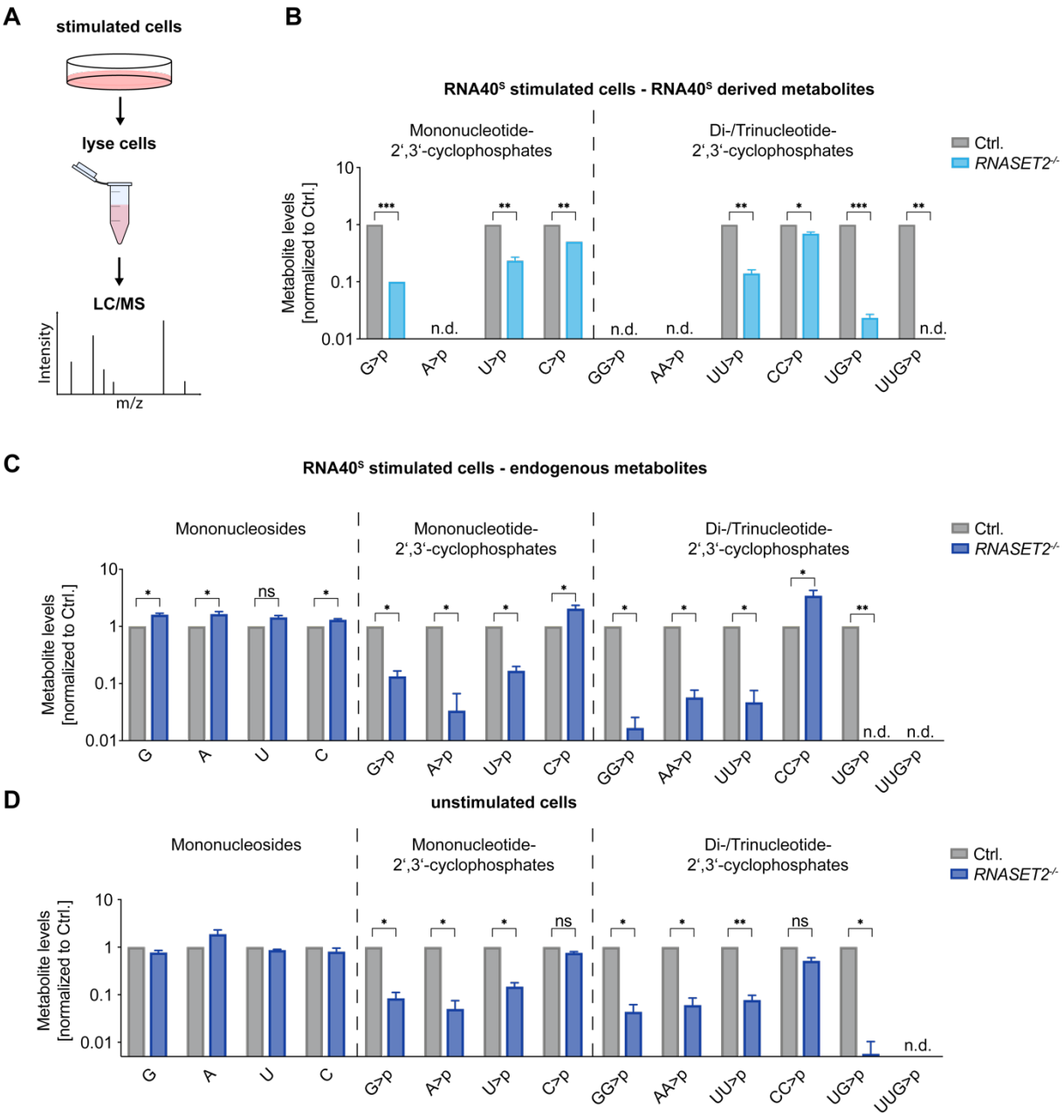

Figure 4.7 RNase T2 deficiency leads to altered RNA metabolism

(A) Schematic overview of experimental workflow: BLaER1 cells were stimulated with RNA40^S for 14 h, lysed and analyzed by liquid chromatography mass spectrometry (LC-MS). **(B and C)** Ctrl and *RNASET2*$^{-/-}$ cells were stimulated with RNA40^S and analyzed by LC-MS. RNA40^S derived metabolites are shown in (B) whereas endogenous ones are shown in (C). Data are normalized to Ctrl cells (note logarithmic scale). **(D)** Whole cell lysate of BLaER1 cells with indicated genotype was analyzed by LC-MS. All data are normalized to Ctrl cells. Statistical significance was calculated using the Welch's unequal variances test: ***p ≤ 0.001; **p ≤ 0.01; *p ≤ 0.05; ns, not significant.

Once the cleavage site of RNase T2 was determined we wanted to address the question, how the enzyme is affecting RNA catabolism *in cellulo*. To this end, we designed a mass

spectrometry approach to measure the abundance of specific metabolites generated by RNase T2, ranging from single nucleosides up to certain trinucleotides (Figure 4.7A). To distinguish between endogenous and stimulation derived fragments, cells were treated with RNA40^{S}, as the backbone modification (oxygen atom is replaced with a sulfur atom) resulted in heavier metabolites allowing the identification of RNA40^{S} derived fragments. To assign the found masses to the appropriate metabolite, we either made use of synthetic standards or of obtained data from RNA40 *in vitro* digests. This allowed us to unequivocally identify mononucleotides as well as di- or trinucleotides with a 2'-3'-cyclophosphate moiety from either endogenous origin or RNA40^{S} degradation.

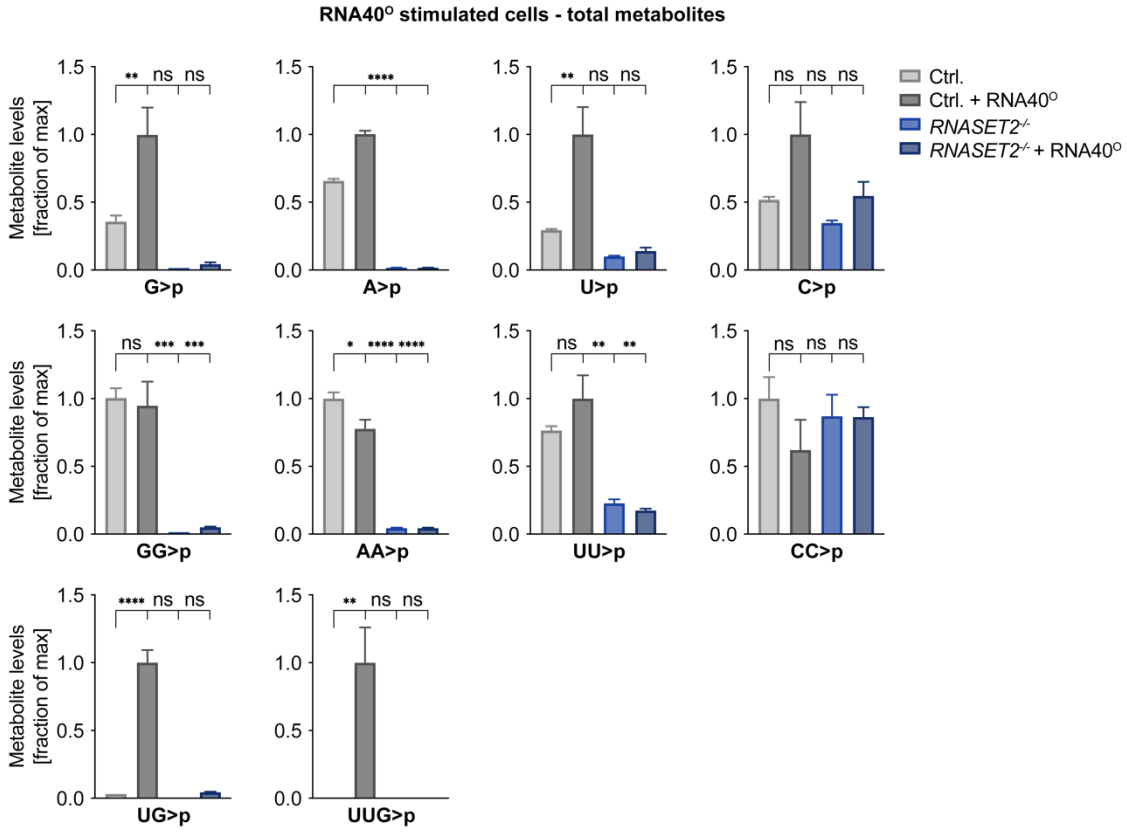

Figure 4.8 Total metabolites of RNA40^{O} stimulated Ctrl and *RNASET2*$^{-/-}$ cells

BLaER1 cells of indicated genotypes were either unstimulated or stimulated with RNA40^{O}. Cell lysates were analyzed by LC-MS. The mean of the highest vale was determined for each metabolite and data are depicted as a fraction thereof. Data are depicted as mean + SEM of three experiments. Statistical significance was calculated using one-way ANOVA: ****p ≤ 0.0001; ***p ≤ 0.001; **p ≤ 0.01; *p ≤ 0.05; ns, not significant.

The analysis of RNA40^{S} derived metabolites containing a 2'-3'-cyclophosphate configuration showed only a slight drop of C>p and CC>p whereas G>p was decreased over 90% in the absence of RNase T2 (Figure 4.7B). Of note, the level of U>p and UU>p was also greatly reduced, whereas A>p could not be detected in either control or *RNASET2*$^{-/-}$ cells. The metabolites GG>p and AA>p could also not be detected, however, this is expected as they are

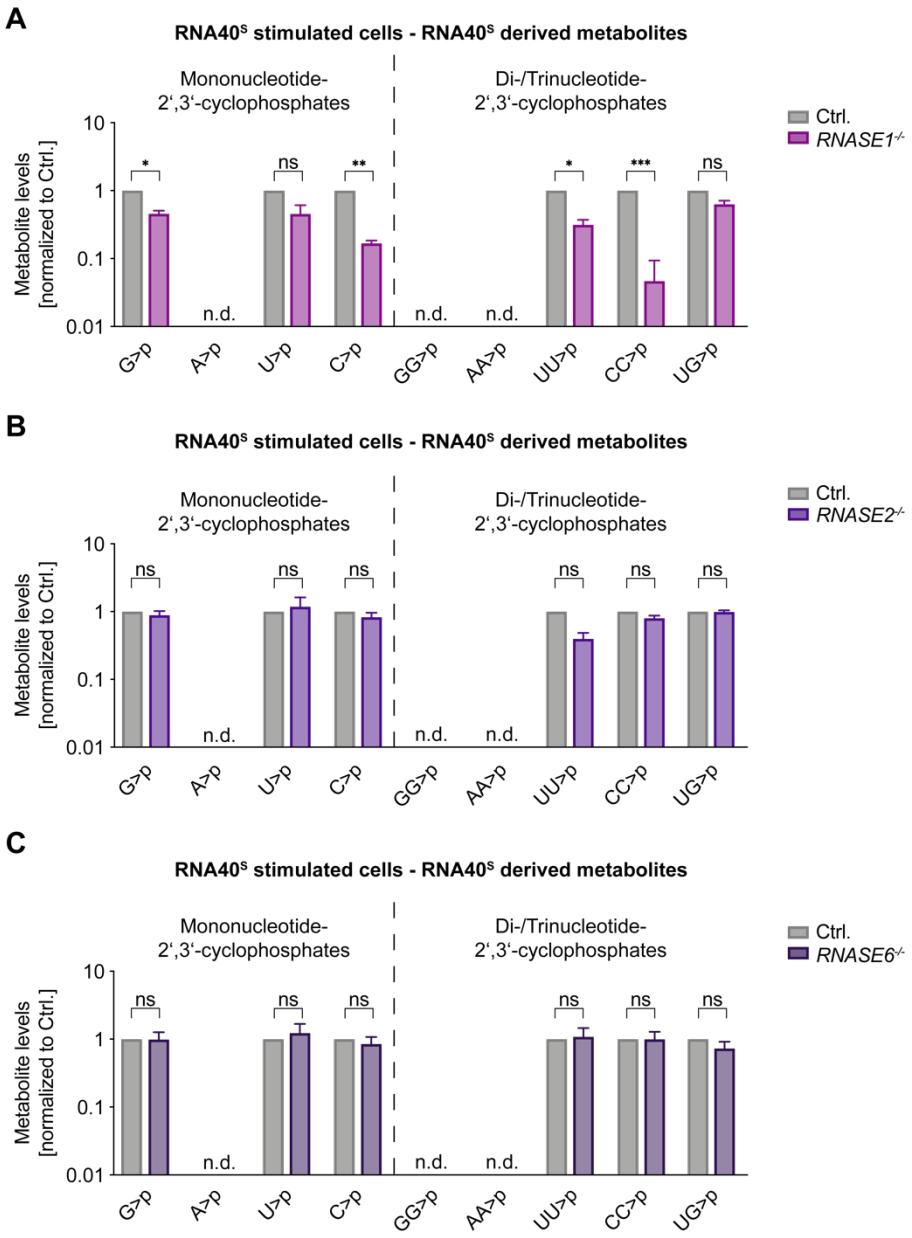

Figure 4.9 Deficiency in RNase A family enzymes leads to altered metabolism distinct from *RNASET2*$^{-/-}$ cells
(A-C) *RNASE1*$^{-/-}$, *RNASE2*$^{-/-}$ and *RNASE6*$^{-/-}$ BLaER1 cells were stimulated with RNA40^{S}, lysed and analyzed by LC-MS. RNA40^{S} derived metabolites are shown and data are normalized to Ctrl cells (note logarithmic scale). All stimulations were carried out for 14 h. Data are depicted as mean + SEM of three independent experiments. Statistical significance was calculated using a Welch's unequal variances t test: ***p ≤ 0.001; **p ≤ 0.01; *p ≤ 0.05; ns, not significant.

not contained in RNA40. Strikingly, the signal of UG>p and UUG>p was robust in control cells whereas the metabolites could barely or not be detected in the absence of RNase T2. Intriguingly, analyzing endogenous metabolites (non-sulfur backbone) in either RNA40^{S} stimulated (Figure 4.7C) or unstimulated cells (Figure 4.7D), largely reflected the results obtained by RNA40^{S} derived degradation products. Similar to RNA40^{S} derived metabolites the level of endogenous C>p and CC>p was largely unaffected in the absence of RNase T2, whereas

U>p, UU>p, UG>p and G>p were significantly reduced. While A>p, AA>p and GG>p could not be detected among RNA40^{S} degradation products, they could readily be identified in the endogenous pool showing significant dependence on RNase T2. For UUG>p on the other hand, it was the other way around: while it could be detected after RNA40^{S} stimulation, it was not found among the endogenous pool, indicating an important role during cell stimulation. However, mononucleotide levels were unaffected under either RNA40^{S} stimulated or unstimulated conditions. These results offer insights about the origin of metabolites during the course of stimulation and their relative abundance in a RNase T2 dependent manner. However, they cannot provide information about the absolute increase of metabolites after stimulation compared to endogenous levels.

To address this question, cells were stimulated with RNA40^{O} to obtain metabolites indistinguishable from the endogenous pool, to monitor the global change of RNA degradation products *in cellulo* (Figure 4.8). This experiment revealed a moderate increase in metabolite levels of G>p, A>p, U>p and C>p (2.8-, 1.5-, 3.4-, and 1.9-fold) after RNA40 treatment as well as a RNase T2 dependence for G>p, A>p and U>p. Of note, U>p was less dependent on RNase T2 than G>p or A>p. As already observed in previous experiments, the level of C>p and CC>p was neither significantly altered after RNA stimulation nor in the absence of RNase T2. Levels of GG>p, AA>p and to a lesser extend UU>p were dependent on RNase T2, however, they were virtually unaffected by RNA40^{O} stimulation. Intriguingly, the metabolites UG>p and UUG>p could almost exclusively be detected after RNA40^{O} stimulation and were completely dependent on RNase T2. Stimulation resulted in 33-times higher UG>p levels, whereas UUG>p could not even be detected in unstimulated cells. This indicates an important role for both metabolites in the course of RNA stimulation. Of note, loss of RNase A family members like *RNASE2* or *RNASE6* did not alter RNA40^{S} derived metabolites in any fashion (Figure 4.9B and C), solely *RNASE1* deficient cells showed a drop in C>p and CC>p levels (Figure 4.9A). Together these results indicate a critical role of RNase T2 in generating certain metabolites with a 2'-3'-cyclophosphate moiety from either endogenous or exogenous origins. Most strikingly, UG>p and UUG>p were completely RNase T2 dependent and exclusively found after RNA stimulation.

4.5 A minimal motif for TLR8 activation

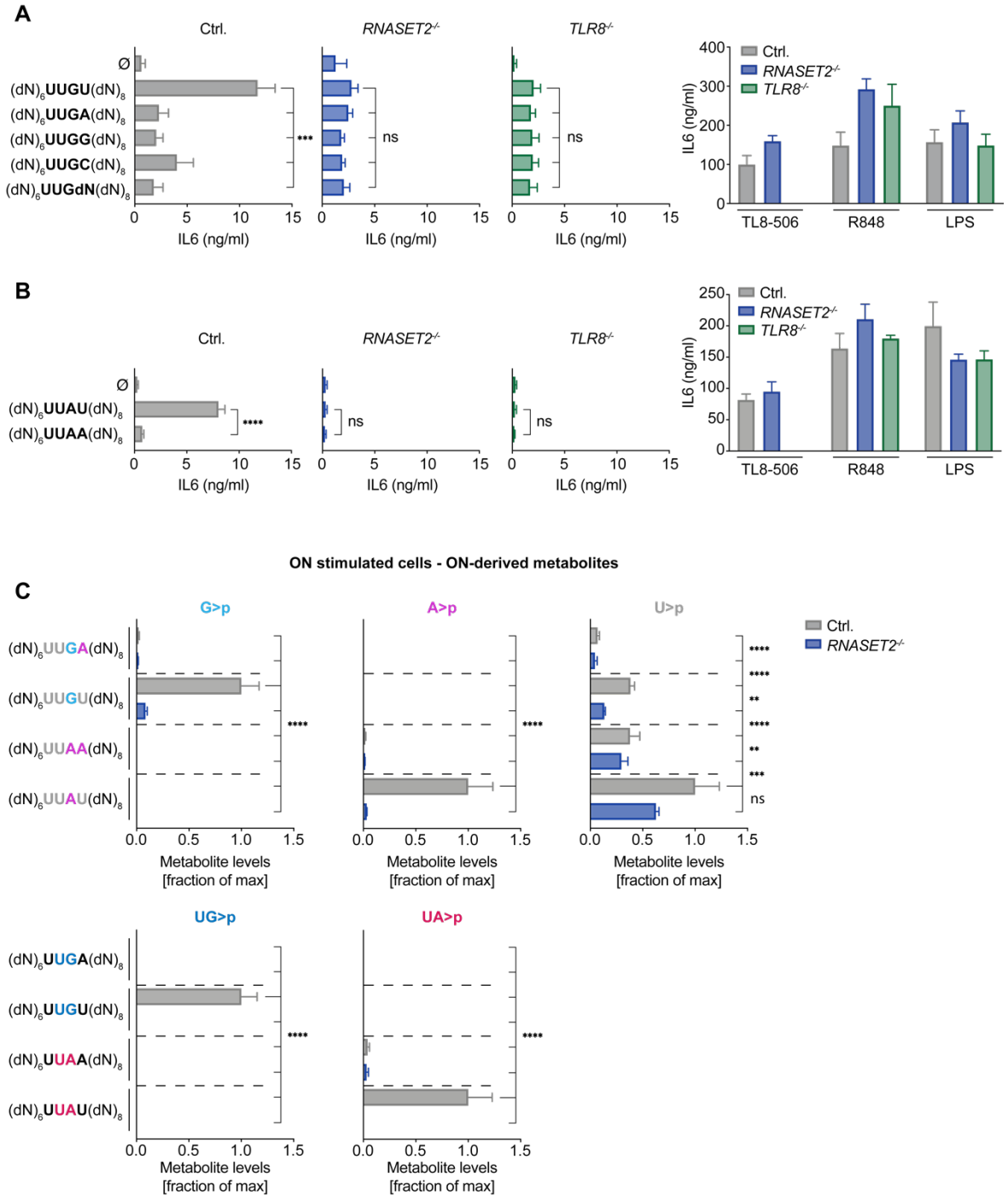

Figure 4.10 A minimal motif for TLR8 activation

(A and B) BLaER1 cells of indicated genotype were stimulated with DNA-RNA hybrids $(dN)_6UUNN(dN)_8$. The four middle bases are ribonucleotides which are flanked by random deoxyribonucleotides. As control, cells were stimulated with TL8-506, R848 and LPS. All supernatants were harvested after 14 h and analyzed by IL-6 ELISA. **(C)** BLaER1 cells of indicated genotype were stimulated with the shown DNA-RNA hybrid oligos and analyzed after 14 h by LC-MS. The mean of the highest vale for each dataset was determined and data are depicted as fractions thereof. Data are depicted as mean + SEM of three independent. Statistical significance was calculated using two-way ANOVA (A and B) or one-way ANOVA (C): ****p ≤ 0.0001; ***p ≤ 0.001; **p ≤ 0.01; *p ≤ 0.05; ns, not significant.

The results above indicate a critical role of UG>p in the course of TLR8 activation. As RNA40 is harboring four GU dinucleotides in its sequence, we switched to oligos containing a minimal motif for TLR8 activation flanked by non-stimulatory sequences. To this end, it was already published that UUGU in the context of deoxyribonucleotides ($(dN)_6UUGU(dN)_8$) leads to pro-inflammatory cytokine release in human myeloid cells, downstream of TLR8 activation (Forsbach et al., 2008). These results are in line with our previous finding, that RNase T2 is capable of cleaving RNA between guanosine and uridine residues explaining its TLR8 agonistic activity. As this hybrid ON offers an excellent platform to investigate the minimal motif for TLR8 activation, we stimulated BLaER1 cells with a phosphorothioate stabilized version of it. Indeed treating cells with $(dN)_6UUGU(dN)_8$ led to IL-6 release in a RNase T2 and TLR8 dependent manner, albeit at lower level then RNA40 (Figure 4.10A). Exchanging the terminal uridine by any other possible ribonucleotide or a random deoxyribonucleotide confirmed the previously found sequence specificity of RNase T2, as all of them rendered the ON non-immunostimulatory. This underlines the importance of uridine at the second position of the cleavage site, being essential to render the ON TLR8 agonistic. As the previous published data showed immunostimulatory effects not only for GU- but also AU-rich ONs the question arouse, whether AU-rich sequences also lead to the release of pro-inflammatory cytokines in a RNase T2 and TLR8 dependent manner. To this end, we modified the RNA bases within the hybrid ON to UUAU or UUAA and tested them in stimulation assays. In line with our previous results only UUAU but not UUAA resulted in RNase T2 as well as TLR8 dependent induction of pro-inflammatory cytokines (Figure 4.10B). To further support these data, ON derived metabolites were measured by LC-MS *in cellulo*. As expected, we could observe increased G>p and UG>p levels exclusively in cells stimulated with UUGU, in a completely RNase T2 dependent fashion (Figure 4.10C). The same could be observed for adenosine containing oligos: only cells stimulated with UUAU but not UUAA showed RNase T2 dependent increase of A>p and UA>p levels. Intriguingly, U>p levels were largely uncoupled from the stimulatory capacity of used ONs. Stimulation with the immunostimulatory UUGU ON led to equal U>p level compared to the non-activating UUAA ON. Furthermore, U>p level of UUAA was largely independent of RNase T2, whereas for UUGU a clear dependence could be observed. In line with these results, UUAU led to the highest induction of U>p in a partially RNase T2 dependent manner. Together this data suggests that, UURU is a minimal motif for RNase T2 dependent TLR8 activation. Furthermore, the release of at least a dinucleotide with the sequence UR>p seems to be critically required for TLR8 activation, however, exclusively increased U>p level seems to be insufficient to trigger an immune response under physiological conditions.

4.6 RNase T2 degradation products bypass the lack of RNase T2 to exert TLR8 agonism

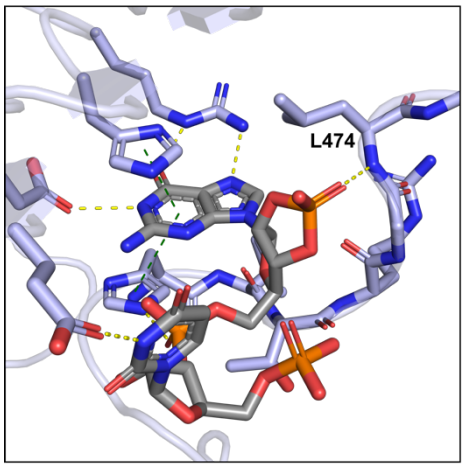

Figure 4.11 Crystal structure of the second TLR8 binding pocket
Part of the TLR8 crystal structure showing the second binding pocket of the protein bound to UG>p (PDB, 4R07). Yellow dashed lines indicate hydrogen bonds whereas green lines show π-π-interactions. The following color code was used: nitrogen, blue; oxygen, red; phosphor, orange; carbon, light blue and gray.

Some years ago the crystal structure of TLR8 was solved revealing the binding of YG as well as YYG di- or trinucleotides with a 2'- 3'-cyclophosphate configuration to the second pocket of TLR8 (Figure 4.11) (Tanji et al., 2015). They found, that the cyclophosphate structure of these oligonucleotides was coordinated by the amino bond of residue L474. These results, together with our previous data are in line with the notion, that RNase T2 derived metabolites could play a critical role in TLR8 activation. Therefore, we hypothesized that RNase T2 is essential to generate ligands with (Y)YG>p motif, fitting into the second binding pocket of TLR8. To test if TLR8 can be directly activated by delivering second pocket ligands, we digested RNA40^S *in vitro* with either RNase T2 or RNase A and stimulated BLaER1 cells with the respective degradation mixture (Schematic overview, Figure 4.12A). Of note, for RNA40^S digests with RNase A, three different concentrations were used reaching from complete degradation (+++) to partial degradation with distinct bands (+) (Figure 4.12B), whereas for RNase T2 only undercutting conditions were used. As expected, stimulation with untreated RNA40^S could potently stimulate Ctrl cells, whereas *RNASET2*$^{-/-}$ and *TLR8*$^{-/-}$ cells showed no IL-6 release (Figure 4.12C, gray bars). However, after *in vitro* digest with RNase T2, the degradation products of RNA40^S were able to induce a robust immune response in *RNASET2*$^{-/-}$ cells and even boosted IL-6 levels in Ctrl cells. In line with previous results, the stimulation was completely TLR8 dependent (Figure 4.12C, green bars). For RNase A, on the other hand, only the lowest enzyme concentration (+), containing full-length as well as long RNA40^S fragments, was still capable of inducing comparable IL-6 level, however, the stimulation was significantly dependent on

RNase T2 and TLR8 (Figure 4.12C, magenta bars). This indicates that RNase A degradation products are not capable of directly activating TLR8, but that intracellular RNase T2 is digesting either remaining full length RNA40^S or at least large fragments of it, to generate TLR8 ligands.

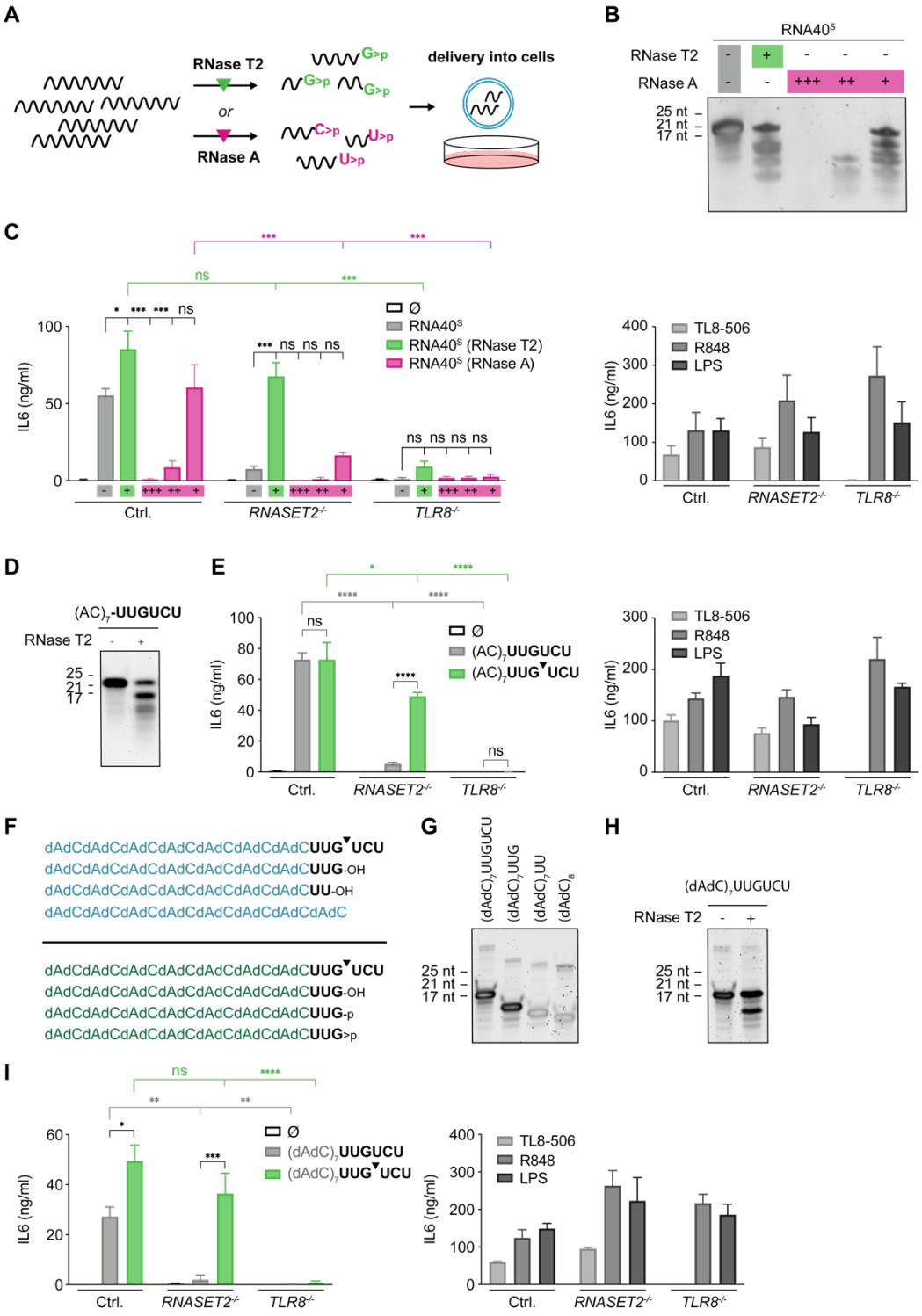

Figure 4.12 RNase T2 degradation products can bypass RNase T2 deficiency

(A) Schematic overview of experimental setup: RNA fragments were digested with either RNase T2 or RNase A and delivered into BLaER1 cells by transfection. **(B)** Urea gel of digested RNA40^S with either RNase T2 or different

concentrations of RNase A. **(C)** BLaER1 cells were either stimulated with full length RNA40^S or digested RNA40^S from (B). Control stimulations are shown on the right. **(D)** Urea gel of the full length and RNase T2 digested $(AC)_7$UUGUCU. **(E)** BLaER1 cells were stimulated with either full length or RNaseT2 digested $(AC)_7$-UUGUCU. Respective control stimulations are shown on the right. **(F)** List of ONs used for the stimulation in Figure 4.13. Arrows indicate RNase T2 cleavage site. **(G)** Urea gel of the following fragments: $(dAdC)_7$UUGUCU, $(dAdC)_7$UUG, $(dAdC)_7$UU and $(dAdC)_8$. **(H)** Urea gel of full length and RNase T2 digested $(dAdC)_7$UUGUCU. **(I)** BLaER1 cells were stimulated with full length and RNase T2 digested $(dAdC)_7$UUGUCU (0.9 µg/condition). Respective controls are shown at the right. Data are depicted as mean + SEM of three independent experiments or one of two representative gels. Statistical significance was calculated using two-way ANOVA: ****p ≤ 0.0001; ***p ≤ 0.001; **p ≤ 0.01; *p ≤ 0.05; ns, not significant.

To further study the generation of second pocket ligands for TLR8, we switched to a more reductionistic ON with the following sequence: $(AC)_7$UUGUCU. According to our cleavage analysis this ON harbors only a single cutting site for RNase T2 resulting in an UUG>p terminated RNA fragment and the trinucleotide UCU (Figure 4.12D). Experiments showed, that its stimulatory capacity was very similar to RNA40: the full-length ON could stimulate BLaER1 cells in a RNase T2 and TLR8 dependent manner, whereas the *in vitro* digest with RNase T2 could rescue its phenotype in *RNASET2*$^{-/-}$ cells (Figure 4.12E). Next, we wanted to test if UUG terminated ONs, as they are generated by RNase T2, can exert TLR8 activity on their own and how their stimulatory capacity is influenced by their 3' phosphate configuration. To this end, we tried to purify $(AC)_7$UUG>p by high-performance liquid chromatography (HPLC) from RNase T2 digests, however, it turned out to be nearly impossible due to the huge number of diastereomers caused by phosphorothioate linkages. Therefore, we exchanged the inert part of $(AC)_7$UUGUCU by phosphodiester linked deoxynucleotides resulting in $(dAdC)_7$UUGUCU (Figure 4.12F and G). Similar to the phosphorothioate stabilized ON, degradation of $(dAdC)_7$UUGUCU by RNase T2 showed only one large degradation product, as the trinucleotide cannot be detected on the urea gel (Figure 4.12H). Furthermore, stimulation of BLaER1 cells with *in vitro* digested $(dAdC)_7$UUGUCU did rescue RNase T2 but not TLR8 deficiency (Figure 4.12I). Having established the phosphodiester ON, we investigated the stimulatory capacity of two shortened derivates of $(dAdC)_7$UUGUCU terminating with either UUG or UU. Whereas the UUG terminated fragment was able to stimulate TLR8, the shorter UU variant was completely inert (Figure 4.13A, insert). Intriguingly, stimulation with UUG was dramatically weaker compared to *ex cellulo* digested full-length ON and surprisingly partially dependent on RNase T2 (Figure 4.13A). We hypothesized, that the lower stimulatory capacity could have two possible reasons: on the one hand the lacking trinucleotide UCU could serve as uridine donor and therefore be needed for first pocket ligand generation. In this scenario uridine is potentially released by another lysosomal RNase, possibly also in cooperation with RNase T2. On the other hand, the stimulatory capacity could be influenced by the 3' phosphate configuration, as the synthetic UUG-p terminated fragment has an open 3'-

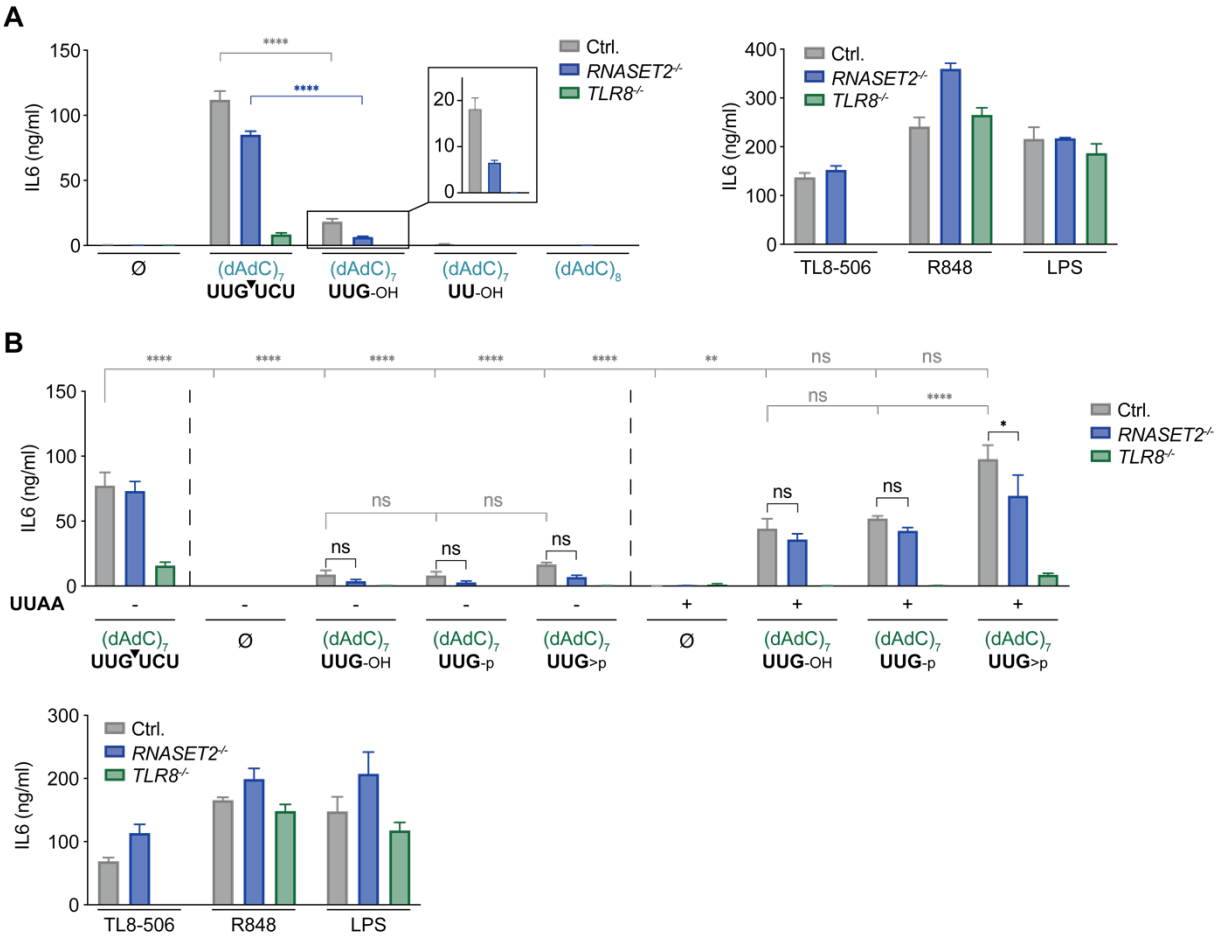

Figure 4.13 A purine terminated fragment and uridine are required for robust TLR8 activation

(A) BLaER1 cells were stimulated with the ONs from (Figure 4.12F) (top panel). **(B)** ONs from (Figure 4.12F) (bottom panel) were purified by HPLC and used for BLaER1 stimulation. To obtain cyclophosphate terminated $(dAdC)_7$UUG>p the parental ON $(dAdC)_7$UUGUCU was digested by RNase T2 and subsequentially purified by HPLC. Control stimuli are shown below. All ONs were either transfected alone or together with the DNA-RNA hybrid (dN_6)UUAA(dN_8) (1.2 µg) which served as uridine donor. All stimulations were carried out for 14 h and IL-6 ELSA was measured afterwards. Data are depicted as mean + SEM of three independent experiments. Statistical significance was calculated using two-way ANOVA: ****p ≤ 0.0001; ***p ≤ 0.001; **p ≤ 0.01; *p ≤ 0.05; ns, not significant.

phosphate moiety, whereas the *in vitro* digested ON has a 2'- 3'-cyclophosphate structure. To address this question, we stimulated BLaER1 cells with $(dAdC)_7$UUG, terminated with either an OH group, a 3'-phosphate or a 2'- 3'-cyclophosphate. As synthesizing 2'- 3'-cyclophosphate structures is chemically very challenging and not commercially available, we generated it enzymatically: after *in vitro* digesting $(dAdC)_7$UUGUCU the two degradation products were separated by HPLC, obtaining highly pure $(dAdC)_7$UUG>p. To exclude possible influence of HPLC purification on cell stimulation, all commercially available ONs were also purified according to the same protocol. To address the second scenario involving the release of uridine as first pocket ligand, all stimulations were performed with and without co-delivery of

a uridine donor. Therefore, we exploited the already characterized DNA-RNA hybrid $(dN)_6UUAA(dN)_8$, which had no stimulatory capacity but led to equal amounts of catabolic U>p compared to TLR8 agonistic ONs. These experiments revealed a rather limited induction of pro-inflammatory cytokines after stimulation with either of the three UUG terminated fragments, reaching only 10-20% of the *in vitro* digested ON (Figure 4.13B). However, co-delivering an uridine donor ($(dN)_6UUAA(dN)_8$), which itself exerted no TLR8 activation, led to significantly increased IL-6 production, now equaling *in vitro* digested $(dAdC)_7UUGUCU$. Of note, these stimulations are largely independent of RNase T2. Intriguingly, the 2'- 3'-cyclophosphate moiety was beneficial compared to other 3' configurations, leading to approximately two times increased cytokine levels. Together these results demonstrate, that delivering G-terminated fragments can bypass the requirement for RNase T2 and directly activate TLR8. Furthermore, G-terminated fragments are occupying the second binding pocket of TLR8 and need a certain uridine level for potent activation.

4.7 *Staphylococcus aureus* detection in myeloid cells depends on RNase T2 upstream of TLR8

By using ONs with diverse sequences, we have so far been able to show the cleavage pattern of RNase T2 and the downstream activation mechanism of TLR8. To investigate the involvement of RNase T2 in sensing complex pathogens, we stimulated BLaER1 cells with *Staphylococcus aureus*, as it was previously published that myeloid cells mainly exploit TLR8 to detect these bacteria (Bergstrom et al., 2015; Kruger et al., 2015). To this end, *in vitro* incubation of *S. aureus* derived total RNA with RNase T2 showed potent cleavage (Figure 4.14A and B). To investigate if RNase T2 is involved in TLR8 activation upon *S. aureus* infection *in cellulo*, we first stimulated BLaER1 cells with purified bacterial RNA (Figure 4.14C). Indeed, the stimulation was, like with RNA40, mainly dependent on RNase T2 upstream of TLR8, however, we observed some residual activity under these conditions. This scenario can most likely be explained by the fact, that complex RNA molecules can engage different immune pathways. To take this one step further, we next stimulated BLaER1 cells with live *S. aureus* at different multiplicity of infection (MOI) (Figure 4.14D). This showed potent induction of pro-inflammatory cytokines upon cell infection, which was significantly dependent on RNase T2 and TLR8 (Figure 4.14E). To investigate if *S. aureus* RNA is degraded by RNase T2 *in cellulo,* we metabolically labeled the pathogen by using heavy isotope containing growth medium (^{15}N) and analyzed isotope-labeled metabolites in BLaER1 cells upon infection (Figure 4.15A and C). As expected, stimulation with labeled *S. aureus* was dependent on RNase T2 and TLR8 at all

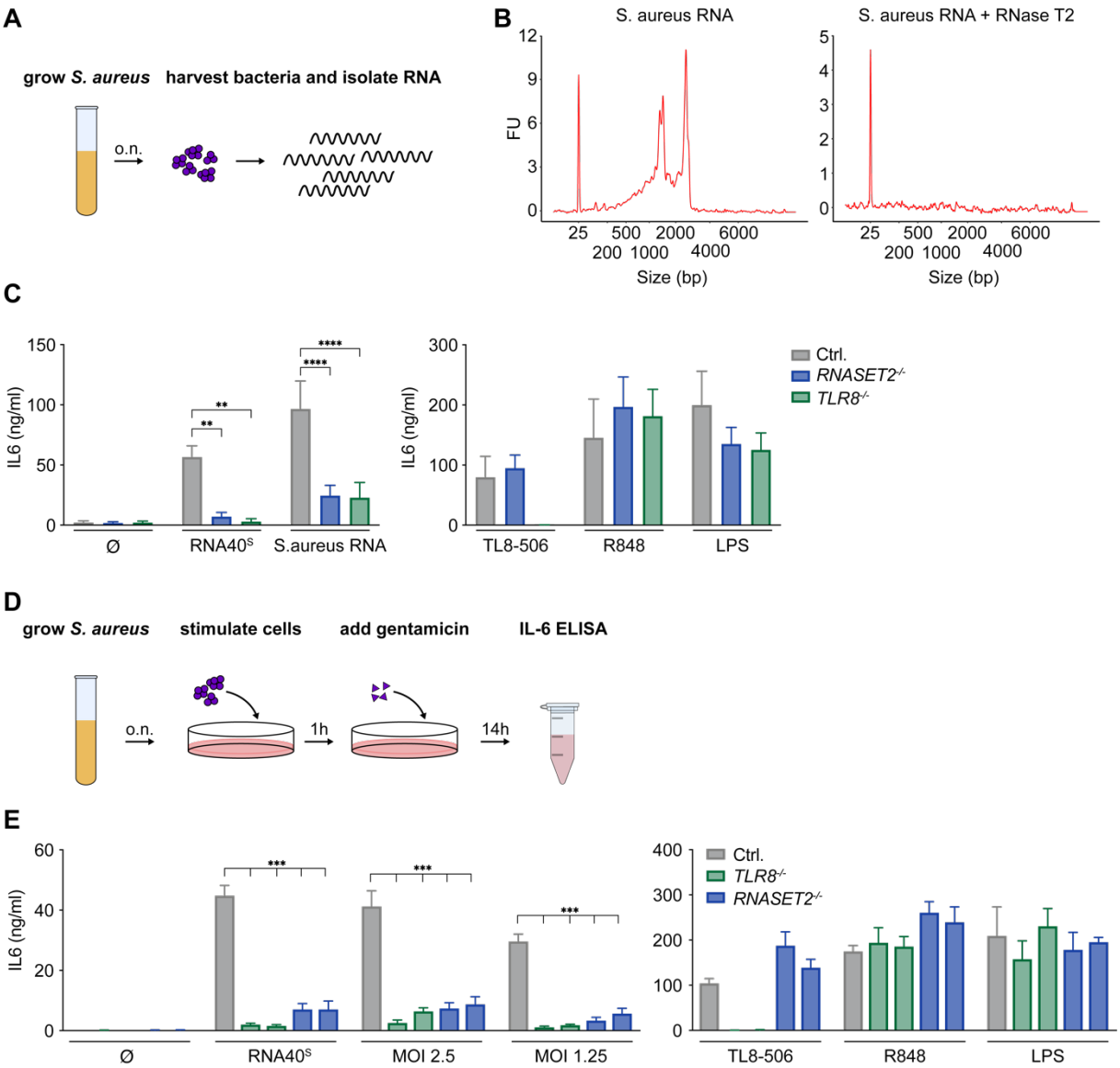

Figure 4.14 RNase T2 is critically involved in *S. aureus* detection upstream of TLR8

(A) Schematic overview of experimental procedure: *S. aureus* was grown over night harvested and total RNA was isolated. **(B)** Full length and RNase T2 digested *S. aureus* RNA was analyzed by Bioanalyzer. **(C)** BLaER1 cells were stimulated with either RNA40^S or *S. aureus* RNA. Controls are shown at the right. **(D)** Schematic overview of BLaER1 stimulation with live *S. aureus*. In brief: *S. aureus* was grown over night, washed and used for stimulation at different MOI. 1 h later gentamicin was added to kill remaining extracellular bacteria. After 14 h supernatant was harvested and IL-6 ELISA was measured. **(E)** *S. aureus* stimulation of BLaER1 cells and associated controls. Data are depicted as mean + SEM three (E) or four (C) independent experiments. Statistical significance was calculated using two-way ANOVA: ****p ≤ 0.0001; ***p ≤ 0.001; **p ≤ 0.01; *p ≤ 0.05; ns, not significant.

MOIs tested (Figure 4.15B). By analyzing stable-isotope-labeled metabolites we could detect all four ribonucleotides derived from degradation of *S. aureus* RNA, however, their abundance was independent of RNase T2 (Figure 4.15D). Yet, in line with the cleavage specificity of RNase T2, the metabolites G>p and A>p could only be detected in control but not in RNase T2 deficient cells. U>p and C>p on the other hand could neither be detected in control nor in

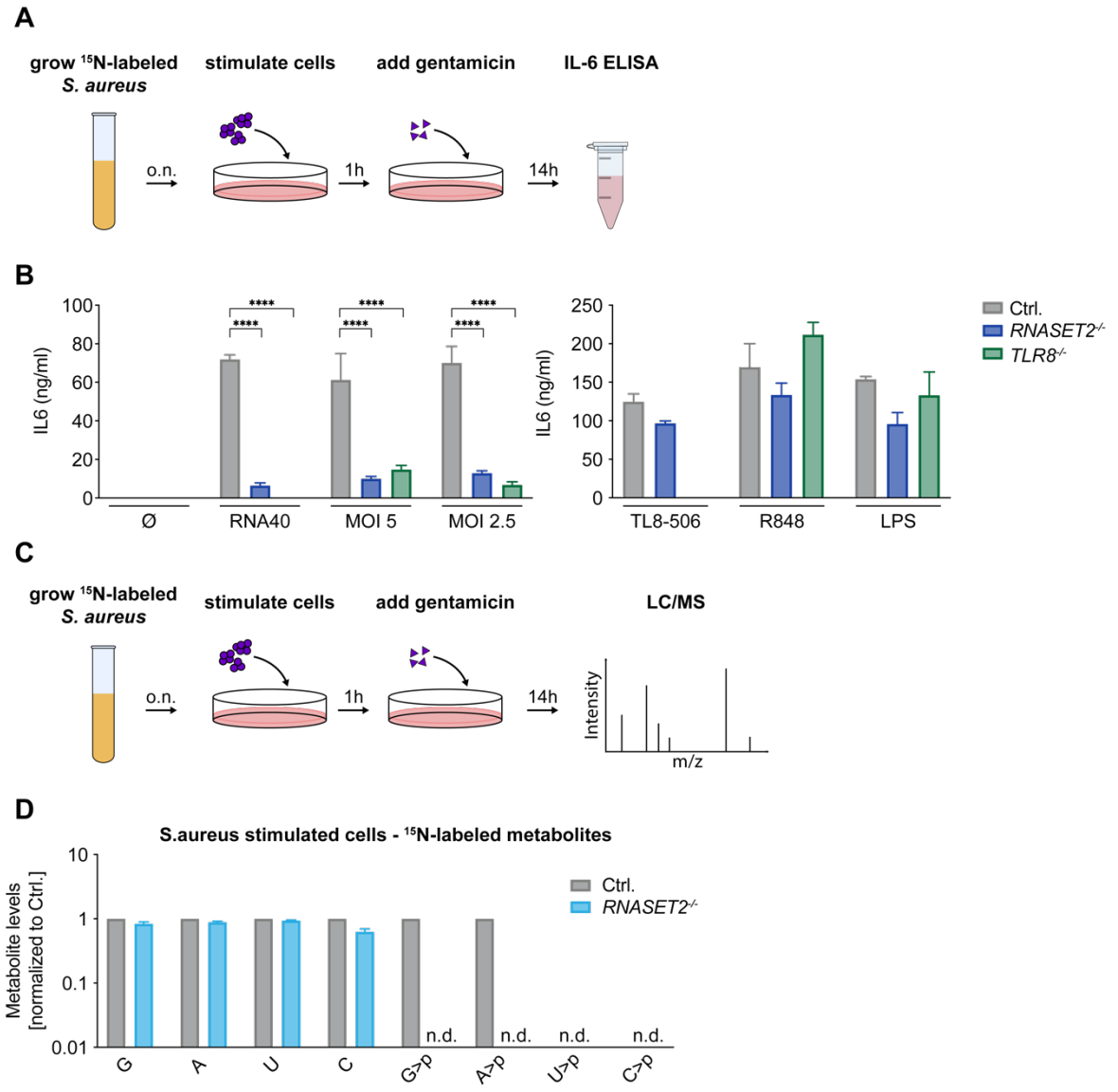

Figure 4.15 *S. aureus* derived RNA metabolites with a cyclophosphate moiety depend on RNase T2

(A) Schematic overview of BLaER1 stimulation with ^{15}N-labeled *S. aureus*: Bacteria were grown over night and used for cells stimulation. After 1 h gentamicin was added and another 14 h later the supernatant was analyzed by IL-6 ELISA. **(B)** BLaER1 stimulation with different MOI of live ^{15}N-labeled *S. aureus*. Controls are shown on the right. **(C)** Schematic overview of generating ^{15}N-labeled *S. aureus* and the subsequent stimulation of BLaER1 cells. Cells were analyzed by LC/MS. **(D)** Metabolites of BLaER1 cells stimulated with ^{15}N-labeled *S. aureus* were analyzed. ^{15}N-labeled metabolites are shown (note logarithmic scale). Data are depicted as mean + SEM of two (D) or three (B) independent experiments. Statistical significance was calculated using two-way ANOVA: ****p ≤ 0.0001; ***p ≤ 0.001; **p ≤ 0.01; *p ≤ 0.05; ns, not significant.

RNASET2$^{-/-}$ cells. Of note, only fully labeled metabolites were taken into account, as they were by far the most abundant species. Together these results indicate that recognition of complex RNA molecules, derived from bacteria like *S. aureus,* is mediated by RNase T2 degradation upstream of TLR8. This shows a very important role of specifically RNase T2 in the course of recognizing bacterial infections.

5 Discussion

Pathogens like bacteria or viruses invade cells of the human body every day challenging the immune system. Thus, the body requires a tightly regulated immune response, which is strong enough to defeat invading pathogens, but without causing severe tissue damage or chronic inflammation. TLRs, a group of pattern recognition receptors, are crucially involved in innate immune defense by recognizing all sorts of molecules derived from pathogens, including DNA, RNA and bacterial cell wall components (PAMPs). To defend against many different bacterial and viral infections, ssRNA recognition inside the lysosome by TLR7/8 is essential. Despite this important function, their mode of action is not fully understood. This is especially true for TLR8, as the receptor can, under physiological conditions, not be activated by RNA ligands in mice (Gorden et al., 2006; Hemmi et al., 2002). However, the crystal structure of both proteins was recently solved and revealed two distinct binding pockets in either receptor (Tanji et al., 2015; Zhang et al., 2016). In both cases the first pocket is occupied by a single nucleotide (uridine for TLR8 and guanosine for TLR7), whereas the second pocket binds to at least a di- or trinucleotide. Yet a minimal motif or the exact identity of the second pocket ligand remains elusive. Furthermore, the studies showed that occupation of the first pocket by a high affinity molecule like R848 is sufficient for receptor activation, nevertheless under physiological conditions the second pocket is essential. It was previously shown that DNase II is critically required upstream of TLR9 for ligand generation (Chan et al., 2015), however it is tempting to assume that a protein with RNase activity is needed upstream of TLR7/8 to degrade complex RNA molecules into appropriate ligands for receptor activation. In this study we exploited the BLaER1 cell system to investigate the sequence specificity and activation mechanism of TLR8, which up to that point was poorly studied due to the lack of a suitable model system. To this end, BLaER1 cells can easily be modified in their B-cell state, using the CRISPR/Cas9 system and then be trans-differentiated into macrophage like cells to investigate their phenotype. In this regard, we systematically knocked out RNases possibly acting upstream of TLR8, as well as the receptor itself. Realizing RNase T2 is critically involved in TLR8 ligand generation, we analyzed its degradation pattern *in vitro* and *in cellulo* by LC/MS. Furthermore, we investigated the requirement of RNase T2 and TLR8 during *Staphylococcus aureus* infections.

5.1 TLR7 and TLR8 recognize RNA inside the endolysosome

To investigate TLR8 activation we first established the BLaER1 human cell system. RNA sequencing data revealed that the receptors TLR4, TLR7 and TLR8 are significantly upregulated upon trans-differentiation of these cells (Figure 4.1A). As expected, stimulation of TLR7 and TLR8 deficient cells showed, that TL8-506 was only capable of stimulating TLR8 whereas R848

was dependent on TLR7 and 8 (Figure 4.1B). Intriguingly, stimulation with RNA40 (phosphorothioate as well as phosphodiester backbone) was completely dependent on TLR8 but not on TLR7, rendering BLaER1 cells a perfect platform to investigate TLR8 activation (Figure 4.1C). To specifically deliver RNA ONs into the endolysosomal compartment, p-L-arginine (pR) was used as a transfection reagent (Ablasser et al., 2009), as lipofectamine 2000 only led to minor IL-6 release (Figure 4.2A). Of note, for most experiments during this study the phosphorothioate stabilized ligand RNA40^{S} was used as it is more stable against degradation. Except for RNA40, we also tested the already published ONs P20 and P20-5M (Ablasser et al., 2009). P20, is forming a hairpin structure and was not able to stimulate either Ctrl, TLR7 or TLR8 deficient cells. However, partially destroying the double stranded structure of P20 by altering its sequence (P20-5M), rendered the ON immunostimulatory in a completely TLR8 dependent fashion (Figure 4.2E). This clearly indicates that only single stranded but not double stranded RNA is essential for TLR8 activation. Together these results establish the BLaER1 trans-differentiation system a good model to investigate TLR8 activation as well as the identity of its ligands.

5.2 RNase T2 is generating unique ligands for TLR8

The systematic KO of endolysosomal RNases revealed, that RNA40 stimulation is completely dependent on RNase T2, suggesting that it is critically responsible for TLR8 ligand generation (Figure 4.3). At first glance this seems rather surprising as several RNases can be found in humans, many of which are located inside the endolysosomal compartment. However, RNase T2 is the only family member of the RNase T2 superfamily found in humans. Generally, endoribonucleases can be divided into three distinct families: RNase A, RNase T1 and RNase T2. All members of these families enter the secretory pathway and can therefore be found in the endolysosomal compartment as well as in the extracellular space. Furthermore, they all belong to the group of transferase-type endoribonucleases, sharing a similar cleavage mechanism: in a first step the substrate is cleaved generating a 2'-3'-cyclophosphate intermediate state, before it is hydrolyzed in a second step, resulting in an open 3'-phosphate structure (MacIntosh, 2011). Although the three families share the same mode of action they can predominantly be found in different kingdoms of life. Whereas RNase A enzymes are very diverse in the vertebrate lineage, RNase T1 enzymes are present in fungi and bacteria. RNase T2 enzymes on the other hand can be found in all kingdoms of life except *Archaea*. Unlike enzymes from the RNase A family, which have undergone extensive duplications and diversifications in humans (13 different genes), only one member of the RNase T2 family is expressed. Like humans most animals express only one RNase T2 enzyme, however, the family has been very successful in plants. The high level of conservation in vertebrates strongly

indicates an important housekeeping function of RNase T2 enzymes. In zebrafish for example, knocking out RNase T2 leads to rRNA accumulation inside the lysosomal compartment of cells of the central nervous system (Haud et al., 2011). This indicates its involvement in ribosome turnover, a process called ribophagy that prevents the accumulation of RNA inside the cells. Structural analysis of RNase T2 enzymes revealed two distinct nucleotide binding pockets, the B1 and B2 site, determining their substrate specificity (MacIntosh, 2011). In bitter gourd, a to human RNase T2 structurally very related RNase called MC1 was found, preferentially binding to uridine at its B2 site. As the B1 site seems to be quite tolerant to all bases, the cleavage site of MC1 appears to be 5'-NU-3' (Numata et al., 2003; Suzuki et al., 2000). Of note, the base coordinating amino acids of the B2 pocket are orthologous between MC1 and human RNase T2 (Thorn et al., 2012), suggesting similar binding patterns of the two proteins. Indeed, all results obtained by *in vitro* digestion of RNA40 showed cutting of RNase T2 exclusively before uridine residues, whereas RNase A showed a distinct degradation pattern. By analyzing 16 ONs with the sequence A_4NNA_2, harboring all possible dinucleotide combinations, we could specify RNase T2 cleavage site to purine-uridine (5'-RU-3') (Figure 4.5 and 4.6). The non-redundant action of RNase T2 strongly indicates, that the enzyme generates purine terminated RNA fragments with a 2'-3'-cyclophosphate moiety, occupying the second binding pocket of human TLR8. Intriguingly, lysosomal ribonucleases of the RNase A family seem to generate degradation products incompatible with TLR8 activation. Hence, it seems like hTLR8 has evolved to specifically recognize RNase T2 degradation products leading to a downstream immune response.

5.3 RNase T2 alters RNA metabolism *in cellulo*

Up to that point, little was known about the identity of lysosomal RNA degradation products and the influence of enzymes like RNase T2 on them. To this end, we investigated cellular RNA metabolite levels under steady state as well as stimulated conditions. We aimed to evaluate the involvement of RNase T2, specifically if the enzyme is only impacting on RNA degradation products derived from foreign RNA, or if it is also influencing the steady-state pool. To distinguish endogenous from exogenous metabolites we stimulated with $RNA40^S$ as due to the phosphorothioate backbone its degradation products can be distinguished from cellular metabolites by mass. This renders $RNA40^S$ degradation products an excellent proxy for the catabolic activity of lysosomal enzymes like RNase T2.

Analyzing metabolite levels from either endogenous or exogenous origin by LC/MS revealed a significant drop of G>p and A>p as well as G>p- and A>p-terminated fragments in *RNASET2*$^{-/-}$ cells. As according to our results RNase T2 cleaves after purines we assumed, that C>p and U>p levels remains unaffected in the absence of RNase T2 but would rather be dependent on

enzymes from the RNase A family, as they were published to cleave after pyrimidines. As expected, C>p levels were unchanged in *RNASET2*$^{-/-}$ cells, whereas they were slightly decreased in the absence of RNase 1. U>p levels on the other hand where significantly decreased in *RNASET2*$^{-/-}$ cells. Theoretically, the absence of RNase T2 can affect U>p levels up to 50% as the enzyme is cleaving upstream of uridine, however, why U>p levels were affected beyond that is not clear. A possible explanation would be, that RNase T2 is accepting uridine in its B1 pocket but with much lower affinity, which would explain why we did not observe this in our under-cutting experiments. Furthermore, it is possible, that the activity of RNase T2 is also affected by other factors than the substrate specificity *in cellulo*. However, these results show a reduced lysosomal concentration of purine terminated fragments as well as uridine in the absence of RNase T2 (Figure 4.7). By stimulating cells with RNA40^{O}, we could also analyze the global change of metabolites *in cellulo*, showing very similar results. G>p, A>p and U>p levels were increased about 2-3-fold upon stimulation and were nearly completely dependent on RNase T2, whereas C>p levels were largely unaffected. The same pattern could be observed for the dinucleotides GG>p, AA>p, UU>p and CC>p. Intriguingly, UG>p and UUG>p were only present after stimulation and completely dependent on RNase T2, implicating an important role of these metabolites in the course of TLR8 activation (Figure 4.8).

These data were also supported by stimulation with more sequence restricted RNA ONs. To further investigate the cleavage behavior of RNase T2 *in cellulo* we stimulated our cells with DNA-RNA hybrid ON, which were published to exert TLR8 activity (Forsbach et al., 2008). The ONs harbor four RNA bases in the middle of their sequence, flanked by random DNA bases. As indicated by our previous results, only DNA-RNA hybrids containing the sequences UUGU or UUAU were able to stimulate BLaER1 cells, in a RNase T2 and TLR8 dependent manner. However, if the last uridine of UUGU was exchanged by any other possible nucleotide (G, A, C or dN) no TLR8 activation could be observed (Figure 4.10A and B). Analyzing ON derived metabolites *in cellulo* could explain this scenario: G>p as well as UG>p were only released from ONs containing UUGU but not UUGA, which was completely dependent on RNase T2. The same is true for the metabolites A>p and UA>p which were found in cells stimulated with UUAU but not UUAA. Intriguingly, the release of U>p was partially uncoupled from the ON sequence as well as from RNase T2. We found the amount of U>p in UUGU and UUAA stimulated cells was equal and largely independent of RNase T2, demonstrating that the sole increase of U>p under stimulation conditions is not sufficient to activate TLR8. However, it renders UUAA a perfect U>p donor without activating the receptor. Taken together these results show, that RNase T2 is critically involved in the generation of purine terminated fragments and that especially dinucleotides like UG>p and UA>p are needed for TLR8 activation. This is in line with the notion that at least a dinucleotide is needed to occupy the second pocket of TLR8, which then facilitates uridine to bind to the first pocket of the receptor.

5.4 Mechanism of TLR8 activation downstream of RNase T2

As TLR8 has two distinct pockets it is important to sort out which of them is occupied by RNase T2 degradation products and if the binding order matters. Interestingly, the occupation of the first binding site by small chemical compounds like R848 is sufficient for TLR8 activation, whereas under physiological conditions always both pockets seem to be occupied. The critical involvement of RNase T2 in TLR8 ligand generation became clear by *in vitro* digestion experiments. Transfecting BLaER1 cells with RNase T2 digested RNA was able to rescue RNase T2 deficiency, however, the stimulation was still TLR8 dependent. Delivering RNase A digested RNA40^{S} on the other hand was not capable of bypassing RNase T2 deficiency. Of note, the stimulatory capacity of degradation mixtures incubated with the lowest amounts of RNase A in control cells, can be explained by the undercutting conditions. It results in remaining full-length RNA fragments which can intracellularly be cleaved by RNase T2, generating appropriate TLR8 ligands (Figure 4.12A-C).

According to literature, the second pocket of TRL8 is preferentially occupied by guanosine terminated di- or trinucleotides of which the other bases are mainly pyrimidines (especially uridine) (Tanji et al., 2015). This together with the observed cleavage of RNase T2 between purine and uridine strongly indicates, that the enzyme is mainly generating ligands for the second pocket of TLR8. However, as the protein is cleaving upstream of uridine it is most likely also enhancing the generation of free uridine which can then occupy the first pocket of the receptor. Indeed, we could observe that RNA derived (U)UR>p fragments were RNase T2 dependent and significantly affecting TLR8 activity. In fact, our experiments suggest RNase T2 being the only endolysosomal RNase capable of generating the afore mentioned 3'-termini, explaining its non-redundant mode of action. As an additional feature, RNase T2 was mainly generating RNA fragments with a 2'-3'-cyclophosphate moiety. Yet, it turned out that the cyclic phosphate at the 3' end is neither needed nor sufficient for TLR8 activation. Nevertheless, the cyclophosphate led to an about 2-fold increased release of pro-inflammatory cytokines compared to RNA fragments with 3'-OH or classical 3'-phosphate termini (Figure 4.13). The first pocket of TLR8 on the other hand binds to uridine and is ultimately leading to TLR8 activation. Even though R848 can directly activate TLR7 and TLR8 by only occupying their first pocket, under physiological conditions RNase T2 generated (U)UR>p fragments play a crucial role in receptor activation. Of note, due to RNase T2 cleaving upstream of uridine, *RNASET2*$^{-/-}$ cells showed a 4-fold reduced U>p level under steady state condition which was even 15-fold reduced after RNA stimulation (Figure 4.8). To this end, stimulation of BLaER1 cells with only a second pocket ligand like $(dAdC)_7$-UUG resulted in significantly decreased IL-6 production compared to stimulation with *in vitro* digested $(dAdC)_7$-UUG↓UCU, in Ctrl as well as RNase T2 deficient cells (Figure 4.13C). These results indicate

that the sole delivery of a second pocket ligand is not sufficient for TLR8 activation, whereas the co-delivery of a uridine donor like the UCU fragment is leading to robust downstream signaling. Indeed, the weaker activation of the second pocket ligand $(dAdC)_7$-UUG could be overcome by co-delivering a non-stimulatory uridine donor like $(dN)_6$UUAA$(dN)_8$. As shown before stimulation with this ON led to comparable uridine levels as TLR8 agonistic RNAs but without the release of pro-inflammatory cytokines (Figure 4.10), however, together with $(dAdC)_7$-UUG the stimulatory capacity was equal to *in vitro* digested $(dAdC)_7$-UUG↓UCU. These results clearly show that sufficient amounts of uridine from exogenous origin are critically required for TLR8 activation. Of note, the sole release of uridine from complex RNA molecules is not sufficient to activate TLR8 and can also be found independently of RNase T2. All in all, RNase T2 is critically required for TLR8 dependent recognition of complex RNA molecules. Dictated by its substrate specificity (RU) the enzyme is essential for the generation of catabolic uridine occupying the first pocket of TLR8, however, this process includes enzymes from the RNase A family cleaving downstream of uridine. On the other hand, RNase T2 is non-redundantly required for the generation of purine terminated fragments occupying the second pocket of TLR8. Together the results suggest that the second pocket ligand is allosterically controlling the binding of uridine to the first pocket, which is an important regulatory step under natural stimulation conditions. Of note, even though the 2'-3'-cyclophosphate moiety is neither required nor sufficient for TLR8 activation, it significantly increases the stimulatory capacity of purine terminated RNA fragments.

5.5 RNase T2 is involved in pathogen sensing

After investigating the RNase T2 mediated activation mechanism of TLR8 by synthetic ONs, we changed to a more natural system – stimulating with living pathogens. To this end, we infected BLaER1 cells with *Staphylococcus aureus,* a gram-positive bacterium to avoid activation of TLR4 by bacterial cell wall components (LPS). Furthermore, the pathogen is well adapted to its human host and leads to sever diseases like endocarditis, bacteraemia and osteomyelitis. Especially resistant strains like Methicillin- resistant *Staphylococcus aureus* (MRSA) represent a big threat, as they became a leading cause of health care associated infections. MRSA induced bacteraemia for example leads to a mortality rate of 15-50%, even with intensive medical attention (Turner et al., 2019). Hence, it is of great interest to further investigate cellular pathways and mechanisms associated with the recognition of pathogens like *S. aureus*.

Before stimulating with living bacteria, we tested purified *S. aureus* RNA. These experiments showed potent degradation of *S. aureus* RNA by RNase T2 and robust IL-6 production upon cell stimulation, in a completely RNase T2 and TLR8 dependent manner. Infection of cells with

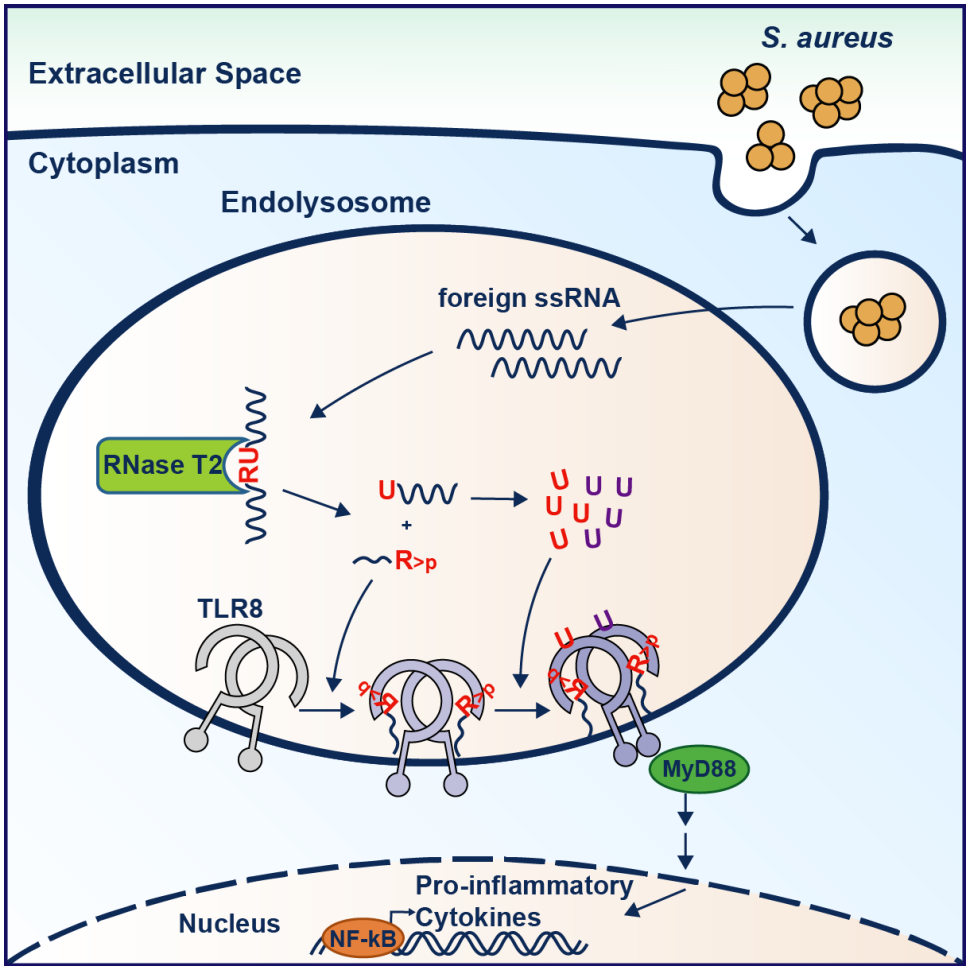

Figure 5.1 Activation mechanism of TLR8 downstream of RNase T2

Bacteria as well as viruses are often entering the cell via the endolysosomal rout or are taken up by phagocytosis. In both cases foreign RNA is ending up in the endosomal or lysosomal compartment. These RNA fragments can be recognized by the cell leading to the release of pro-inflammatory cytokines and interferons. In humans TLR8 is one of the RNA recognizing receptors. It consists of an endolysosomal LRR domain, one transmembrane domain and a cytoplasmic TIR domain. Furthermore, it has two distinct RNA binding pockets located inside the LRR domain. We found, that RNase T2, the only representative of the RNase T2 family present in humans, is critically involved in TLR8 activation. The enzyme is cleaving RNA between purine and uridine residues leaving a 2'-3'-cyclophosphate structure at the 3'-end. These R>p terminated fragments can engage the second pocket of TLR8, allosterically controlling uridine binding. The occupation of the first pocket by uridine is ultimately activating the receptor facilitating downstream signaling. The necessary uridine can either derive from the steady state pool or be released from foreign RNA fragments requiring the help of enzymes from the RNase A family.

living bacteria mirrored these results: the bacteria induced a strong immune response via the RNase T2-TLR8 route, leading to the release of pro-inflammatory cytokines. These data clearly show that TLR8 is critically involved in the recognition of complex pathogens like *S. aureus*, however, it also involves RNA degradation by RNase T2 to generate appropriate ligands for receptor activation (Figure 4.14). Furthermore, we also analyzed *S. aureus* derived RNA degradation products *in cellulo*. To this end, bacteria were labeled with the heavy isotope ^{15}N

prior to stimulation, which allowed us to distinguish between endogenous and exogenous metabolites (Figure 4.15). Analysis of *S. aureus* RNA derived degradation products showed equal levels of ribonucleotides (G, A, U and C) in Ctrl and RNase T2 KO cells. Yet, the metabolites G>p and A>p, carrying a 2'-3'-cyclophosphate moiety, could exclusively be found in control cells. At the same time, we were unable to detect U>p or C>p, in either control or RNase T2 KO cells. Due to the high complexity of ^{15}N-labeled metabolites it was not possible to assign longer RNA fragments than single nucleotides, however, the results suggest that RNase T2 cleaves *S. aureus* RNA *in cellulo* generating G>p- and A>p-terminated RNA fragment, which are needed for TLR8 activation. In conclusion the RNase T2-TLR8 route seems to be critically involved in the recognition of complex RNA molecules in the course of bacterial infections.

Taken together in this study we could identify RNase T2 as a critical factor acting upstream of TLR8. Whereas the majority of RNases belongs to the RNase A family and cleaves after pyrimidines, RNase T2 has a unique substrate specificity, cleaving between purine bases and uridine. This generates RNA fragments with a 2'-3'-cyclophosphate configuration binding to the second pocket of TLR8. Furthermore, it leaves a second RNA fragment with a 5'-uridine, which can be further cleaved by other RNases to release uridine needed for the first pocket. Therefore, RNase T2 not only generates ligands for the second pocket of TLR8 but is also involved in uridine release. As previously published, the occupation of the first pocket is crucial for TLR8 activation. As such our data suggests, that the second pocket of TLR8 is occupied first, increasing the binding affinity of uridine to the first pocket. The binding of uridine then ultimately leads to TLR8 activation and downstream signaling. The uncovered pathway is playing a critical role in detecting infections with bacteria like *S. aureus* (Figure 5.1).

5.6 RNase T2 in health and disease

As RNase T2 is the only member of the RNase T2 superfamily found in humans it strongly suggests a non-redundant function in our body. Thus, it is not very surprising that Loss-of-function mutations within the human *RNASET2* gene cause diseases. Patients with this defect suffer from cystic leukoencephalopathy mimicking a neonatally asymptomatic congenital cytomegalovirus (CMV) brain infection. The MRI (magnetic resonance imaging) pattern is indistinguishable from CMV infection and show multifocal white matter lesions and in some cases calcification. As a result, patients manifest with impairment, spasticity and in rare cases also epilepsy (Henneke et al., 2009). Therefore, it is tempting to assume RNase T2 deficiency and Aicardi-Goutières syndrome (AGS) share a similar pathomechanism (Rice et al., 2017). Patients with AGS have mutations in genes like TREX1, RNase H2, SAMHD1 and ADAR1 leading to defects in intracellular nucleic acid metabolism (Lee-Kirsch et al., 2014). This leads to

accumulation of nucleic acids inside the cell and thus to unwanted activation of PRR, resulting in autoinflammation (Crow and Manel, 2015). At first glance this may seem counterintuitive as our results indicate a pro-inflammatory role of RNase T2. However, if we take a closer look at the impact of RNase T2 deficiency on cells, we can explain the hypothesis: under physiological conditions RNase T2 is generating ligands specifically activating TLR8, leading to a pro-inflammatory immune response. Even though this pathway cannot be engaged in the absence of RNase T2 it is likely, that loss-of-function mutations lead to RNA accumulation inside the endolysosome. Over time the accumulated RNA can leak into the cytoplasm activating cytoplasmic RNA sensors. This would suggest, that due to constant RNA degradation RNase T2 has an important function in nucleic acid homeostasis. To prevent continuous TLR8 activation under steady state conditions, it is likely that a certain RNA threshold has to be reached for receptor activation. Furthermore, the activity of either RNase T2 or TLR8 could also be modulated by RNA modifications like they can be found in tRNA or rRNA (Pereira et al., 2018; Taoka et al., 2018). Interestingly, a similar mechanism was proposed for DNase II, which is also located in the endolysosomal compartment and acts upstream of TLR9. On the one hand, the enzyme is published to digest dsDNA, to generate appropriate ligands for TLR9 (Chan et al., 2015), whereas on the other hand, lack of DNase II leads to DNA leakage into the cytoplasm and the subsequent activation of the cGAS-STING pathway (Ahn et al., 2012; Gao et al., 2015). This underlines the importance of a tightly balanced nucleic acid metabolism. Intriguingly, a study using zebrafish as animal model showed, that RNase T2 deficiency leads to RNA accumulation in the lysosomes of cerebral neurons and white matter lesions. They concluded, that loss of RNase T2 function is associated with lysosomal storage diseases (Haud et al., 2011). This strongly suggests an inhibitory role of RNase T2 in autoinflammatory diseases by preventing RNA accumulation inside the endolysosomal compartment. All in all, it seems like RNase T2 needs to be tightly balanced between its pro-inflammatory role in TLR8 activation and its potential anti-inflammatory role by RNA degradation. However, this would also render lysosomal nucleases protected against pathogen encoded immune modulators, as their downregulation would lead to the activation of cytosolic PRR.

5.7 The BLaER1 cell culture system

Monocytes and macrophages play an important role in the investigation of the properties and function of the innate immune system. This is due to their crucial role to induce and model the immune response. Commonly, murine macrophages are used to study innate immune pathways as loss-of-function studies can be performed in this species. Human myeloid cells can, however, be used for *in vitro* studies. This becomes especially important if proteins like TLR8 are investigated, as the protein is unfunctional in murine cells. Typically used cell lines

like THP-1, however, only mimic human primary myeloid cells to a certain degree (Gaidt et al., 2018). A better model for this purpose is the BLaER1 trans-differentiation system. These cells can easily be genetically edited by the CRISPR/Cas9 system in their B-cell state. Afterwards they can be differentiated into monocytes/macrophages and used to study pathways of the innate immune system. Even though the BLaER1 cell line provides an excellent platform to investigate diverse immune pathways it also has limitations. One of them is the differing gene expression of lysosomal RNases between differentiated BLaER1 cells and primary human monocytes. Whereas RNase T2 is expressed in both cell types, the expression of enzymes from the RNase A family differs. While BLaER1 cells express huge amounts of RNase 1 there is basically no expression in primary monocytes. For RNase 2 it is the other way around whereas RNase 6 can be found in both cell types (Figure 4.3). For THP-1 cells on the other hand the predominantly expressed RNase is RNase 2. The differential expression of RNase A encoding genes could especially influence the release of uridine from RNA fragments as the enzyme class was published to cleave downstream of pyrimidines (Lu et al., 2018; Raines, 1998). To this end, it is likely, that the first pocket ligand for TLR8 is generated by different enzymes from the RNase A family, depending on which cell type is used. Cell culture models always try to mimic primary cells, however, there are always differences that have to be considered.

5.8 Our work in the context of recent publications

Recently Ostendorf and colleagues published their findings on a similar topic (Ostendorf et al., 2020). Even though they confirmed that RNase T2 is critically required for TLR8 activation, there are some differences between the two studies. First, they propose that RNase 2 is equally important for RNA degradation upstream of TLR8. Yet this is only true for THP-1 cells, as they could reproduce our result in BLaER1 cells showing a complete dependence on RNase T2 upon RNA40^{S} stimulation. This result can most likely be explained by the RNase expression pattern of the different cell lines. According to our data, robust TLR8 activation can only occur in the presence of RNase T2, generating ligands for the second binding pocket and a member of the RNase A family needed for uridine release. A closer look at RNase expression levels in different cell types (Ostendorf et al., 2020) shows high amounts of RNase T2, RNase 1 and RNase 6 in differentiated BLaER1 cells, whereas THP-1 cells mainly express RNase T2 and RNase 2. Thus, it is not surprising that RNase 2 is also critical to THP-1 cells being the only RNase from the RNase A family expressed in these cells. In BLaER1 cells on the other hand we could not observe reduced stimulation in the absence of RNase 2, which is most likely due to redundant cleavage patterns between RNase A type enzymes. A key difference of the two studies is the proposed cleavage pattern of RNase T2. In contrast to our results, suggesting cleavage occurring between purine and uridine residues, Ostendorf and colleagues are

proposing a much broader specificity. In line with our findings they state that RNase T2 has a quite strong preference for uridine in the second pocket, but they propose it also accepts adenosine to some extent. Strikingly, it is claimed that RNase T2 has basically no preference at its first binding position. For instance, they show that RNase T2 is capable of cleaving poly(U). Indeed, we have also observed that high concentrations of poly(U) can stimulate TLR8, however, this is largely independent of RNase T2 (data not shown). In light of our data we hypothesize that poly(U) is degraded via RNase A family members overwhelming the first pocket of TLR8, bypassing the need of the second pocket. This situation, however, does not reflect the natural role of TLR8 in detecting the presence of complex RNA molecules, for which both binding pockets are required (Tanji et al., 2015). Interestingly, they used phosphorothioate stabilized RNA for LC/MS analysis of the cleavage site, although phosphodiester RNA was used throughout most of their paper. This might result in difficulties determining the relative amount of found fragments caused by diastereomers. As such, every phosphorothioate linkage added to an RNA molecule increases the number of possible diastereomers by a factor of two. Consequently, a ORN with 19 phosphorothioate linkages consists of 2^{19} diastereomers that produce distinct peaks in HPLC analysis. Therefore, whenever possible, we tried to employ phosphodiester linked ORNs for experiments involving HPLC. In addition to ssRNA40 and 9.2s RNA, Ostendorf and colleagues also included R2152 (CGCG**U**GCGCAGAAGCGC**G**CGC) into their cleavage analysis. R2152 is a hairpin ON with a GU dinucleotide in the double stranded area and the sequence AGAA in the single stranded loop (base pairing nucleotides are underlined, whereas the wobble G:U pair is shown in bold). Of note, the U residue of the single GU dinucleotide is paired with a G, forming a wobble base pair. The major cleavage sites they propose are between the GU dinucleotide and AG as well as AA inside the single stranded loop. This indicates a preference of RNase T2 for GU – accessible due to the wobble base pairing and the single stranded stretch. This is in line with our results, showing that RNase T2 has a bias towards ssRNA. To this end, it is conceivable that RNase T2 is showing off-target cleavage at the AG and AA site as they are located inside the single stranded stretch of the ON. To, therefore, unequivocally identify the true cleavage pattern of RNase T2 it might be best to only take ssRNA molecules in order to avoid that the results get blurred by the influence of ds versus ssRNA. However, in their cleavage analysis this bias was not accounted for. Unfortunately, due to technical issues, they did not include the ONs ORN002 ($(UUA)_6UU$) and ORN006 ($(UUG)_6UU$) to their cleavage analysis, even though these would have been the perfect choice to investigate the preference of RNase T2 between G/A-U and U-U cleavage. Interestingly, it is shown that incubation of RNase T2 with either of these ONs mainly led to RNA fragments with a length of a multiple of three, which would be consistent with a cleavage between GU or AU. Furthermore, Ostendorf et al. proposed that RNase T2 is potently cleaving dsRNA, whereas our data suggest that RNase T2 has a strong

preference for ssRNA. Although they saw cleavage of 9.2s dsRNA there was a clear quality difference as the single stranded 9.2s RNA was digested more efficiently at the same enzyme concentration. This points into the direction that RNase T2 having a preference for ssRNA but is also capable of digesting dsRNA at higher concentrations. It is important to note that our findings only identified the major cleavage site of RNase T2. Like most enzymes it is highly likely that under specific circumstances like high protein concentration or the lack of the target sequence, off-target effects can be seen, especially if very sensitive readout methods are used.

Ultimately, the two papers differ in several points. However, some of the differences like the need of RNase 2 in THP-1 cells, might be resolved by additional experiments demonstrating that RNase A enzymes in BLaER1 cells are redundant. Where the two studies diverge is the cleavage pattern of RNase T2. However, as outlined above, these presumptive differences are less evident, when taking the above considerations into account.

6 Summary

TLR8 is one of the highest-expressed pattern recognition receptors in the myeloid system, yet its mode of action is only poorly understood. This is mainly due to the lack of functional TLR8 in mice, where only the closely related receptor TLR7 can be activated under physiological conditions. TLR8 belongs to the family of toll-like receptors and is together with TLR3, TLR7 and TLR9 located inside the endolysosomal compartment. Whereas TLR9 is sensing CpG-DNA and TLR3 dsRNA, the ligand for both TLR7 and TLR8 is ssRNA. Upon activation of TLR7/8 the adaptor protein MyD88 is recruited, leading to downstream signaling and the activation of the NF-κB as well as the interferon pathway. Several years ago, the crystal structure of human TLR8 was solved showing that the receptor is composed of a cytoplasmic TIR domain, one transmembrane domain and a lysosomal domain built up by leucine-rich repeats (LRR). Inside the LRR domain a flexible structure called Z-loop is located, which has to be cleaved to obtain mature TLR8. Furthermore, the crystal structure revealed two distinct RNA binding pockets located inside the LRR domain, however, it remained elusive how theses short RNA ligands are formed *in cellulo* in the context of sensing complex RNA molecules.

In this study we set out to investigate TLR8 ligand generation and its activation mechanism. A systematic gene targeting approach of endolysosomal RNases revealed RNase T2 as a non-redundant upstream component of TLR8-dependent RNA recognition. The enzyme is critically required to break down complex RNA molecules into small fragments, rendering them detectible for TLR8. RNase T2 belongs to the RNase T2 superfamily and is the only representative found in humans. Even though, several other RNases of the RNase A family are present in the endolysosomal compartment, RNase T2 is due to its distinct cleavage pattern critically required for TLR8 ligand generation. Its preferential cleavage between purine and uridine residues leads to the generation of purine-2',3'-cyclophosphate-terminated oligoribonucleotides, which can encounter the second binding pocket of TLR8. Furthermore, RNase T2 is critically involved in the release of catabolic uridine, binding to the first pocket of TLR8. However, our experiments show, that even though the occupation of the first pocket by chemical compounds like R848 is sufficient for TLR8 activation, the sole increase of uridine seen in the context of a complex RNA molecule stimulation is not enough to trigger TLR8 signaling. To this end, RNase T2 generated purine-2',3'-cyclophosphate-terminated fragments are critically involved in TLR8 signaling by allosterically controlling uridine binding, which ultimately leads to receptor activation. Of note, even though the 2',3'- cyclophosphate configuration did enhance TLR8 activity it was neither required nor sufficient, as also purine terminated fragments with an open phosphate, or a hydroxyl group were immunostimulatory. Finally, we could show, that the RNase T2-TLR8 route is involved in sensing pathogens like *Staphylococcus aureus*.

7 Bibliography

Ablasser, A., Poeck, H., Anz, D., Berger, M., Schlee, M., Kim, S., Bourquin, C., Goutagny, N., Jiang, Z., Fitzgerald, K.A*., et al.* (2009). Selection of molecular structure and delivery of RNA oligonucleotides to activate TLR7 versus TLR8 and to induce high amounts of IL-12p70 in primary human monocytes. J Immunol *182*, 6824-6833.

Ahn, J., Gutman, D., Saijo, S., and Barber, G.N. (2012). STING manifests self DNA-dependent inflammatory disease. Proc Natl Acad Sci U S A *109*, 19386-19391.

Akira, S., and Hoshino, K. (2003). Myeloid differentiation factor 88-dependent and -independent pathways in toll-like receptor signaling. J Infect Dis *187 Suppl 2*, S356-363.

Amarante-Mendes, G.P., Adjemian, S., Branco, L.M., Zanetti, L.C., Weinlich, R., and Bortoluci, K.R. (2018). Pattern Recognition Receptors and the Host Cell Death Molecular Machinery. Front Immunol *9*, 2379.

Anwar, M.A., Shah, M., Kim, J., and Choi, S. (2019). Recent clinical trends in Toll-like receptor targeting therapeutics. Med Res Rev *39*, 1053-1090.

Ban, T., Sato, G.R., and Tamura, T. (2018). Regulation and role of the transcription factor IRF5 in innate immune responses and systemic lupus erythematosus. Int Immunol *30*, 529-536.

Bell, J.K., Mullen, G.E., Leifer, C.A., Mazzoni, A., Davies, D.R., and Segal, D.M. (2003). Leucine-rich repeats and pathogen recognition in Toll-like receptors. Trends Immunol *24*, 528-533.

Bella, J., Hindle, K.L., McEwan, P.A., and Lovell, S.C. (2008). The leucine-rich repeat structure. Cell Mol Life Sci *65*, 2307-2333.

Bentham, J., Morris, D.L., Graham, D.S.C., Pinder, C.L., Tombleson, P., Behrens, T.W., Martin, J., Fairfax, B.P., Knight, J.C., Chen, L*., et al.* (2015). Genetic association analyses implicate aberrant regulation of innate and adaptive immunity genes in the pathogenesis of systemic lupus erythematosus. Nat Genet *47*, 1457-1464.

Bergstrom, B., Aune, M.H., Awuh, J.A., Kojen, J.F., Blix, K.J., Ryan, L., Flo, T.H., Mollnes, T.E., Espevik, T., and Stenvik, J. (2015). TLR8 Senses Staphylococcus aureus RNA in Human Primary Monocytes and Macrophages and Induces IFN-beta Production via a TAK1-IKKbeta-IRF5 Signaling Pathway. J Immunol *195*, 1100-1111.

Blasius, A.L., Arnold, C.N., Georgel, P., Rutschmann, S., Xia, Y., Lin, P., Ross, C., Li, X., Smart, N.G., and Beutler, B. (2010). Slc15a4, AP-3, and Hermansky-Pudlak syndrome proteins are required for Toll-like receptor signaling in plasmacytoid dendritic cells. Proc Natl Acad Sci U S A *107*, 19973-19978.

Boix, E., and Nogues, M.V. (2007). Mammalian antimicrobial proteins and peptides: overview on the RNase A superfamily members involved in innate host defence. Mol Biosyst *3*, 317-335.

Bonham, K.S., Orzalli, M.H., Hayashi, K., Wolf, A.I., Glanemann, C., Weninger, W., Iwasaki, A., Knipe, D.M., and Kagan, J.C. (2014). A promiscuous lipid-binding protein diversifies the subcellular sites of toll-like receptor signal transduction. Cell *156*, 705-716.

Botos, I., Segal, D.M., and Davies, D.R. (2011). The structural biology of Toll-like receptors. Structure *19*, 447-459.

Bottazzi, B., Doni, A., Garlanda, C., and Mantovani, A. (2010). An integrated view of humoral innate immunity: pentraxins as a paradigm. Annu Rev Immunol *28*, 157-183.

Brogden, K.A. (2005). Antimicrobial peptides: pore formers or metabolic inhibitors in bacteria? Nat Rev Microbiol *3*, 238-250.

Cao, Z., Henzel, W.J., and Gao, X. (1996). IRAK: a kinase associated with the interleukin-1 receptor. Science *271*, 1128-1131.

Celhar, T., Magalhaes, R., and Fairhurst, A.M. (2012). TLR7 and TLR9 in SLE: when sensing self goes wrong. Immunol Res *53*, 58-77.

Chacko, R., and Shankar, V. (1998). Extracellular ribonuclease from Rhizopus stolonifer: characteristics of an atypical--guanylic acid preferential--enzyme from ribonuclease T2 family. Biochim Biophys Acta *1379*, 264-272.

Chakrabarti, A., Jha, B.K., and Silverman, R.H. (2011). New insights into the role of RNase L in innate immunity. J Interferon Cytokine Res *31*, 49-57.

Chan, M.P., Onji, M., Fukui, R., Kawane, K., Shibata, T., Saitoh, S., Ohto, U., Shimizu, T., Barber, G.N., and Miyake, K. (2015). DNase II-dependent DNA digestion is required for DNA sensing by TLR9. Nat Commun *6*, 5853.

Chiffoleau, E. (2018). C-Type Lectin-Like Receptors As Emerging Orchestrators of Sterile Inflammation Represent Potential Therapeutic Targets. Front Immunol *9*, 227.

Chmiest, D., Sharma, N., Zanin, N., Viaris de Lesegno, C., Shafaq-Zadah, M., Sibut, V., Dingli, F., Hupe, P., Wilmes, S., Piehler, J.*, et al.* (2016). Spatiotemporal control of interferon-induced JAK/STAT signalling and gene transcription by the retromer complex. Nat Commun *7*, 13476.

Cho, S., Beintema, J.J., and Zhang, J. (2005). The ribonuclease A superfamily of mammals and birds: identifying new members and tracing evolutionary histories. Genomics *85*, 208-220.

Cojocaru, M., Cojocaru, I.M., Silosi, I., and Vrabie, C.D. (2011). Manifestations of systemic lupus erythematosus. Maedica (Buchar) *6*, 330-336.

Condon, C., and Putzer, H. (2002). The phylogenetic distribution of bacterial ribonucleases. Nucleic Acids Res *30*, 5339-5346.

Crow, Y.J., and Manel, N. (2015). Aicardi-Goutieres syndrome and the type I interferonopathies. Nat Rev Immunol *15*, 429-440.

D'Arcy, M.S. (2019). Cell death: a review of the major forms of apoptosis, necrosis and autophagy. Cell Biol Int *43*, 582-592.

Dambuza, I.M., and Brown, G.D. (2015). C-type lectins in immunity: recent developments. Curr Opin Immunol *32*, 21-27.

de Crecy-Lagard, V., Boccaletto, P., Mangleburg, C.G., Sharma, P., Lowe, T.M., Leidel, S.A., and Bujnicki, J.M. (2019). Matching tRNA modifications in humans to their known and predicted enzymes. Nucleic Acids Res *47*, 2143-2159.

Deshpande, R.A., and Shankar, V. (2002). Ribonucleases from T2 family. Crit Rev Microbiol *28*, 79-122.

Dhuriya, Y.K., and Sharma, D. (2018). Necroptosis: a regulated inflammatory mode of cell death. J Neuroinflammation *15*, 199.

Dobbs, N., Burnaevskiy, N., Chen, D., Gonugunta, V.K., Alto, N.M., and Yan, N. (2015). STING Activation by Translocation from the ER Is Associated with Infection and Autoinflammatory Disease. Cell Host Microbe *18*, 157-168.

Dobin, A., Davis, C.A., Schlesinger, F., Drenkow, J., Zaleski, C., Jha, S., Batut, P., Chaisson, M., and Gingeras, T.R. (2013). STAR: ultrafast universal RNA-seq aligner. Bioinformatics *29*, 15-21.

Doria, A., Zen, M., Bettio, S., Gatto, M., Bassi, N., Nalotto, L., Ghirardello, A., Iaccarino, L., and Punzi, L. (2012). Autoinflammation and autoimmunity: bridging the divide. Autoimmun Rev *12*, 22-30.

Dunkelberger, J.R., and Song, W.C. (2010). Complement and its role in innate and adaptive immune responses. Cell Res *20*, 34-50.

Elmore, S. (2007). Apoptosis: a review of programmed cell death. Toxicol Pathol *35*, 495-516.

Emmerich, C.H., Ordureau, A., Strickson, S., Arthur, J.S., Pedrioli, P.G., Komander, D., and Cohen, P. (2013). Activation of the canonical IKK complex by K63/M1-linked hybrid ubiquitin chains. Proc Natl Acad Sci U S A *110*, 15247-15252.

Everts, B., Amiel, E., Huang, S.C., Smith, A.M., Chang, C.H., Lam, W.Y., Redmann, V., Freitas, T.C., Blagih, J., van der Windt, G.J.*, et al.* (2014). TLR-driven early glycolytic reprogramming via the kinases TBK1-IKKvarepsilon supports the anabolic demands of dendritic cell activation. Nat Immunol *15*, 323-332.

Ewald, S.E., Engel, A., Lee, J., Wang, M., Bogyo, M., and Barton, G.M. (2011). Nucleic acid recognition by Toll-like receptors is coupled to stepwise processing by cathepsins and asparagine endopeptidase. J Exp Med *208*, 643-651.

Ferrao, R., Zhou, H., Shan, Y., Liu, Q., Li, Q., Shaw, D.E., Li, X., and Wu, H. (2014). IRAK4 dimerization and trans-autophosphorylation are induced by Myddosome assembly. Mol Cell *55*, 891-903.

Fitzgerald, K.A., and Kagan, J.C. (2020). Toll-like Receptors and the Control of Immunity. Cell *180*, 1044-1066.

Flannagan, R.S., Jaumouille, V., and Grinstein, S. (2012). The cell biology of phagocytosis. Annu Rev Pathol *7*, 61-98.

Forsbach, A., Nemorin, J.G., Montino, C., Muller, C., Samulowitz, U., Vicari, A.P., Jurk, M., Mutwiri, G.K., Krieg, A.M., Lipford, G.B., and Vollmer, J. (2008). Identification of RNA sequence motifs stimulating sequence-specific TLR8-dependent immune responses. J Immunol *180*, 3729-3738.

Fukui, R., Yamamoto, C., Matsumoto, F., Onji, M., Shibata, T., Murakami, Y., Kanno, A., Hayashi, T., Tanimura, N., Yoshida, N., and Miyake, K. (2018). Cleavage of Toll-Like Receptor 9 Ectodomain Is Required for In Vivo Responses to Single Strand DNA. Front Immunol *9*, 1491.

Gaidt, M.M., Ebert, T.S., Chauhan, D., Ramshorn, K., Pinci, F., Zuber, S., O'Duill, F., Schmid-Burgk, J.L., Hoss, F., Buhmann, R.*, et al.* (2017). The DNA Inflammasome in Human Myeloid Cells Is Initiated by a STING-Cell Death Program Upstream of NLRP3. Cell *171*, 1110-1124 e1118.

Gaidt, M.M., Ebert, T.S., Chauhan, D., Schmidt, T., Schmid-Burgk, J.L., Rapino, F., Robertson, A.A., Cooper, M.A., Graf, T., and Hornung, V. (2016). Human Monocytes Engage an Alternative Inflammasome Pathway. Immunity *44*, 833-846.

Gaidt, M.M., and Hornung, V. (2016). Pore formation by GSDMD is the effector mechanism of pyroptosis. EMBO J *35*, 2167-2169.

Gaidt, M.M., Rapino, F., Graf, T., and Hornung, V. (2018). Modeling Primary Human Monocytes with the Trans-Differentiation Cell Line BLaER1. Methods Mol Biol *1714*, 57-66.

Gao, D., Li, T., Li, X.D., Chen, X., Li, Q.Z., Wight-Carter, M., and Chen, Z.J. (2015). Activation of cyclic GMP-AMP synthase by self-DNA causes autoimmune diseases. Proc Natl Acad Sci U S A *112*, E5699-5705.

Gao, W., Xiong, Y., Li, Q., and Yang, H. (2017). Inhibition of Toll-Like Receptor Signaling as a Promising Therapy for Inflammatory Diseases: A Journey from Molecular to Nano Therapeutics. Front Physiol *8*, 508.

Gehrke, N., Mertens, C., Zillinger, T., Wenzel, J., Bald, T., Zahn, S., Tuting, T., Hartmann, G., and Barchet, W. (2013). Oxidative damage of DNA confers resistance to cytosolic nuclease TREX1 degradation and potentiates STING-dependent immune sensing. Immunity *39*, 482-495.

Globisch, D., Pearson, D., Hienzsch, A., Bruckl, T., Wagner, M., Thoma, I., Thumbs, P., Reiter, V., Kneuttinger, A.C., Muller, M.*, et al.* (2011). Systems-based analysis of modified tRNA bases. Angew Chem Int Ed Engl *50*, 9739-9742.

Gorden, K.K., Qiu, X.X., Binsfeld, C.C., Vasilakos, J.P., and Alkan, S.S. (2006). Cutting edge: activation of murine TLR8 by a combination of imidazoquinoline immune response modifiers and polyT oligodeoxynucleotides. J Immunol *177*, 6584-6587.

Gould, T.J., Lysov, Z., and Liaw, P.C. (2015). Extracellular DNA and histones: double-edged swords in immunothrombosis. J Thromb Haemost *13 Suppl 1*, S82-91.

Gupta, S.K., Haigh, B.J., Griffin, F.J., and Wheeler, T.T. (2013). The mammalian secreted RNases: mechanisms of action in host defence. Innate Immun *19*, 86-97.

Han, J.W., Zheng, H.F., Cui, Y., Sun, L.D., Ye, D.Q., Hu, Z., Xu, J.H., Cai, Z.M., Huang, W., Zhao, G.P.*, et al.* (2009). Genome-wide association study in a Chinese Han population identifies nine new susceptibility loci for systemic lupus erythematosus. Nat Genet *41*, 1234-1237.

Haud, N., Kara, F., Diekmann, S., Henneke, M., Willer, J.R., Hillwig, M.S., Gregg, R.G., Macintosh, G.C., Gartner, J., Alia, A., and Hurlstone, A.F. (2011). rnaset2 mutant zebrafish model familial cystic leukoencephalopathy and reveal a role for RNase T2 in degrading ribosomal RNA. Proc Natl Acad Sci U S A *108*, 1099-1103.

Hayashi, F., Smith, K.D., Ozinsky, A., Hawn, T.R., Yi, E.C., Goodlett, D.R., Eng, J.K., Akira, S., Underhill, D.M., and Aderem, A. (2001). The innate immune response to bacterial flagellin is mediated by Toll-like receptor 5. Nature *410*, 1099-1103.

Heil, F., Hemmi, H., Hochrein, H., Ampenberger, F., Kirschning, C., Akira, S., Lipford, G., Wagner, H., and Bauer, S. (2004). Species-specific recognition of single-stranded RNA via toll-like receptor 7 and 8. Science *303*, 1526-1529.

Heinz, L.X., Lee, J., Kapoor, U., Kartnig, F., Sedlyarov, V., Papakostas, K., Cesar-Razquin, A., Essletzbichler, P., Goldmann, U., Stefanovic, A.*, et al.* (2020). TASL is the SLC15A4-associated adaptor for IRF5 activation by TLR7-9. Nature *581*, 316-322.

Hemmi, H., Kaisho, T., Takeuchi, O., Sato, S., Sanjo, H., Hoshino, K., Horiuchi, T., Tomizawa, H., Takeda, K., and Akira, S. (2002). Small anti-viral compounds activate immune cells via the TLR7 MyD88-dependent signaling pathway. Nat Immunol *3*, 196-200.

Henneke, M., Diekmann, S., Ohlenbusch, A., Kaiser, J., Engelbrecht, V., Kohlschutter, A., Kratzner, R., Madruga-Garrido, M., Mayer, M., Opitz, L.*, et al.* (2009). RNASET2-deficient cystic leukoencephalopathy resembles congenital cytomegalovirus brain infection. Nat Genet *41*, 773-775.

Hillwig, M.S., Liu, X., Liu, G., Thornburg, R.W., and Macintosh, G.C. (2010). Petunia nectar proteins have ribonuclease activity. J Exp Bot *61*, 2951-2965.

Hillwig, M.S., Rizhsky, L., Wang, Y., Umanskaya, A., Essner, J.J., and MacIntosh, G.C. (2009). Zebrafish RNase T2 genes and the evolution of secretory ribonucleases in animals. BMC Evol Biol *9*, 170.

Horng, T., Barton, G.M., Flavell, R.A., and Medzhitov, R. (2002). The adaptor molecule TIRAP provides signalling specificity for Toll-like receptors. Nature *420*, 329-333.

Hornung, V., Ablasser, A., Charrel-Dennis, M., Bauernfeind, F., Horvath, G., Caffrey, D.R., Latz, E., and Fitzgerald, K.A. (2009). AIM2 recognizes cytosolic dsDNA and forms a caspase-1-activating inflammasome with ASC. Nature *458*, 514-518.

Hornung, V., Ellegast, J., Kim, S., Brzozka, K., Jung, A., Kato, H., Poeck, H., Akira, S., Conzelmann, K.K., Schlee, M.*, et al.* (2006). 5'-Triphosphate RNA is the ligand for RIG-I. Science *314*, 994-997.

Hornung, V., Hartmann, R., Ablasser, A., and Hopfner, K.P. (2014). OAS proteins and cGAS: unifying concepts in sensing and responding to cytosolic nucleic acids. Nat Rev Immunol *14*, 521-528.

Hugot, K., Ponchet, M., Marais, A., Ricci, P., and Galiana, E. (2002). A tobacco S-like RNase inhibits hyphal elongation of plant pathogens. Mol Plant Microbe Interact *15*, 243-250.

Idzko, M., Ferrari, D., and Eltzschig, H.K. (2014). Nucleotide signalling during inflammation. Nature *509*, 310-317.

Igic, B., and Kohn, J.R. (2001). Evolutionary relationships among self-incompatibility RNases. Proc Natl Acad Sci U S A *98*, 13167-13171.

Imler, J.L., and Hoffmann, J.A. (2002). Toll receptors in Drosophila: a family of molecules regulating development and immunity. Curr Top Microbiol Immunol *270*, 63-79.

Inokuchi, N., Kobayashi, H., Hara, J., Itagaki, T., Koyama, T., Iwama, M., Ohgi, K., and Irie, M. (2000). Amino acid sequence of an unique ribonuclease with a C-terminus rich in O-glycosylated serine and threonine from culture medium of Lentinus edodes. Biosci Biotechnol Biochem *64*, 44-51.

Irie, M. (1999). Structure-function relationships of acid ribonucleases: lysosomal, vacuolar, and periplasmic enzymes. Pharmacol Ther *81*, 77-89.

Ishikawa, H., and Barber, G.N. (2008). STING is an endoplasmic reticulum adaptor that facilitates innate immune signalling. Nature *455*, 674-678.

Ivashkiv, L.B., and Donlin, L.T. (2014). Regulation of type I interferon responses. Nat Rev Immunol *14*, 36-49.

Jin, M.S., Kim, S.E., Heo, J.Y., Lee, M.E., Kim, H.M., Paik, S.G., Lee, H., and Lee, J.O. (2007). Crystal structure of the TLR1-TLR2 heterodimer induced by binding of a tri-acylated lipopeptide. Cell *130*, 1071-1082.

Kang, J.Y., Nan, X., Jin, M.S., Youn, S.J., Ryu, Y.H., Mah, S., Han, S.H., Lee, H., Paik, S.G., and Lee, J.O. (2009). Recognition of lipopeptide patterns by Toll-like receptor 2-Toll-like receptor 6 heterodimer. Immunity *31*, 873-884.

Kariko, K., Buckstein, M., Ni, H., and Weissman, D. (2005). Suppression of RNA recognition by Toll-like receptors: the impact of nucleoside modification and the evolutionary origin of RNA. Immunity *23*, 165-175.

Kato, H., Takeuchi, O., Sato, S., Yoneyama, M., Yamamoto, M., Matsui, K., Uematsu, S., Jung, A., Kawai, T., Ishii, K.J*., et al.* (2006). Differential roles of MDA5 and RIG-I helicases in the recognition of RNA viruses. Nature *441*, 101-105.

Kawai, T., and Akira, S. (2010). The role of pattern-recognition receptors in innate immunity: update on Toll-like receptors. Nat Immunol *11*, 373-384.

Kawano, S., Kakuta, Y., and Kimura, M. (2002). Guanine binding site of the Nicotiana glutinosa ribonuclease NW revealed by X-ray crystallography. Biochemistry *41*, 15195-15202.

Kawasaki, T., and Kawai, T. (2014). Toll-like receptor signaling pathways. Front Immunol *5*, 461.

Kawata, Y., Sakiyama, F., Hayashi, F., and Kyogoku, Y. (1990). Identification of two essential histidine residues of ribonuclease T2 from Aspergillus oryzae. Eur J Biochem *187*, 255-262.

Kayagaki, N., Stowe, I.B., Lee, B.L., O'Rourke, K., Anderson, K., Warming, S., Cuellar, T., Haley, B., Roose-Girma, M., Phung, Q.T*., et al.* (2015). Caspase-11 cleaves gasdermin D for non-canonical inflammasome signalling. Nature *526*, 666-671.

Kayagaki, N., Warming, S., Lamkanfi, M., Vande Walle, L., Louie, S., Dong, J., Newton, K., Qu, Y., Liu, J., Heldens, S*., et al.* (2011). Non-canonical inflammasome activation targets caspase-11. Nature *479*, 117-121.

Kerr, J.F., Wyllie, A.H., and Currie, A.R. (1972). Apoptosis: a basic biological phenomenon with wide-ranging implications in tissue kinetics. Br J Cancer *26*, 239-257.

Kim, H.M., Park, B.S., Kim, J.I., Kim, S.E., Lee, J., Oh, S.C., Enkhbayar, P., Matsushima, N., Lee, H., Yoo, O.J., and Lee, J.O. (2007). Crystal structure of the TLR4-MD-2 complex with bound endotoxin antagonist Eritoran. Cell *130*, 906-917.

Kim, Y.M., Brinkmann, M.M., Paquet, M.E., and Ploegh, H.L. (2008). UNC93B1 delivers nucleotide-sensing toll-like receptors to endolysosomes. Nature *452*, 234-238.

Koczera, P., Martin, L., Marx, G., and Schuerholz, T. (2016). The Ribonuclease A Superfamily in Humans: Canonical RNases as the Buttress of Innate Immunity. Int J Mol Sci *17*.

Kroese, L.J., and Scheffer, P.G. (2014). 8-hydroxy-2'-deoxyguanosine and cardiovascular disease: a systematic review. Curr Atheroscler Rep *16*, 452.

Kruger, A., Oldenburg, M., Chebrolu, C., Beisser, D., Kolter, J., Sigmund, A.M., Steinmann, J., Schafer, S., Hochrein, H., Rahmann, S*., et al.* (2015). Human TLR8 senses UR/URR motifs in bacterial and mitochondrial RNA. EMBO Rep *16*, 1656-1663.

Kumar, A., and McClure, B. (2010). Pollen-pistil interactions and the endomembrane system. J Exp Bot *61*, 2001-2013.

Lamkanfi, M., and Dixit, V.M. (2014). Mechanisms and functions of inflammasomes. Cell *157*, 1013-1022.

Latz, E., Verma, A., Visintin, A., Gong, M., Sirois, C.M., Klein, D.C., Monks, B.G., McKnight, C.J., Lamphier, M.S., Duprex, W.P.*, et al.* (2007). Ligand-induced conformational changes allosterically activate Toll-like receptor 9. Nat Immunol *8*, 772-779.

Lee, A.J., and Ashkar, A.A. (2018). The Dual Nature of Type I and Type II Interferons. Front Immunol *9*, 2061.

Lee, J., Chuang, T.H., Redecke, V., She, L., Pitha, P.M., Carson, D.A., Raz, E., and Cottam, H.B. (2003). Molecular basis for the immunostimulatory activity of guanine nucleoside analogs: activation of Toll-like receptor 7. Proc Natl Acad Sci U S A *100*, 6646-6651.

Lee-Kirsch, M.A., Wolf, C., and Gunther, C. (2014). Aicardi-Goutieres syndrome: a model disease for systemic autoimmunity. Clin Exp Immunol *175*, 17-24.

Lehmann, S.M., Kruger, C., Park, B., Derkow, K., Rosenberger, K., Baumgart, J., Trimbuch, T., Eom, G., Hinz, M., Kaul, D.*, et al.* (2012). An unconventional role for miRNA: let-7 activates Toll-like receptor 7 and causes neurodegeneration. Nat Neurosci *15*, 827-835.

Lemaitre, B., Nicolas, E., Michaut, L., Reichhart, J.M., and Hoffmann, J.A. (1996). The dorsoventral regulatory gene cassette spatzle/Toll/cactus controls the potent antifungal response in Drosophila adults. Cell *86*, 973-983.

Leonard, J.N., Ghirlando, R., Askins, J., Bell, J.K., Margulies, D.H., Davies, D.R., and Segal, D.M. (2008). The TLR3 signaling complex forms by cooperative receptor dimerization. Proc Natl Acad Sci U S A *105*, 258-263.

Li, B., and Dewey, C.N. (2011). RSEM: accurate transcript quantification from RNA-Seq data with or without a reference genome. BMC Bioinformatics *12*, 323.

Li, Z., Michael, I.P., Zhou, D., Nagy, A., and Rini, J.M. (2013). Simple piggyBac transposon-based mammalian cell expression system for inducible protein production. Proc Natl Acad Sci U S A *110*, 5004-5009.

Lin, S.C., Lo, Y.C., and Wu, H. (2010). Helical assembly in the MyD88-IRAK4-IRAK2 complex in TLR/IL-1R signalling. Nature *465*, 885-890.

Liu, S., Cai, X., Wu, J., Cong, Q., Chen, X., Li, T., Du, F., Ren, J., Wu, Y.T., Grishin, N.V., and Chen, Z.J. (2015). Phosphorylation of innate immune adaptor proteins MAVS, STING, and TRIF induces IRF3 activation. Science *347*, aaa2630.

Liu, T., Zhang, L., Joo, D., and Sun, S.C. (2017). NF-kappaB signaling in inflammation. Signal Transduct Target Ther *2*.

Lomaga, M.A., Yeh, W.C., Sarosi, I., Duncan, G.S., Furlonger, C., Ho, A., Morony, S., Capparelli, C., Van, G., Kaufman, S.*, et al.* (1999). TRAF6 deficiency results in osteopetrosis and defective interleukin-1, CD40, and LPS signaling. Genes Dev *13*, 1015-1024.

Lu, L., Li, J., Moussaoui, M., and Boix, E. (2018). Immune Modulation by Human Secreted RNases at the Extracellular Space. Front Immunol *9*, 1012.

Ma, Y.J., and Garred, P. (2018). Pentraxins in Complement Activation and Regulation. Front Immunol *9*, 3046.

MacIntosh, G.C. (2011). RNase T2 Family: Enzymatic Properties, Functional Diversity, and Evolution of Ancient Ribonucleases. In Ribonucleases, A.W. Nicholson, ed. (Berlin, Heidelberg: Springer Berlin Heidelberg), pp. 89-114.

MacIntosh, G.C., Bariola, P.A., Newbigin, E., and Green, P.J. (2001). Characterization of Rny1, the Saccharomyces cerevisiae member of the T2 RNase family of RNases: unexpected functions for ancient enzymes? Proc Natl Acad Sci U S A *98*, 1018-1023.

MacIntosh, G.C., Hillwig, M.S., Meyer, A., and Flagel, L. (2010). RNase T2 genes from rice and the evolution of secretory ribonucleases in plants. Mol Genet Genomics *283*, 381-396.

Man, S.M., Karki, R., and Kanneganti, T.D. (2017). Molecular mechanisms and functions of pyroptosis, inflammatory caspases and inflammasomes in infectious diseases. Immunol Rev *277*, 61-75.

Mandal, A., and Viswanathan, C. (2015). Natural killer cells: In health and disease. Hematol Oncol Stem Cell Ther *8*, 47-55.

Marshak-Rothstein, A. (2006). Toll-like receptors in systemic autoimmune disease. Nat Rev Immunol *6*, 823-835.

Martin, L., Koczera, P., Simons, N., Zechendorf, E., Hoeger, J., Marx, G., and Schuerholz, T. (2016). The Human Host Defense Ribonucleases 1, 3 and 7 Are Elevated in Patients with Sepsis after Major Surgery--A Pilot Study. Int J Mol Sci *17*, 294.

Martinon, F., Burns, K., and Tschopp, J. (2002). The inflammasome: a molecular platform triggering activation of inflammatory caspases and processing of proIL-beta. Mol Cell *10*, 417-426.

Medzhitov, R., Preston-Hurlburt, P., and Janeway, C.A., Jr. (1997). A human homologue of the Drosophila Toll protein signals activation of adaptive immunity. Nature *388*, 394-397.

Meng, X., Sun, P., and Kao, T.H. (2011). S-RNase-based self-incompatibility in Petunia inflata. Ann Bot *108*, 637-646.

Miyake, K., Shibata, T., Ohto, U., and Shimizu, T. (2017). Emerging roles of the processing of nucleic acids and Toll-like receptors in innate immune responses to nucleic acids. J Leukoc Biol *101*, 135-142.

Montague, T.G., Cruz, J.M., Gagnon, J.A., Church, G.M., and Valen, E. (2014). CHOPCHOP: a CRISPR/Cas9 and TALEN web tool for genome editing. Nucleic Acids Res *42*, W401-407.

Morizot, A., and Saleh, M. (2012). Non-apoptotic functions of cell death effectors in inflammation and innate immunity. Microbes Infect *14*, 1241-1253.

Motwani, M., Pesiridis, S., and Fitzgerald, K.A. (2019). DNA sensing by the cGAS-STING pathway in health and disease. Nat Rev Genet *20*, 657-674.

Mukai, K., Konno, H., Akiba, T., Uemura, T., Waguri, S., Kobayashi, T., Barber, G.N., Arai, H., and Taguchi, T. (2016). Activation of STING requires palmitoylation at the Golgi. Nat Commun *7*, 11932.

Murakami, M., Hibi, M., Nakagawa, N., Nakagawa, T., Yasukawa, K., Yamanishi, K., Taga, T., and Kishimoto, T. (1993). IL-6-induced homodimerization of gp130 and associated activation of a tyrosine kinase. Science *260*, 1808-1810.

Murphy, K., Travers, P., Walport, M., and Janeway, C. (2012). Janeway's immunobiology (New York: Garland Science).

Nakagawa, A., Tanaka, I., Sakai, R., Nakashima, T., Funatsu, G., and Kimura, M. (1999). Crystal structure of a ribonuclease from the seeds of bitter gourd (Momordica charantia) at 1.75 A resolution. Biochim Biophys Acta *1433*, 253-260.

Numata, T., Suzuki, A., Kakuta, Y., Kimura, K., Yao, M., Tanaka, I., Yoshida, Y., Ueda, T., and Kimura, M. (2003). Crystal structures of the ribonuclease MC1 mutants N71T and N71S in complex with 5'-GMP: structural basis for alterations in substrate specificity. Biochemistry *42*, 5270-5278.

Nurnberger, T., Abel, S., Jost, W., and Glund, K. (1990). Induction of an Extracellular Ribonuclease in Cultured Tomato Cells upon Phosphate Starvation. Plant Physiol *92*, 970-976.

Odhams, C.A., Roberts, A.L., Vester, S.K., Duarte, C.S.T., Beales, C.T., Clarke, A.J., Lindinger, S., Daffern, S.J., Zito, A., Chen, L.*, et al.* (2019). Interferon inducible X-linked gene CXorf21 may contribute to sexual dimorphism in Systemic Lupus Erythematosus. Nat Commun *10*, 2164.

Ohto, U., Ishida, H., Shibata, T., Sato, R., Miyake, K., and Shimizu, T. (2018). Toll-like Receptor 9 Contains Two DNA Binding Sites that Function Cooperatively to Promote Receptor Dimerization and Activation. Immunity *48*, 649-658 e644.

Ohto, U., Shibata, T., Tanji, H., Ishida, H., Krayukhina, E., Uchiyama, S., Miyake, K., and Shimizu, T. (2015). Structural basis of CpG and inhibitory DNA recognition by Toll-like receptor 9. Nature *520*, 702-705.

Okabe, Y., Kawane, K., Akira, S., Taniguchi, T., and Nagata, S. (2005). Toll-like receptor-independent gene induction program activated by mammalian DNA escaped from apoptotic DNA degradation. J Exp Med *202*, 1333-1339.

Ostendorf, T., Zillinger, T., Andryka, K., Schlee-Guimaraes, T.M., Schmitz, S., Marx, S., Bayrak, K., Linke, R., Salgert, S., Wegner, J.*, et al.* (2020). Immune Sensing of Synthetic, Bacterial, and Protozoan RNA by Toll-like Receptor 8 Requires Coordinated Processing by RNase T2 and RNase 2. Immunity *52*, 591-605 e596.

Parry, S., Newbigin, E., Currie, G., Bacic, A., and Oxley, D. (1997). Identification of active-site histidine residues of a self-incompatibility ribonuclease from a wild tomato. Plant Physiol *115*, 1421-1429.

Pelka, K., Bertheloot, D., Reimer, E., Phulphagar, K., Schmidt, S.V., Christ, A., Stahl, R., Watson, N., Miyake, K., Hacohen, N.*, et al.* (2018). The Chaperone UNC93B1 Regulates Toll-like Receptor Stability Independently of Endosomal TLR Transport. Immunity *48*, 911-922 e917.

Pereira, M., Francisco, S., Varanda, A.S., Santos, M., Santos, M.A.S., and Soares, A.R. (2018). Impact of tRNA Modifications and tRNA-Modifying Enzymes on Proteostasis and Human Disease. Int J Mol Sci *19*.

Petes, C., Odoardi, N., and Gee, K. (2017). The Toll for Trafficking: Toll-Like Receptor 7 Delivery to the Endosome. Front Immunol *8*, 1075.

Pichlmair, A., Schulz, O., Tan, C.P., Naslund, T.I., Liljestrom, P., Weber, F., and Reis e Sousa, C. (2006). RIG-I-mediated antiviral responses to single-stranded RNA bearing 5'-phosphates. Science *314*, 997-1001.

Platnich, J.M., and Muruve, D.A. (2019). NOD-like receptors and inflammasomes: A review of their canonical and non-canonical signaling pathways. Arch Biochem Biophys *670*, 4-14.

Poltorak, A., He, X., Smirnova, I., Liu, M.Y., Van Huffel, C., Du, X., Birdwell, D., Alejos, E., Silva, M., Galanos, C.*, et al.* (1998). Defective LPS signaling in C3H/HeJ and C57BL/10ScCr mice: mutations in Tlr4 gene. Science *282*, 2085-2088.

Potenza, N., Salvatore, V., Migliozzi, A., Martone, V., Nobile, V., and Russo, A. (2006). Hybridase activity of human ribonuclease-1 revealed by a real-time fluorometric assay. Nucleic Acids Res *34*, 2906-2913.

Qureshi, S.T., Lariviere, L., Leveque, G., Clermont, S., Moore, K.J., Gros, P., and Malo, D. (1999). Endotoxin-tolerant mice have mutations in Toll-like receptor 4 (Tlr4). J Exp Med *189*, 615-625.

Raines, R.T. (1998). Ribonuclease A. Chem Rev *98*, 1045-1066.

Rapino, F., Robles, E.F., Richter-Larrea, J.A., Kallin, E.M., Martinez-Climent, J.A., and Graf, T. (2013). C/EBPalpha induces highly efficient macrophage transdifferentiation of B lymphoma and leukemia cell lines and impairs their tumorigenicity. Cell Rep *3*, 1153-1163.

Rice, G.I., Melki, I., Fremond, M.L., Briggs, T.A., Rodero, M.P., Kitabayashi, N., Oojageer, A., Bader-Meunier, B., Belot, A., Bodemer, C.*, et al.* (2017). Assessment of Type I Interferon Signaling in Pediatric Inflammatory Disease. J Clin Immunol *37*, 123-132.

Roalson, E.H., and McCubbin, A.G. (2003). S-RNases and sexual incompatibility: structure, functions, and evolutionary perspectives. Mol Phylogenet Evol *29*, 490-506.

Rodriguez, S.M., Panjikar, S., Van Belle, K., Wyns, L., Messens, J., and Loris, R. (2008). Nonspecific base recognition mediated by water bridges and hydrophobic stacking in ribonuclease I from Escherichia coli. Protein Sci *17*, 681-690.

Rosenberg, H.F. (2008). RNase A ribonucleases and host defense: an evolving story. J Leukoc Biol *83*, 1079-1087.

Rowe, D.C., McGettrick, A.F., Latz, E., Monks, B.G., Gay, N.J., Yamamoto, M., Akira, S., O'Neill, L.A., Fitzgerald, K.A., and Golenbock, D.T. (2006). The myristoylation of TRIF-related adaptor molecule is essential for Toll-like receptor 4 signal transduction. Proc Natl Acad Sci U S A *103*, 6299-6304.

Santiago-Raber, M.L., Baudino, L., and Izui, S. (2009). Emerging roles of TLR7 and TLR9 in murine SLE. J Autoimmun *33*, 231-238.

Satake, H., and Sekiguchi, T. (2012). Toll-like receptors of deuterostome invertebrates. Front Immunol *3*, 34.

Sborgi, L., Ruhl, S., Mulvihill, E., Pipercevic, J., Heilig, R., Stahlberg, H., Farady, C.J., Muller, D.J., Broz, P., and Hiller, S. (2016). GSDMD membrane pore formation constitutes the mechanism of pyroptotic cell death. EMBO J *35*, 1766-1778.

Scaffidi, P., Misteli, T., and Bianchi, M.E. (2002). Release of chromatin protein HMGB1 by necrotic cells triggers inflammation. Nature *418*, 191-195.

Schmacke, N.A., and Hornung, V. (2020). Fourth defence molecule completes antiviral line-up. Nature *581*, 266-267.

Schmid-Burgk, J.L., Chauhan, D., Schmidt, T., Ebert, T.S., Reinhardt, J., Endl, E., and Hornung, V. (2016). A Genome-wide CRISPR (Clustered Regularly Interspaced Short Palindromic Repeats) Screen Identifies NEK7 as an Essential Component of NLRP3 Inflammasome Activation. J Biol Chem *291*, 103-109.

Schmid-Burgk, J.L., Schmidt, T., Gaidt, M.M., Pelka, K., Latz, E., Ebert, T.S., and Hornung, V. (2014). OutKnocker: a web tool for rapid and simple genotyping of designer nuclease edited cell lines. Genome Res *24*, 1719-1723.

Schmidt, T., Schmid-Burgk, J.L., and Hornung, V. (2015). Synthesis of an arrayed sgRNA library targeting the human genome. Sci Rep *5*, 14987.

Schneider, R., Unger, G., Stark, R., Schneider-Scherzer, E., and Thiel, H.J. (1993). Identification of a structural glycoprotein of an RNA virus as a ribonuclease. Science *261*, 1169-1171.

Schoenemeyer, A., Barnes, B.J., Mancl, M.E., Latz, E., Goutagny, N., Pitha, P.M., Fitzgerald, K.A., and Golenbock, D.T. (2005). The interferon regulatory factor, IRF5, is a central mediator of toll-like receptor 7 signaling. J Biol Chem *280*, 17005-17012.

Scofield, R.H., Bruner, G.R., Namjou, B., Kimberly, R.P., Ramsey-Goldman, R., Petri, M., Reveille, J.D., Alarcon, G.S., Vila, L.M., Reid, J.*, et al.* (2008). Klinefelter's syndrome (47,XXY) in male systemic lupus erythematosus patients: support for the notion of a gene-dose effect from the X chromosome. Arthritis Rheum *58*, 2511-2517.

Shi, J., Zhao, Y., Wang, K., Shi, X., Wang, Y., Huang, H., Zhuang, Y., Cai, T., Wang, F., and Shao, F. (2015). Cleavage of GSDMD by inflammatory caspases determines pyroptotic cell death. Nature *526*, 660-665.

Shi, J., Zhao, Y., Wang, Y., Gao, W., Ding, J., Li, P., Hu, L., and Shao, F. (2014). Inflammatory caspases are innate immune receptors for intracellular LPS. Nature *514*, 187-192.

Shi, Y., Evans, J.E., and Rock, K.L. (2003). Molecular identification of a danger signal that alerts the immune system to dying cells. Nature *425*, 516-521.

Shibata, T., Ohto, U., Nomura, S., Kibata, K., Motoi, Y., Zhang, Y., Murakami, Y., Fukui, R., Ishimoto, T., Sano, S.*, et al.* (2016). Guanosine and its modified derivatives are endogenous ligands for TLR7. Int Immunol *28*, 211-222.

Sisirak, V., Ganguly, D., Lewis, K.L., Couillault, C., Tanaka, L., Bolland, S., D'Agati, V., Elkon, K.B., and Reizis, B. (2014). Genetic evidence for the role of plasmacytoid dendritic cells in systemic lupus erythematosus. J Exp Med *211*, 1969-1976.

Sorrentino, S. (2010). The eight human "canonical" ribonucleases: molecular diversity, catalytic properties, and special biological actions of the enzyme proteins. FEBS Lett *584*, 2194-2200.

Steinbachs, J.E., and Holsinger, K.E. (2002). S-RNase-mediated gametophytic self-incompatibility is ancestral in eudicots. Mol Biol Evol *19*, 825-829.

Stojan, G., and Petri, M. (2018). Epidemiology of systemic lupus erythematosus: an update. Curr Opin Rheumatol *30*, 144-150.

Suzuki, A., Yao, M., Tanaka, I., Numata, T., Kikukawa, S., Yamasaki, N., and Kimura, M. (2000). Crystal structures of the ribonuclease MC1 from bitter gourd seeds, complexed with 2'-UMP or 3'-UMP, reveal structural basis for uridine specificity. Biochem Biophys Res Commun *275*, 572-576.

Szondy, Z., Sarang, Z., Kiss, B., Garabuczi, E., and Koroskenyi, K. (2017). Anti-inflammatory Mechanisms Triggered by Apoptotic Cells during Their Clearance. Front Immunol *8*, 909.

Tait, S.W., Ichim, G., and Green, D.R. (2014). Die another way--non-apoptotic mechanisms of cell death. J Cell Sci *127*, 2135-2144.

Takeda, K., Kaisho, T., and Akira, S. (2003). Toll-like receptors. Annu Rev Immunol *21*, 335-376.

Takeuchi, O., and Akira, S. (2009). Innate immunity to virus infection. Immunol Rev *227*, 75-86.

Takeuchi, O., Hoshino, K., Kawai, T., Sanjo, H., Takada, H., Ogawa, T., Takeda, K., and Akira, S. (1999). Differential roles of TLR2 and TLR4 in recognition of gram-negative and gram-positive bacterial cell wall components. Immunity *11*, 443-451.

Tamirou, F., Arnaud, L., Talarico, R., Scire, C.A., Alexander, T., Amoura, Z., Avcin, T., Bortoluzzi, A., Cervera, R., Conti, F.*, et al.* (2018). Systemic lupus erythematosus: state of the art on clinical practice guidelines. RMD Open *4*, e000793.

Tan, Y., and Kagan, J.C. (2019). Innate Immune Signaling Organelles Display Natural and Programmable Signaling Flexibility. Cell *177*, 384-398 e311.

Tanaka, N., Arai, J., Inokuchi, N., Koyama, T., Ohgi, K., Irie, M., and Nakamura, K.T. (2000). Crystal structure of a plant ribonuclease, RNase LE. J Mol Biol *298*, 859-873.

Tanaka, T., Narazaki, M., and Kishimoto, T. (2014). IL-6 in inflammation, immunity, and disease. Cold Spring Harb Perspect Biol *6*, a016295.

Tanji, H., Ohto, U., Motoi, Y., Shibata, T., Miyake, K., and Shimizu, T. (2016). Autoinhibition and relief mechanism by the proteolytic processing of Toll-like receptor 8. Proc Natl Acad Sci U S A *113*, 3012-3017.

Tanji, H., Ohto, U., Shibata, T., Miyake, K., and Shimizu, T. (2013). Structural reorganization of the Toll-like receptor 8 dimer induced by agonistic ligands. Science *339*, 1426-1429.

Tanji, H., Ohto, U., Shibata, T., Taoka, M., Yamauchi, Y., Isobe, T., Miyake, K., and Shimizu, T. (2015). Toll-like receptor 8 senses degradation products of single-stranded RNA. Nat Struct Mol Biol *22*, 109-115.

Taoka, M., Nobe, Y., Yamaki, Y., Sato, K., Ishikawa, H., Izumikawa, K., Yamauchi, Y., Hirota, K., Nakayama, H., Takahashi, N., and Isobe, T. (2018). Landscape of the complete RNA chemical modifications in the human 80S ribosome. Nucleic Acids Res *46*, 9289-9298.

Teghanemt, A., Zhang, D., Levis, E.N., Weiss, J.P., and Gioannini, T.L. (2005). Molecular basis of reduced potency of underacylated endotoxins. J Immunol *175*, 4669-4676.

Thompson, D.M., and Parker, R. (2009). The RNase Rny1p cleaves tRNAs and promotes cell death during oxidative stress in Saccharomyces cerevisiae. J Cell Biol *185*, 43-50.

Thorn, A., Steinfeld, R., Ziegenbein, M., Grapp, M., Hsiao, H.H., Urlaub, H., Sheldrick, G.M., Gartner, J., and Kratzner, R. (2012). Structure and activity of the only human RNase T2. Nucleic Acids Res *40*, 8733-8742.

Tran, N.L., Manzin-Lorenzi, C., and Santiago-Raber, M.L. (2015). Toll-like receptor 8 deletion accelerates autoimmunity in a mouse model of lupus through a Toll-like receptor 7-dependent mechanism. Immunology *145*, 60-70.

Tsujimoto, H., Ono, S., Efron, P.A., Scumpia, P.O., Moldawer, L.L., and Mochizuki, H. (2008). Role of Toll-like receptors in the development of sepsis. Shock *29*, 315-321.

Turner, M.D., Nedjai, B., Hurst, T., and Pennington, D.J. (2014). Cytokines and chemokines: At the crossroads of cell signalling and inflammatory disease. Biochim Biophys Acta *1843*, 2563-2582.

Turner, N.A., Sharma-Kuinkel, B.K., Maskarinec, S.A., Eichenberger, E.M., Shah, P.P., Carugati, M., Holland, T.L., and Fowler, V.G., Jr. (2019). Methicillin-resistant Staphylococcus aureus: an overview of basic and clinical research. Nat Rev Microbiol *17*, 203-218.

Ullah, M.O., Sweet, M.J., Mansell, A., Kellie, S., and Kobe, B. (2016). TRIF-dependent TLR signaling, its functions in host defense and inflammation, and its potential as a therapeutic target. J Leukoc Biol *100*, 27-45.

Unterholzner, L., Keating, S.E., Baran, M., Horan, K.A., Jensen, S.B., Sharma, S., Sirois, C.M., Jin, T., Latz, E., Xiao, T.S*., et al.* (2010). IFI16 is an innate immune sensor for intracellular DNA. Nat Immunol *11*, 997-1004.

Vande Walle, L., and Lamkanfi, M. (2016). Pyroptosis. Curr Biol *26*, R568-R572.

Venereau, E., Ceriotti, C., and Bianchi, M.E. (2015). DAMPs from Cell Death to New Life. Front Immunol *6*, 422.

Vijay-Kumar, M., Aitken, J.D., Carvalho, F.A., Cullender, T.C., Mwangi, S., Srinivasan, S., Sitaraman, S.V., Knight, R., Ley, R.E., and Gewirtz, A.T. (2010). Metabolic syndrome and altered gut microbiota in mice lacking Toll-like receptor 5. Science *328*, 228-231.

Walport, M.J. (2001). Complement. First of two parts. N Engl J Med *344*, 1058-1066.

Walsh, D., McCarthy, J., O'Driscoll, C., and Melgar, S. (2013). Pattern recognition receptors--molecular orchestrators of inflammation in inflammatory bowel disease. Cytokine Growth Factor Rev *24*, 91-104.

Wang, C., Deng, L., Hong, M., Akkaraju, G.R., Inoue, J., and Chen, Z.J. (2001). TAK1 is a ubiquitin-dependent kinase of MKK and IKK. Nature *412*, 346-351.

Wiseman, H., and Halliwell, B. (1996). Damage to DNA by reactive oxygen and nitrogen species: role in inflammatory disease and progression to cancer. Biochem J *313 (Pt 1)*, 17-29.

Wu, J., Sun, L., Chen, X., Du, F., Shi, H., Chen, C., and Chen, Z.J. (2013). Cyclic GMP-AMP is an endogenous second messenger in innate immune signaling by cytosolic DNA. Science *339*, 826-830.

Wu, Y.W., Tang, W., and Zuo, J.P. (2015). Toll-like receptors: potential targets for lupus treatment. Acta Pharmacol Sin *36*, 1395-1407.

Yamamoto, M., Sato, S., Hemmi, H., Hoshino, K., Kaisho, T., Sanjo, H., Takeuchi, O., Sugiyama, M., Okabe, M., Takeda, K., and Akira, S. (2003). Role of adaptor TRIF in the MyD88-independent toll-like receptor signaling pathway. Science *301*, 640-643.

Yan, N., and Chen, Z.J. (2012). Intrinsic antiviral immunity. Nat Immunol *13*, 214-222.

Yoneyama, M., and Fujita, T. (2008). Structural mechanism of RNA recognition by the RIG-I-like receptors. Immunity *29*, 178-181.

Zanoni, I., Ostuni, R., Marek, L.R., Barresi, S., Barbalat, R., Barton, G.M., Granucci, F., and Kagan, J.C. (2011). CD14 controls the LPS-induced endocytosis of Toll-like receptor 4. Cell *147*, 868-880.

Zhang, Z., Ohto, U., Shibata, T., Krayukhina, E., Taoka, M., Yamauchi, Y., Tanji, H., Isobe, T., Uchiyama, S., Miyake, K., and Shimizu, T. (2016). Structural Analysis Reveals that Toll-like Receptor 7 Is a Dual Receptor for Guanosine and Single-Stranded RNA. Immunity *45*, 737-748.

8 List of abbreviation

8-OHdG	8-hydroxy-2' -Deoxyguanosine
8-OHG	8-Hydroxyguanosine
A	Adenosine
ACS	Aicardi-Goutières syndrome
AIM2	Absent In Melanoma 2
bp	Base pair
C	Cytidine
cGAMP	Cyclic GMP-AMP
cGAS	Cyclic GMP-AMP synthase
CLRs	C-type lectin receptors
CMV	Cytomegalovirus
CNS	Central nervous system
CSF	Cerebrospinal fluid
CSFV	Classical swine fever virus
CXorf21	Chromosome X Open Reading Frame 21
dA	Deoxyadenosine
DAMP	Damage-associated molecular pattern
dC	Deoxycytidine
DCs	Dendritic cells
DD	Death domain
dG	Deoxyguanosine
DNA	Deoxyribonucleic acid
dNTPs	Deoxynucleoside triphosphates
ds	Double stranded
dT	Deoxythymidine
ELISA	Enzyme-linked Immunosorbent Assay
ER	Endoplasmic reticulum
EtOH	Ethanol
FACS	Fluorescence-activated cell sorting
FCS	Fetal cow serum
G	Guanosine
GPCR	G protein-coupled receptors
GSDMD	Gasdermin D
H2O	Water

HIV	Human immunodeficiency virus
HSCs	Hematopoietic stem cells
IFN	Interferon
IKK	Inhibitor of nuclear factor kappa-B kinase
IL	Interleukin
iNOS	Inducible nitric oxide synthase
IRAK	IL-1 receptor-activated protein kinase
IRF	Interferon regulatory factor
JAK	Janus kinase
LGP2	Laboratory of genetics and physiology 2
LPS	Lipopolysaccharide
LRR	Leucine-rich repeat
M-CSF	Macrophage colony-stimulating factor
MAC	Membrane attack complex
MAL	MyD88 adaptor like protein
MAPK	Mitogen-activated protein kinase
MAVS	Mitochondrial antiviral-signaling protein
MDA5	Melanoma differentiation-associated protein 5
MHC	Major histocompatibility complex
MLKL	mixed lineage kinase domain-like protein
MRI	Magnetic resonance imaging
MyD88	Myeloid differentiation factor 88
NADPH	nicotinamide adenine dinucleotide phosphate
NF-κB	Nuclear factor kappa-light-chain-enhancer of activated B cells
NLRP	NOD-, LRR- and pyrin domain-containing protein
NLRs	NOD like receptors
OAS	2’-5’-oligoadenylate synthetase
ONs	Oligoribonucleotides
PAMP	Pathogen associated molecular pattern
PCR	Polymerase chain reaction
PMA	Phorbol 12-myristate 13-acetate
pR	Poly-L-arginine
PRR	Pattern recognition receptors
RIG-I	Retinoic acid-inducible gene I
RIPK	Receptor-interacting serine/threonine-protein kinase
RLRs	RIG-I like receptors
RNA	Ribonucleic acid

Rnase L	Ribonuclease L
RNP	Ribonucleoprotein
ROS	Reactive oxygen species
rRNA	Ribosomal ribonucleic acid
SAMHD1	SAM domain and HD domain-containing protein 1
SLC15A4	Central nervous system
ss	Single stranded
STAT	Signal transducers and activators of transcription
STING	Stimulator of interferon genes
T	Thymidine
TAK1	transforming growth factor b activated protein kinase 1
TASL	TLR adaptor interacting with SLC15A4 on the lysosome
TBK1	TANK-binding kinase1
TIR domain	Toll/Interleuchin-1 domain
TLR	Toll-like receptors
TNF	Tumor necrosis factor
TRAF	tumor necrosis factor receptor associated factor
TRAF	tumor necrosis factor receptor associated factor
TRIF	TIR-domain-containing adapter-inducing interferon-β
tRNA	Transfer ribonucleic acid
U	Uridine
UV	Ultraviolet

9 Acknowledgments

First, I want to thank Veit Hornung who gave me the opportunity to do my Ph.D. thesis in his lab. He was always available to discuss the project and came up with very helpful ideas and suggestions. Thanks for the close supervision especially during the paper time!

Next, I want to thank Mirko Wagner and Thomas Carell for a very nice and fruitful collaboration. Mirko Wagner did measure all mass spectrometry samples, really contributing to this study.

Furthermore, I want to thank Moritz Gaidt, who did the initial experiments for this project.

I also really want to thank Andreas Wegerer and Larissa Hansbauer for all the technical support and hours of ELISA that made my life much easier! I also want to thank the rest of the Hornung group. It was really fun to work with you guys and I could always ask for help if something did not work out. Furthermore, I enjoyed all the social activities like skiing trips or boulder sessions.

I also want to thank Sara for always supporting me and cheering me up if something did not go as planned. It helped me to survive stressful times. Thanks for the nice everyday life together with you.

In the end, I also want to thank my parents and family, who supported me throughout my whole studies.